UNIVERSIDADE ESTADUAL DE CAMPINAS
Faculdade de Engenharia Mecânica

GIOVANNA PISICCHIO ZANONI

Acoustical characterization of double porosity materials using mineral wools

Caracterização acústica de materiais com dupla porosidade usando lãs minerais

CAMPINAS
2018

GIOVANNA PISICCHIO ZANONI

Acoustical characterization of double porosity materials using mineral wools

Caracterização acústica de materiais com dupla porosidade usando lãs minerais

Master Thesis presented to the School of Mechanical Engineering of the Univesity of Campinas in partial fulfillment of the requirements for the degree of Master in Mechanical Engineering, in the Area of Solid Mechanics and Mechanical Design.

Dissertação de Mestrado apresentada à Faculdade de Engenharia Mecânica da Universidade Estadual de Campinas como parte dos requisitos exigidos para a obtenção do título de Mestra em Engenharia Mecânica, na Área de Mecânica dos Sólidos e Projeto Mecânico.

Orientador: Prof. Dr. Alberto Luiz Serpa

ESTE EXEMPLAR CORRESPONDE À VERSÃO FINAL DA DISSERTAÇÃO DEFENDIDA PELA ALUNA GIOVANNA PISICCHIO ZANONI, E ORIENTADA PELO PROF. DR. ALBERTO LUIZ SERPA.

CAMPINAS

2018

Agência(s) de fomento e nº(s) de processo(s): CAPES, 33003017
ORCID: https://orcid.org/0000-0003-1907-2525

Ficha catalográfica
Universidade Estadual de Campinas
Biblioteca da Área de Engenharia e Arquitetura
Luciana Pietrosanto Milla - CRB 8/8129

Z17a

Zanoni, Giovanna Pisicchio, 1990-
Acoustical characterization of double porosity materials using mineral wools / Giovanna Pisicchio Zanoni. – Campinas, SP : [s.n.], 2018.

Orientador: Alberto Luiz Serpa.
Dissertação (mestrado) – Universidade Estadual de Campinas, Faculdade de Engenharia Mecânica.

1. Materiais porosos. 2. Absorção do som. 3. Isolamento acústico. 4. Lã mineral. I. Serpa, Alberto Luiz, 1967-. II. Universidade Estadual de Campinas. Faculdade de Engenharia Mecânica. III. Título.

Informações para Biblioteca Digital

Título em outro idioma: Caracterização acústica de materiais com dupla porosidade usando lãs minerais
Palavras-chave em inglês:
Porous materials
Sound absorption
Sound insulation
Mineral wool
Área de concentração: Mecânica dos Sólidos e Projeto Mecânico
Titulação: Mestra em Engenharia Mecânica
Banca examinadora:
Alberto Luiz Serpa [Orientador]
Bruno Sanches Masiero
Flávio de Campos Bannwart
Data de defesa: 28-02-2018
Programa de Pós-Graduação: Engenharia Mecânica

UNIVERSIDADE ESTADUAL DE CAMPINAS
FACULDADE DE ENGENHARIA MECÂNICA
COMISSÃO DE PÓS-GRADUAÇÃO EM ENGENHARIA MECÂNICA
DEPARTAMENTO DE MECÂNICA COMPUTACIONAL

DISSERTAÇÃO DE MESTRADO ACADÊMICO

Acoustical characterization of double porosity materials using mineral wools

Caracterização acústica de materiais com dupla porosidade usando lãs minerais

Autor: Giovanna Pisicchio Zanoni
Orientador: Prof. Dr. Alberto Luiz Serpa

A Banca Examinadora composta pelos membros abaixo aprovou esta Dissertação:

Prof. Dr. Alberto Luiz Serpa
FEM/UNICAMP

Prof. Dr. Bruno Sanches Masiero
FEEC/UNICAMP

Prof. Dr. Flávio de Campos Bannwart
FEM/UNICAMP

A Ata da defesa com as respectivas assinaturas dos membros encontra-se no processo de vida acadêmica da aluna.

Campinas, 28 de fevereiro de 2018.

Dedico este trabalho aos meus pais, Angela e Jose.

ACKNOWLEDGEMENTS

A Deus por ter me feito perseverar perante as dificuldades pessoais e acadêmicas. Ao meus pais, Angela e Jose, por todo o tipo de suporte, carinho e incentivo para que eu seja sempre uma pessoa e profissional melhor. A minha irmã Juliana e meu cunhado Nelson pelo incentivo e aos meus sobrinhos João Pedro (em memória), Beatriz e Francisco por terem sempre adoçado minha vida.

Ao meu orientador Prof. Dr. Alberto Luiz Serpa pela oportunidade do mestrado, sua orientação e ajuda.

À Dr[a]. Rita Aparecida Zoppi pela colaboração em diversas etapas desse projeto.

A Guilherme L. L. Alves pelo carinho, ajuda e por sempre acreditar em mim.

As minhas amigas Ana, Aline, Camila C., Camila S., Danielle, Letícia e Lígia por terem torcido por mim e pelas palavras de apoio, mesmo a distância. Aos meus colegas de pós-graduação pela ajuda acadêmica e pessoal e por terem tornado esse período ainda mais agradável com a amizade de vocês. Aos meu amigos de graduação por terem me ensinado a perseverar sempre diante das dificuldades acadêmicas.

Àqueles que muito contribuíram com a parte prática deste trabalho, seja com ideias para o preparo e corte de amostras, disposição de maquinários e confecção de peças de corte e suporte para amostras: Andre Pissolati (IFGW-Unicamp), Jose Luis C. Almeida (FEM-Unicamp) e Prof. João F. Foganholi (Cotuca-Unicamp). A Fernando Ortolano (FEM-Unicamp) pelo suporte com a instrumentação utilizada nos testes e auxílios gerais durante o período de mestrado. Ao Laboratório de Vibroacústica da FEM-Unicamp, onde realizei a caracterização acústica dos materiais, representado pelos seus docentes, colaboradores e pós-graduandos.

Ao Laboratório Nacional de Nanotecnologia (LNNano) pela liberação para realização de experimentos em suas instalações, e em especial à equipe de Microtomografia de Raios-X e Microscopia Eletrônica de Varredura. Ao Laboratório de Ensaios Mecânicos do DEMM-FEM-Unicamp pelo ensaio de compressão das amostras de Lãs Minerais, em especial a Jose Luis Lisboa. Ao Laboratório de Ensaios Não-destrutivos da Feagri-Unicamp pela ajuda com o ensaio de ultrassom, em especial a Paulo G. K. Nunes e a Prof[a]. Dr[a]. Raquel Gonçalves.

Ao Prof. Dr. Flávio de Campos Bannwart e ao Prof. Dr. Bruno Sanches Masiero pelas sugestões realizadas a esse trabalho.

À Faculdade de Engenharia Mecânica da Unicamp por fornecer os meios necessários para realização deste trabalho.

A Coordenação de Aperfeiçoamento do Pessoal de Nível Superior (Capes) pelo suporte financeiro.

"Por vezes sentimos que aquilo que fazemos não é senão uma gota de água no mar. Mas o mar seria menor se lhe faltasse uma gota"

(Madre Teresa de Calcutá)

RESUMO

O controle de ruído passivo é umas das formas mais comuns de se controlar o ruído em diversos campos de aplicação, devido ao menor custo e simplicidade quando comparado ao controle ativo de ruído. Materiais porosos são amplamente usados no controle de ruído passivo, e nos últimos anos, diferentes conceitos de materiais acústicos têm sido criados. O uso de macroperforações em um material poroso leva à formação de materiais de dupla porosidade, que são materiais com duas redes de poros que são interconectadas. Nesse estudo, materiais de dupla porosidade feitos de lã de rocha e lã de vidro foram avaliados. Diversas configurações de macroperfurações ou mesoporos foram testados em termos de absorção e perda por transmissão sonora. As amostras de dupla porosidade foram confeccionadas com mesoporos sem preenchimento ou com mesoporos preenchidos com outro material poroso. Estes testes foram realizados usando dois tubos de impedância distintos, um com seção transversal circular de 60 *mm* (125 - 2500 *Hz*) e outro com seção transversal retangular de 240×160 *mm* (20 - 717 *Hz*). Os resultados de absorção sonora indicaram um ganho em absorção para as amostras de lã de rocha, com os mesoporos preenchidos ou não, acima dos 1000 *Hz* (amostras circulares). Já para a lã de vidro, foram observados ganho para algumas amostras ao redor de 250 *Hz* e 2000 *Hz* (amostras circulares). Para os ensaios de absorção sonora no tubo retangular ganhos foram encontrados para quatros tipos de amostras de lã de vidro em torno de 250 *Hz* e todos os tipos de amostra de lã de rocha com mesoporos preenchidos em torno de 500 *Hz*. Para a perda por transmissão sonora, somente testes no tubo de impedância de seção circular foram realizados e mostraram a possibilidade de aumentar o isolamento sonoro adicionando uma proporção de outro material poroso em comparação com a amostra de porosidade única. Além disso, a porosidade e tortuosidade da lã de rocha e lã de vidro de porosidade única foram estimadas. Este parâmetros foram usados como dados de entrada para um modelo de predição de absorção sonora para dupla porosidade, que foi comparado com os dados experimentais do tubo de impedância de seção transversal retangular.

Palavras-chaves: Materiais porosos, Dupla porosidade, Absorção do som, Isolamento acústico, Lã mineral.

ABSTRACT

Passive noise control is one of the most common forms for noise control at different fields of applications, because of the lower cost and simplicity compared to the active noise control. Porous materials are widely used in passive noise control, and different concepts of acoustical materials have been created in the past years. The use of macroperforations in a porous material lead to double porosity materials, which are materials with two different networks of interconnected pores. In this study, double porosity materials made by rockwool and glasswool are evaluated. Different configurations of macroperforations or mesopores were tested in terms of sound absorption and sound transmission loss. The double porosity samples were made with mesopores not filled or with mesopores filled with another porous material. These tests were performed using two different impedance tubes, one with a circular cross-section of 60 *mm* (125 - 2500 *Hz*) and other with a rectangular cross-section of 240$\times$160 *mm* (20 - 717 *Hz*). Results of sound absorption indicated gains for rockwool samples, with mesopores filled and not filled, above 1000 *Hz* (circular samples). For glasswool, gains were observed for some samples around 250 *Hz* and 2000 *Hz* (circular samples). In the sound absorption tests at the rectangular tube, gains were found for four types of glasswool samples around 250 *Hz* and for all rockwool samples with mesopores filled around 500 *Hz*. For sound transmission loss, only the tests in the circular cross-section tube were made and they showed the possibility to enhance sound insulation by adding a proportion of other porous material in comparison to the pure case. Also, porosity and tortuosity were estimated for single porosity rockwool and glasswool. These parameters were used as input data for a double porosity sound absorption prediction model, that was compared with the experimental data of sound absorption test at the impedance tube of rectangular cross-section.

Keywords: Porous materials, Double porosity, Sound absorption, Sound insulation, Mineral wool.

LIST OF FIGURES

LIST OF TABLES

NOTATION

Latin Letters

c	Sound speed in air
C_i	Wave speed in fluid
C_{is}	Wave speed in the same fluid when it saturates a porous frame
C_p	Specific heat at constant pressure
C_v	Specific heat at constant volume
e	Thickness
f	Frequency in Hertz
G_{rr}	Loudspeaker Autospectrum
H_I	Transfer function between microphones for the incident wave
H_R	Transfer function between microphones for the reflected wave
H_{12}	Transfer function between microphones 1 and 2
k	Wavenumber
K_m	Dynamic Bulk Modulus for microporosity medium
K_p	Dynamic Bulk Modulus for macroporosity medium
K_{dp}	Dynamic Bulk Modulus for double porosity material
L_c	Size of one unit cell
l_p	Mesosocopic characteristic size
l_m	Microporosity characteristic size
L	Macroporosity characteristic size
m	Mass per unit area
P_0	Atmospheric pressure
$P_{x=0}$	Sound pressure at sample surface
$P_{x=d}$	Pressure at sample termination

P_{up} Pressure upstream the sample

P_{down} Pressure downstream the sample

R Mesopore radius with circular cross section

$V_{x=0}$ Particle Velocity at sample surface

$V_{x=d}$ Particle Velocity at sample termination

r Sound reflection coefficient

s Mechanical stiffness

T Temperature

T_a Transmission coefficient for an anechoic termination

TL Sound transmission loss

Z_C Characteristic impedance

Z_{dp} Surface impedance for double porosity media

Greek Letters

α Sound absorption coefficient

α_∞ Tortuosity

τ Sound transmission coefficient

ϕ Porosity

ϕ_m Microporosity

ϕ_p Mesoporosity

Π_{dp} Dynamic Permeability for double porosity media

Pi_m Dynamic Permeability for microporous media

Pi_p Dynamic Permeability for macroscopic media

δ_v Viscous boundary layer thickness

δ_t Thermal boundary layer thickness

η Air dynamic viscosity

Λ Viscous characteristic length

Λ' Thermal characteristic length

$\Theta(0)$ Static thermal permeability

$\Theta(\omega)$ Dynamic thermal permeability

κ Air thermal conductivity

ρ_0 Air density

ρ_{dp} Effective density in the case of double porosity media

ω Angular frequency

ω_0 Resonance frequency

ω_{vp} Mesosocopic viscous characteristic frequency

ω_{vm} Microscopic viscous characteristic frequency

ω_d Diffusion frequency

Abbreviations

TL Sound transmission loss

SEM Scanning electron microscopy

SE Secondary electrons

BSE Backscattered electrons

EDS Energy dispersion sensor

O Oxygen

Ca Calcium

Si Silicon

Na Sodium

Mg Magnesium

CONTENTS

1 INTRODUCTION

Materials with interesting acoustic properties are used in various noise control solutions, in different fields of application: architectural, environmental, automobile, aeronautical, and industrial in general. Acoustic materials used for noise control are mainly porous: foams, mineral wools and fabric (for example, the curtains and carpets used for acoustics architectural purpose) (COX; D'ANTONIO, 2009).

In this study, perforations were made in rockwool and glasswool, two types of mineral wools used as thermal insulators and acoustic materials, in order to create a double porosity material with the objective of evaluating acoustical properties .

1.1 Motivation

Nowadays, an interesting field of study is the improvement of sound absorption of acoustic porous materials, especially at low frequencies, as these materials generally present a good performance at middle and high frequencies. This effect can be observed in Tab. 1, which presents sound absorption values for roockwool for various thickness and densities and for other porous material. Additionally, in Fig. 1, we see the different sound absorption values when using carpets, also a porous material are described and it is easy to observe the increase of sound absorption as the frequency increases.

Table 1 – Sound absorption for different porous acoustic materials.

Material	**Octave Band Center Frequency (*Hz*)**				
Fiber Glass or rockwool blanket	125	250	500	1000	2000
16 kg/m^3, 25 *mm* thick	0.12	0.28	0.55	0.74	0.83
16 $kg/m^3$3, 50 *mm* thick	0.17	0.45	0.80	0.97	0.94
16 kg/m^3, 75 *mm* thick	0.30	0.69	0.94	1.0	1.0
16 kg/m^3, 100 *mm* thick	0.43	0.86	1.0	1.0	1.0
24 kg/m^3, 25 *mm* thick	0.11	0.32	0.56	0.77	0.91
24 kg/m^3, 50 *mm* thick	0.27	0.54	0.94	1.0	1.0
24 kg/m^3, 75 *mm* thick	0.28	0.79	1.0	1.0	1.0
24 kg/m^3, 100 *mm* thick	0.46	1.0	1.0	1.0	1.0
48 kg/m^3, 50 *mm* thick	0.30	1.0	1.0	1.0	1.0
48 kg/m^3, 75 *mm* thick	0.43	1.0	1.0	1.0	1.0
48 kg/m^3, 100 *mm* thick	0.65	1.0	1.0	1.0	1.0
60 kg/m^3, 25 *mm* thick	0.18	0.24	0.68	1.0	1.0
60 kg/m^3, 50 *mm* thick	0.25	0.83	1.0	1.0	1.0
Polyurethane foam, 27 kg/m^3, 15 *mm* thick	0.08	0.22	0.55	0.85	0.75

Reference:Bies and Hansen (1996)

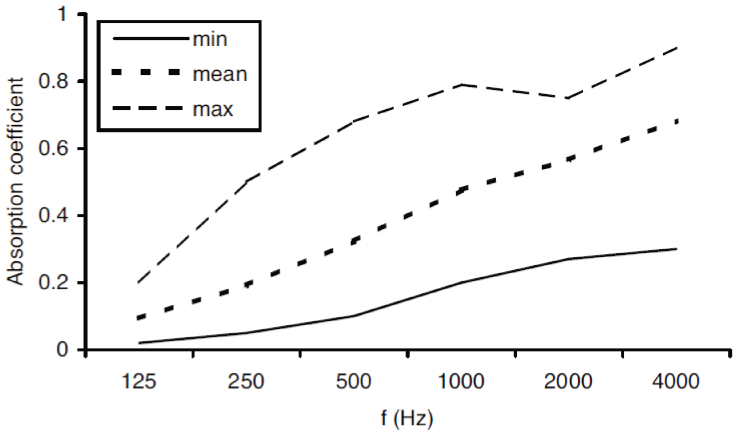

Figure 1 – Minimum, mean and maximum values of sound absorption found for carpets.
Reference:Cox and D'Antonio (2009)

The problem related to the absorption at low frequencies is that in some situations where it is necessary to apply noise control solutions, noise needs to be atenuatted at different frequency ranges, including the low frequency range. One example is the case of ventilating systems, which can be placed outside or inside a room. This is a problem presented both for architectural room acoustics and industrial noise control. The spectrum of a ventilating system is characterized by a larger bandwidth, including significant components at low frequencies (GERGES, 1992). Another case is the sound pressure level of a power transformer. It has an important component at low and medium frequencies, including many tonal noises, represented by harmonics of a frequency, as shown in Fig. 2. To obtain a global effect of sound reduction in these cases, it is necessary to reduce noise also at low frequencies, a region where porous materials usually do not have their best performance.

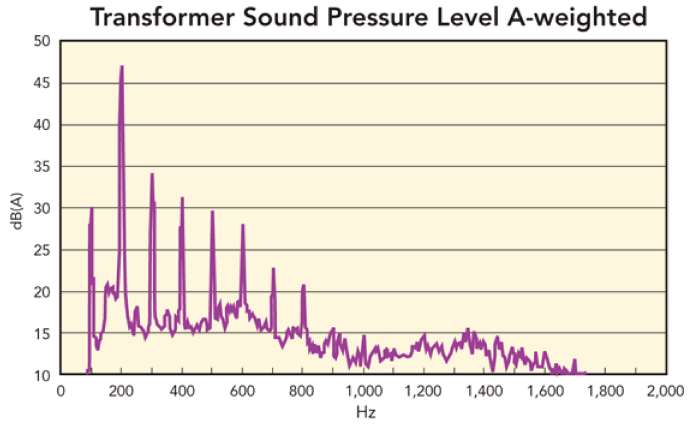

Figure 2 – Sound pressure level of a typical power tranformer.
Reference:$http:$
$//www.elp.com/articles/powergrid_international/print/volume-15/issue-1/features/the-sound-of-silence.html$

In this context, the insertion of macroperforations in porous materials to obtain better performance for sound absorption at low frequencies and in the entire frequency range is

studied in order to improve sound absorption. Materials with micropores and macroperfurations are called double porosity materials. The macroperforation is also called mesopore. In a general way, a double porosity material is defined as a material with two interconnected pore networks with different characteristics lengths (OLNY; BOUTIN, 2003).

By the study of past works, the double porosity materials are presented as a good solution for improvement of sound absorption. An alternative approach is the use of multi-layered systems, with layers of different materials. However, a parametric study by Atalla *et al.* (2001) has shown that heterogeneous materials have a better acoustical performance for sound absorption than homogeneous materials with different layers.

Atalla *et al.* (2001) studied the case where a glasswool panel had mesopores filled by rockwool instead of air. The absorption coefficient of this panel was compared to a double layered panel with a five centimeters layer of rockwool and a one-centimeter layer of glasswool. The sample with double porosity presented better sound absorption for all frequencies and a significant proportional increase of absorption at low frequencies when compared to the double layered panel.

Another alternative approach is the use of hybrid systems, as the ones with an active sound control at low frequencies and a passive sound control at middle and high frequencies. But the use of active control demands power supply, which can be undesirable in harsh work environment (GOURDON; SEPPI, 2010). Also, the developing of an active noise control system requires a lot of signal processing work, which is not necessary in the case of passive control solutions.

On average, the passive sound control solutions are easier to be developed for noise control solutions, especially at the industrial and civil construction area. Porous materials, like mineral wools, are very common in the acoustical market, and the modifications, like the perforations, are easy to be made by means of simple tools. In this context, the use of double porosity in this type of material is an interesting topic to study the improvement of sound absorption. Also, it is a relatively new field of study in the area of acoustic materials. The studies began about 20 years ago.

In the case of transmission loss using double porosity, few studies related to the topic are reported. Transmission loss can be investigated to verify if the use of double porosity in acoustic porous materials can lead to an interesting sound insulation performance.

In this study, low frequencies refer to frequencies below 600 Hz and high frequencies from 600 Hz to 2500 Hz (which is the highest frequency value evaluated experimentally).

1.2 Related works

The double porosity materials for acoustical purposes were first studied by authors in the late 1990s (AURIALT; BOUTIN, 1994), (BOUTIN *et al.*, 1998) and (OLNY; BOUTIN,

2000). These authors stated some theoretical aspects, and after Atalla *et al.* (2001) and Sgard *et al.* (2005) developed numerical and analytical models and performed experiments using double porosity, especially with mesopores filled with air. In 2010, Gourdon and Seppi (2010) developed analytical expressions and made experimental verification for the case where the perforations are filled with another porous material.

In the article of Olny and Boutin (2003), they defined what is a double porosity media and explained the proper separation of scales between pores and mesopores. They used the homogenization theory to give the governing equations of sound propagation in this type of media and studied two types of situation: the low and high contrast of permeability, which is characterized by the differences of the characteristic sizes of mesopores and micropores of the material. They observed the macroscopic behavior of these situations. For high contrast situation, the mesopores governed the macroscopic flow.

Atalla *et al.* (2001) developed a 3D numerical model to predict the sound absorption of a double porosity material in a semi-infinite hard-walled rectangular waveguide. They presented experimental results for two different thickness samples and, with these results, validated their model. However, their model was limited to air-filled mesopores. They found that it is possible to increase sound absorption at low frequency by the proper design of the macroperforations, for the case of mesoporosity (mesopore area proportion compared to the substrate area) between an especific interval. Additionally, they studied numerically the influence of the macroporosity, the size of the hole and the macropore distribution on the sound absorption and compared a double porosity material with porous inclusion to a multilayered panel.

Sgard *et al.* (2005) also present an analytical model for double porosity materials based on physical parameters. Using this model, they provided practical rules to the design of a double porosity material, which are equations based on physical parameters. They investigated the influence of the transversal profile of the mesopore and the influence of an impervious screen with double porosity material.

Gourdon and Seppi (2010) studied composite material by the use of double porosity materials with porous inclusions. They developed the analytical model for porous inclusions, based on the previous studies. They showed that when the inclusion is filled, the behavior at very low frequencies (between 50 to 200 Hz) is better than for the case of not filled mesopores.They validated their model using experiments in three different Kundt Tubes, wich have different cross-sections.

The hypotheses that the inclusions are periodic and the frame is rigid were considered for all the studies discussed above.

Finally, Sgard and Atalla (2000) studied the sound transmission loss in a composite material. The material is a porous material filled with solid inclusions of polystyrene. They showed, using a numeric methodology, that there is a small gain in transmission loss around

1000 *Hz* by the use of the solid inclusions, compared to the case without inclusions (SGARD; ATALLA, 2000). Although they did not name it a double porosity material, it can be considered one, because the inclusions in a double porosity material can be fluid (air), poroelastic or elastic (SGARD *et al.*, 2005).

In this study, a higher number of samples with different mesoporosities were tested experimentally, for samples with perforations and porous inclusions, when compared to the previous studies of Atalla *et al.* (2001) and Gourdon and Seppi (2010). Also, transmission loss was experimentally evaluated for porous inclusions different from the case of solid inclusions presented by Sgard and Atalla (2000).

1.3 Objective

The main objective of this study is the experimental investigation of sound absorption and sound transmission loss behavior when using the concept of macroperforations or mesopores at a given porous material.

The specific objectives are:

- Analyze acoustic measurements of sound absorption and sound transmission loss for materials with macroperforations filled with air and macroperforations filled with another porous material;
- Analyze the influence of mesoporosity and the number of mesopores;
- Characterize physical properties of porous materials which are related to the material sound absorption;
- Compare experimental results of sound absorption coefficient with an analytical models that predicts sound absorption for double porosity materials.

1.4 Work structure

This study is divided into the following chapters:

- Chapter 2 presents the theoretical background with the main theoretical concepts of this study;
- Chapter 3 presents the methodology of the acoustic and non-acoustic tests realized;
- Chapter 4 presents the results of this study;
- Chapter 5 presents the conclusions based on the results and the theoretical aspects studied.

2 THEORETICAL BACKGROUND

2.1 Sound absorption

Sound absorption coefficient (α) is defined as the amount of energy that is absorbed by the material considering the amount of incident sound energy. If the material is rigidly backed, as in Fig. 3, there is only absorption and reflection of sound waves at this material. One portion of the incident sound wave is absorbed and the other is reflected. The reflection coefficient r is defined as:

$$r = \frac{A_{rw}}{A_{iw}}, \tag{2.1}$$

where A_{rw} is the complex amplitude of the reflected wave and A_{iw} is the complex amplitude of the incident wave.

The sound energy density of a wave, the sound energy contained in one unit volume, is related to pressure (p), the sound speed (c) and the air density (ρ_0) by (KUTRUFF, 2000):

$$w = \frac{p^2}{\rho_0 c}. \tag{2.2}$$

The sound absorption coefficient is related to the amount of energy which was not reflected, so, considering Eq. 2.2 this leads to (RAICHEL, 2006):

$$\alpha = 1 - |r|^2. \tag{2.3}$$

α is a real value coefficient that ranges from 0 to 1, totally reflective and totally absorptive, respectively.

2.2 Sound transmission loss

The measurement of the sound insulation of a material or a structure (wall, barrier) is given by the transmission loss. When there is an incident sound wave at a structure or material, sound can be reflected, absorbed and transmitted, as in Fig. 4. The sound transmission coefficient (τ) is given by the ratio of incident sound energy (W_i) to the transmitted sound energy (W_t):

$$\tau = \frac{W_t}{W_i}. \tag{2.4}$$

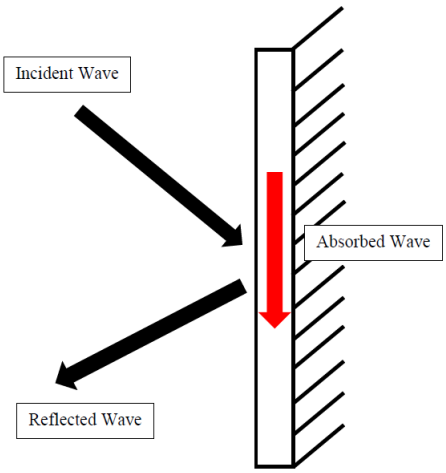

Figure 3 – Sound absorption at a material.
Reference: adapted from http://alfaacoustics.com/sound-absorption-coefficient/

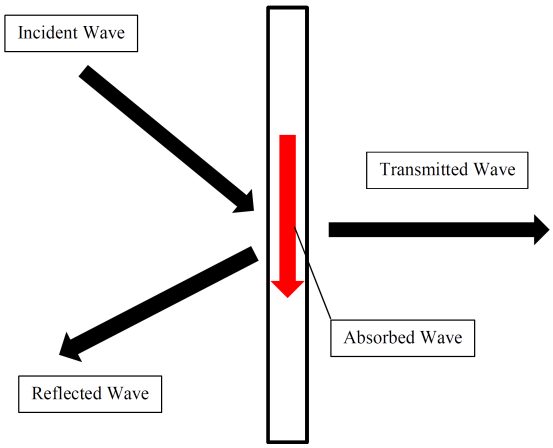

Figure 4 – Sound transmission through a material.
Reference: adapted from http://alfaacoustics.com/sound-transmission-loss/

The sound transmission loss (TL) is expressed in decibel scale and is given by (RAICHEL, 2006):

$$TL = 10log_{10}\left(\frac{1}{\tau}\right). \tag{2.5}$$

Considering an idealized system, which is represented by a mass per unit area (m) plate, mounted on an elastic suspension with stiffness (s) and damping coefficient (r)[1] per unit area as in Fig. 5, the sound transmission loss is studied considering a normal incidence sound wave. This idealized system is an approximate representation of a large panel. The assumption is that the panel is uniform, unbounded and non-flexible (FAHY; GARDONIO, 2007).

[1] Symbol r is only valid for Fig. 5, to maintain the original author's notation.

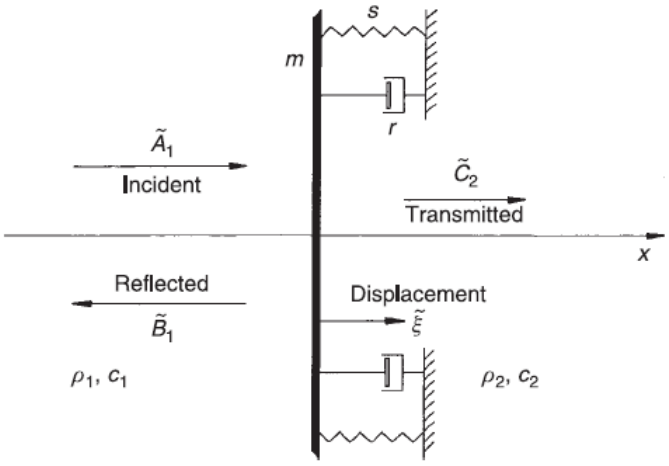

Figure 5 – Idealized panel.
Reference: Fahy and Gardonio (2007)

The incident pressure (p_i)and the reflected pressure (p_r) in the region of $x < 0$ are given by:

$$p_i = A_1 e^{j(\omega t - kx)}, \tag{2.6}$$

$$p_r = B_1 e^{j(\omega t + kx)}, \tag{2.7}$$

where A_1 and B_1 are complex amplitudes, ω is the angular frequency and $k = \omega/c$ is the wavenumber.

As a consequence of the plate displacement (ζ), a radiated sound pressure field is generated. This implies that two other radiated pressure fields are created, one for the region of $x > 0$ and another for $x < 0$.

$$p^-_{rad} = C_1 e^{j(\omega t + kx)}, \tag{2.8}$$

$$p^+_{rad} = C_2 e^{j(\omega t - kx)}, \tag{2.9}$$

Considering that the fluid in both sides of the plate is air, A_1, B_1, C_1 and C_2 are related to the plate displacement (ζ) by:

$$A_1 + B_1 = j\omega\rho_0 c\zeta, \tag{2.10}$$

$$C_1 = -j\omega\rho_0 c\zeta, \tag{2.11}$$

$$C_2 = j\omega\rho_0 c\zeta, \tag{2.12}$$

The sound pressure field before the plate $p(x = 0^-,t)$ and after the plate $p(x = 0^+,t)$, can be described as sum of the individual components in $x < 0$ and $x > 0$:

$$p(x = 0^-,t) = p_i + p_r + p^-_{rad}, \tag{2.13}$$

$$p(x = 0^-,t) = p^+_{rad}. \tag{2.14}$$

Also, the plate equation of motion is described by:

$$m\ddot{\zeta} + r\dot{\zeta} + s\zeta = p(x = 0^-,t) - p(x = 0^+,t), \tag{2.15}$$

By substituting Eqs. 2.13 and 2.14 in Eq. 2.15 and using the relations stated in Eqs. 2.10, 2.12 and 2.11 it is possible to find that the complex amplitude A_1 and the complex amplitude C_2 are related by (FAHY; GARDONIO, 2007):

$$C_2 = \frac{2A_1}{j(\omega m - s/\omega)\rho_0 c + (r/\rho_0 c + 2)}. \tag{2.16}$$

As the transmission coefficient is defined by the transmitted to incident sound powers, it is given by:

$$\tau = \frac{|C_2|^2/\rho_0 c}{|A_1|^2/\rho_0 c} = \frac{4}{(\omega m - s/\omega)^2 + (\omega_0 m\eta/\rho_0 c + 2)^2}, \tag{2.17}$$

where ω_0 is the natural frequency of an unbounded plate ($\omega_0 = \sqrt{s/m}$) and η_s is the loss factor, which is related to damping by the expression $\eta_s = r/(\omega_0 m)$.

Stiffness controls the TL at lower frequencies. In the frequency region near to the resonance frequency of the system, the plate presents higher amplitudes and consequently TL is decreased (RAICHEL, 2006). Considering ω_0 it is possible to describe three different situations.

First, the situation where the frequency is below ω_0 ($\omega << \omega_0$). The Eq. 2.17 can be approximated in this case to:

$$\tau = (2\rho_0 c\omega/s)^2, \tag{2.18}$$

considering that η_s is normally much less than a unit and that the ratios $(s/\omega)\rho_0 c$ and $(m\omega_0)/\rho_0 c$ are not greater than one for air.

In this case, transmission loss is only dependent on elastic stiffness and insensitive to mass and damping, so TL, using Eq. 2.5 is given by:

$$TL = 20log_{10}(s) - 20log_{10}(f) - 20log_{10}(4\pi\rho_0 c), \tag{2.19}$$

where f is the frequency in Hertz.

Second, at the region where the frequency $\omega = \omega_0$, τ (Eq. 2.17) can be approximated to:

$$\tau = (2\rho_0 c/\eta_s \omega_0 m)^2, \tag{2.20}$$

considering that $\eta_s >> \rho_0 c/\omega m$, which leads to this expression for TL:

$$TL = 20log_{10}(m) + 20log_{10}(\omega_0/2\pi) + 20log_{10}(\eta_s) - 20log_{10}(\rho_0 c/\pi). \tag{2.21}$$

Third, when $\omega >> \omega_0$, sound transmission coefficient (Eq. 2.17) is approximated to:

$$\tau = (2\rho_0 c/\omega m)^2, \tag{2.22}$$

considering that $\eta_s < 1$ and $\omega m/\rho_0 c << 1$ for air.

This case is known as the mass control region, where stiffness and damping are neglected and the TL can be given by the expression (FAHY; GARDONIO, 2007):

$$TL = 20log_{10}(m) + 20log_{10}(f) - 20log_{10}(\rho_0 c/\pi). \tag{2.23}$$

The example of sound transmission in a partition is important to understand the phenomenon of transmission loss. However, for the case of a porous material, the calculation of the TL is computed in a different way. One model to the prediction of transmission loss regarding the material thickness and the flow resistivity can be used (BIES; HANSEN, 2003). According to this model, TL varies with frequency, and, in this case, three ranges are defined: low, middle and high frequency (BIES; HANSEN, 2003). The range is determined as a function of the thickness of the material, as can be seen at Fig. 6.

For Fig. 6, λ_m is the sound wavelength in the porous material (regarding the different wave velocity between fluid media and the porous media); the flow resistivity is represented by R_1; the thickness of the material by l; and ρ is the air density.

For the low frequency range, the wavelength is large compared to the porous structure, so the structure vibrates at the same speed as the particle velocity of the sound wave

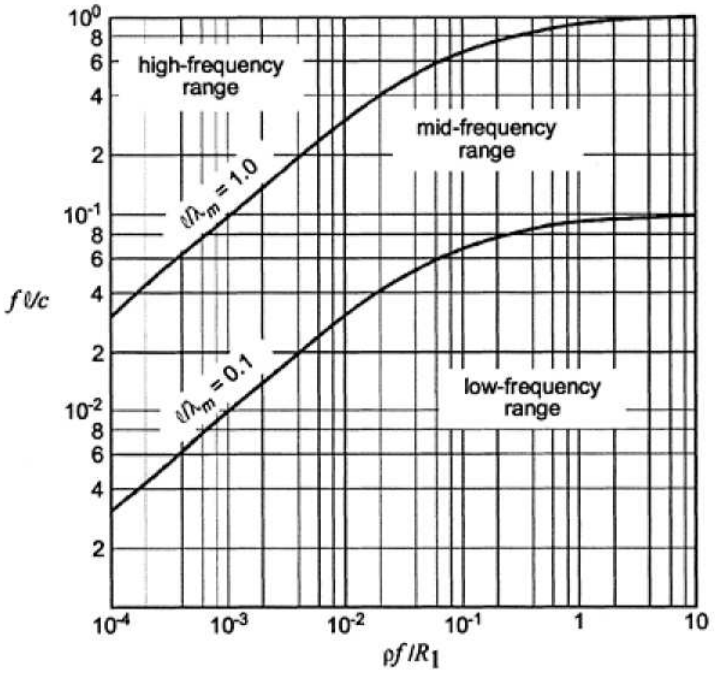

Figure 6 – Limits of low and high-frequency models when estimating the transmission loss through a porous layer.
Reference: Bies and Hansen (2003)

passing through it. However, for the high frequency range, the porous material has a thickness corresponding to some wavelengths and the reflections on both surfaces and losses through the material should be also considered.

For the prediction of TL, in the low frequency range, the plot showed in Fig. 7 can be used. It defines transmission loss as a function of the frequency, thickness, air density, flow resistivity, sound speed and the density of the material (ρ_B), which considers the void part in the material (Bulk Density). Additionally, for the prediction of TL at high frequencies, the chart in Fig. 8 can be used, where TL is given in function of the frequency, the flow resistivity and the air density [2]. For middle frequencies, the TL is calculated interpolating the values for low and high frequencies (BIES; HANSEN, 2003).

To compare experimental values of TL with the prediction model described above it would be necessary the knowledge of the material flow resistivity (σ) and the wavelength in the material (λ_m), considering the heterogeneities introduced by the double porosity, discussed later in this chapter.

2.3 Porous materials

In porous materials, the sound absorption occurs in the interconnected pores by viscous and thermal losses. The viscous part is due to the friction between air and pore walls while

[2] Symbols λ_m, R_1, l and ρ are only valid for Figs. 6, 7 and 8, to maintain original authors notation.

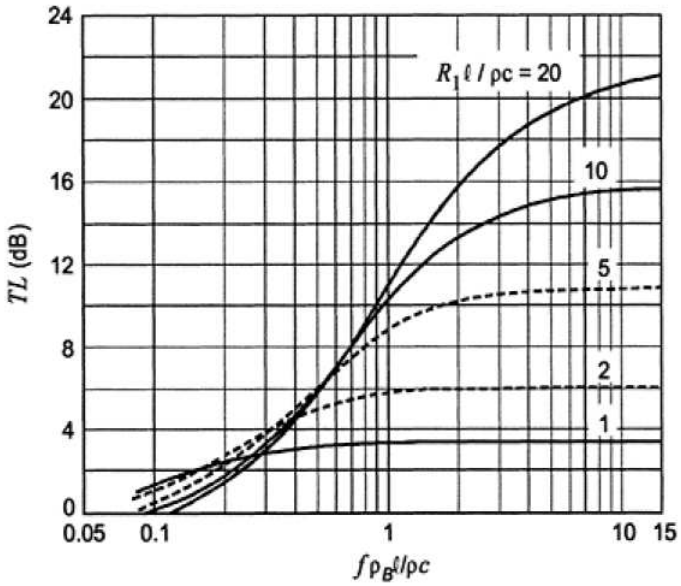

Figure 7 – Transmission loss for low frequency range of a porous material.
Reference: Bies and Hansen (2003)

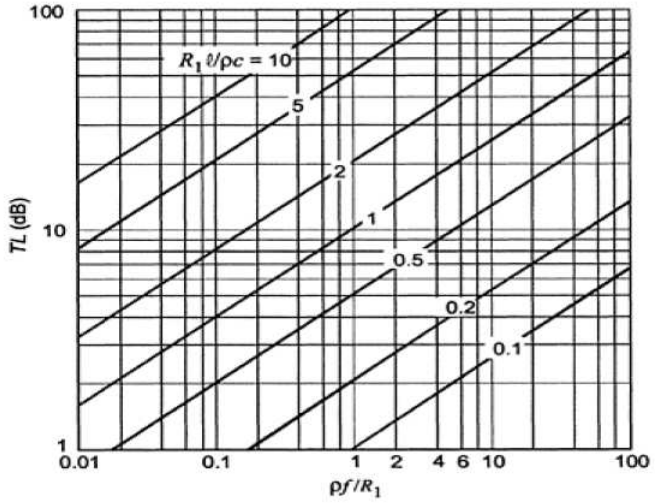

Figure 8 – Transmission loss for high frequency range of a porous material.
Reference: Bies and Hansen (2003)

the thermal part is caused by thermal conduction in the same interaction. For the occurrence of these two types of energy losses, it is necessary that the material presents an open cell structure that provides a proper air flow inside the material (COX; D'ANTONIO, 2009).

The material thickness influences the sound absorption. In the case of porous material which are rigidly backed, insignificant absorption occurs at the surface of the rigid wall because at this position the particle velocity is null. In this case, significant absorption is obtained with a porous material thickness of a quarter of the wavelength, where particle velocity is maximum. This is why for low frequencies it is necessary larger thickness of the porous materials or the use of an air cavity between the material and the rigid wall (BIES; HANSEN, 2003).

2.3.1 Mineral wools

Porous materials for acoustical purposes often used are mineral wools. They are made of sand and basaltic rock. Their sound absorption depend on the fiber diameter, density, fiber orientation and the nature of the binder. They are often sold in panels and they are anisotropic. However, for the sake of simplicity, anisotropy is ignored in most prediction models and they are developed not depending on the direction of propagation (COX; D'ANTONIO, 2009).

The chemical composition of mineral wools, as rockwool and glasswool are slightly different. Rockwool is mainly made of aluminium and silicion oxides. However, compared to glasswool, it has a higher alkaline earth content of MgO and CaO and a lower alkaline metal content of Na_2O and K_2O (WILLIAMS; MCCLURE, 1994). Table 2 shows the percentage quantity of each chemical component for rockwool and glaswool (HUMANS, 1988).

The production of rockwool and glasswool is made in a centrifugal or rotary process, which lead to a nominal fiber diameter of $3-7\mu m$ for rockwool and a $3-15\mu m$ fiber diameter for glasswool (WILLIAMS; MCCLURE, 1994).

Table 2 – Chemical composition of mineral wools.

Component	Material	
	Glasswool	Rockwool
SiO_2	73%	53%
Al_2O_3	2%	7%
CaO	5.5%	31%
MgO	3.5%	0%
Na_2O	16%	3%
K_2O	0%	2%
Others	0%	4%

Reference: adapted from IARC (1988)

2.4 Properties of porous materials

Some physical parameters are needed to describe a porous material, especially for models used for sound absorption and sound transmission loss prediction. The most important ones are porosity and flow resistivity, and they are the basis for the simplest models (COX; D'ANTONIO, 2009). Also, the pore shapes influences the sound absorption. Different pore shapes give different surface areas and influence the thermal and viscous losses. These losses could be represented by tortuosity and characteristic lengths (COX; D'ANTONIO, 2009). For the case of sound absorption prediction models, the higher the complexity of pore profile, more parameters are needed to describe sound absorption. The models utilized to predict sound absorption according to the pore complexity are described in Fig. 9. However, it is difficult to

directly measure all the physical parameters necessary for more detailed models. In this case, simpler models, with less parameters, can be used for an estimation of sound absorption.

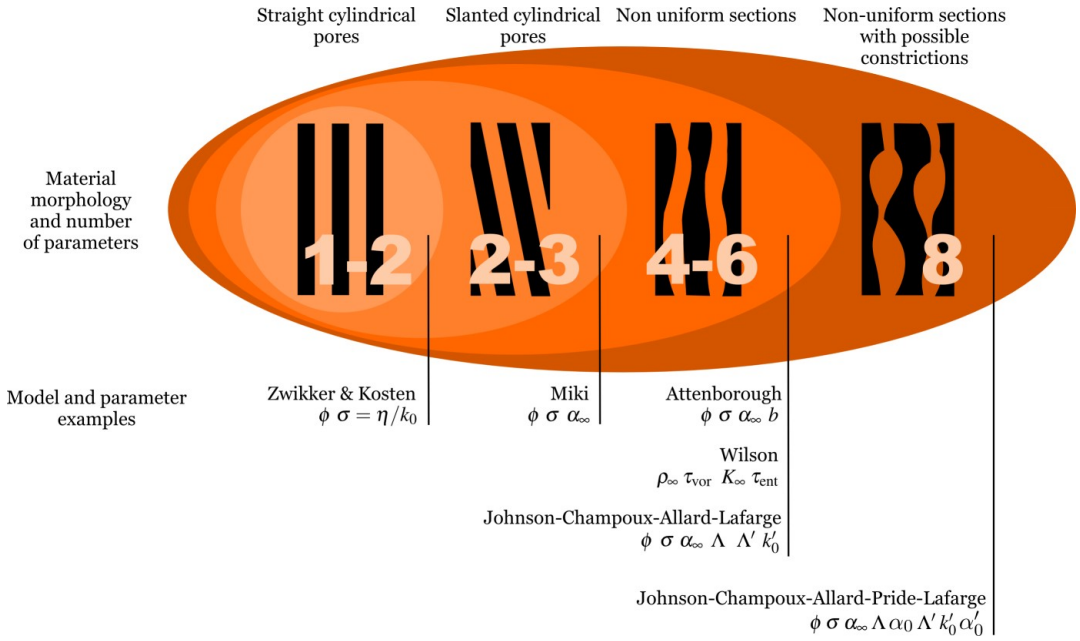

Figure 9 – Models and parameters according to pore section complexity.
Reference: Jaouen (2018)

The double porosity analytical model studied in this work was based on the parameters of Johnson-Champoux-Allard-Lafarge single porosity model. The physical parameters of this model are discussed in the next sections.

2.4.1 Porosity

Porosity (ϕ) is the ratio of the pore volume (V_p) to the total volume of the porous material (V_t):

$$\phi = \frac{V_p}{V_t}. \tag{2.24}$$

Closed pores are not accounted for the porosity because they do not influence the sound absorption (COX; D'ANTONIO, 2009), so this parameter is also known as open porosity or connected porosity (ALLARD; ATALLA, 2009).

2.4.2 Air flow resistivity

Air flow resistivity (σ) expresses the resistance of the air flow through the porous material structure. It is defined as the ratio of the pressure drop (ΔP) to the normal air flow

velocity (U) and the thickness (e), considering that the material is submitted to a steady flow, i.e.,

$$\sigma = \frac{\Delta P}{Ue}, \tag{2.25}$$

and this is only valid for small flow velocities.

In this study, the term flow resistivity always refers to air flow resistivity. For typical acoustical materials, the values of flow resistivity lie in the range of 10^3 to 10^6 Ns/m^4 (JAOUEN, 2018).

2.4.3 Tortuosity

Tortuosity (α_∞) is the parameter that describes the orientation of the pores compared to the incident sound wave, and is one of the parameters used to describe the complexity of the path for the sound wave at the material pores (COX; D'ANTONIO, 2009) (ALLARD; ATALLA, 2009). It relates the effective density (ρ_{eff}) to the nonviscous fluid density ρ_0 when it when it saturates a porous frame, i.e.,

$$\rho_{eff} = \alpha_\infty \rho_0. \tag{2.26}$$

This effect of density increasing can be explained considering the macroscopic and microscopic velocities of the flow. Considering the microscopic velocity (υ_m) of a nonviscous fluid at a material M, the macroscopic velocity ($\upsilon(M_0)$) at a point M_0 is obtained by averaging ($< . >$) over a representative volume V around (M_0) (ALLARD; ATALLA, 2009):

$$\upsilon(M_0) =< \upsilon_m(M) >_V . \tag{2.27}$$

Tortuosity is defined as:

$$\alpha_\infty = \frac{< \upsilon_m^2(M) >_V}{\upsilon(M_0)^2}. \tag{2.28}$$

If the macroscopic velocity is analyzed, it is necessary to consider a fluid of density $\alpha_\infty \rho_0$ instead of the nonviscous fluid density ρ_0, because of the interaction between the fluid and the porous frame (ALLARD; ATALLA, 2009). For the evaluation of tortuosity, using Eq. 2.28, it is considered the value of microscopic velocity (υ_m) for high frequencies, i.e, α_∞ is defined as the high frequency limit of the dynamic tortuosity.

For a typical acoustical material, the values of tortuosity lie between approximately 1 to 3, depending on the pores complexity (BOUTIN; GEINDREAU, 2008). The lowest value 1, for example, can corresponds to cylindrical pores with central axis parallel to the velocity field (JAOUEN, 2018).

2.4.4 Characteristic lengths

The viscous characteristic length Λ is the weighted ratio of the volume to the surface area of the pores. It is weighted by the square of the microscopic velocity and represents viscous losses:

$$\Lambda = \frac{1}{2}\frac{\int_V \upsilon_i^2(r)dV}{\int_A \upsilon_i^2(r_w)dA}, \tag{2.29}$$

where $\upsilon_i(r_w)$is the velocity of the fluid at the pore surface, $\upsilon_i(r)$ is the velocity inside the pore and V and A are representative pore volume and area, respectively (ALLARD; ATALLA, 2009).

For more complex pore shapes, a second characteristic length is also needed: Λ'. This one represents thermal losses and it is defined as half of the ratio of the pore volume to the pore area. Using A and V as representatives volumes and areas, Λ' is given by:

$$\Lambda' = \frac{1}{2}\frac{V}{A}. \tag{2.30}$$

For the simplest case, identical cylindrical pores, these two characteristic lengths have the same value (ALLARD; ATALLA, 2009). The ratio between Λ and Λ' indicates something about the pores shapes. In the case where $\Lambda < \Lambda'$, the connection between pores are small and narrow. Because Λ is influenced by the contributions of areas with large velocity amplitudes, the value of the velocity at the pore surface becomes higher, which occurs in the narrow connections (VIGRAN, 2008).

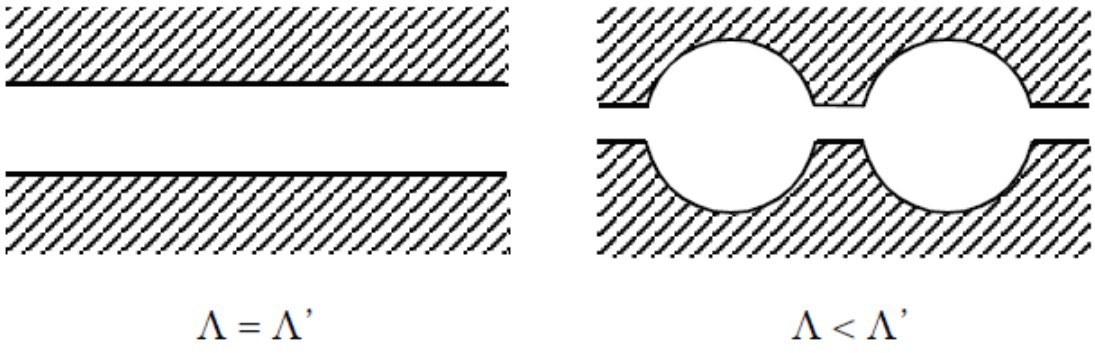

Figure 10 – Relationship between characteristic lengths values according to the pore shape.
Reference: Vigran (2008)

Both characteristic lengths are geometrical parameters, as can be seen by their definitions at Eq. 2.29 and 2.30, so their unit is expressed in meters (m).

2.4.5 Static thermal permeability

The static thermal permeability (Θ_0) is a parameter introduced by Lafarge *et al.* (1997) to enhance the description of thermal effects at low frequencies for models of sound

absorption. It is the limit of the dynamic thermal permeability when the frequency tends to zero. At low frequencies, the thermal boundary layer is of the same order of magnitude of the characteristic size of the pores, so the static thermal permeability helps to described losses related to thermal effects (JAOUEN, 2018).

The dynamic thermal permeability $\Theta(\omega)$ is a parameter that relates the pressure time derivative to the mean temperature inside the pore (T) by the expression (ALLARD; ATALLA, 2009):

$$\phi T = \frac{\Theta(\omega)}{\kappa} \frac{\partial p}{\partial t}, \tag{2.31}$$

where κ is the air thermal conductivity.

Then, the static thermal permeability (Θ_0) is given by (LAFARGE *et al.*, 1997):

$$\lim_{\omega \to 0} \Theta(\omega) = \Theta_0. \tag{2.32}$$

This parameter is a geometrical parameter, which has the unit of area (m^2). Values of static thermal permeability varies from 10^{-10} to 10^{-8} m^2 (JAOUEN, 2018).

2.5 Double porosity materials

As mentioned in Chapter 1.1, a material that has two interconnected pore networks is considered a double porosity material (OLNY; BOUTIN, 2003). Double porosity materials can be manufactured or can be a natural state. Perforations can be done in porous materials in order to create another pore network, or double porosity can be found naturally in materials, as the granular ones (COX; D'ANTONIO, 2009) (ATALLA *et al.*, 2001). The grains that form the material have pores between each one and also the grain itself is perforated. Figures 11a and 11b shows two types of double porosity material. Also, double porosity materials can be made by using elastic or poroelastic inclusions in a matrix material (SGARD *et al.*, 2005).

2.5.1 Physical aspects of double porosity materials

In the study of Olny and Boutin (2003), the physical parameters of a double porosity material and the physical model of sound propagation in a double porosity medium using the homogenization technique are described. The homogenization method is only valid for periodic structures and is used to describe the sound absorption in porous materials using the idea of representing the sound propagation in an equivalent fluid with an effective density (ρ_{eff}) and bulk modulus (ALLARD; ATALLA, 2009) which are functions of the physical parameters of the porous materials, described in Sec.2.4. This technique is valid under rigid frame assumption.

When dealing with double porosity material, two types of porosity are defined:

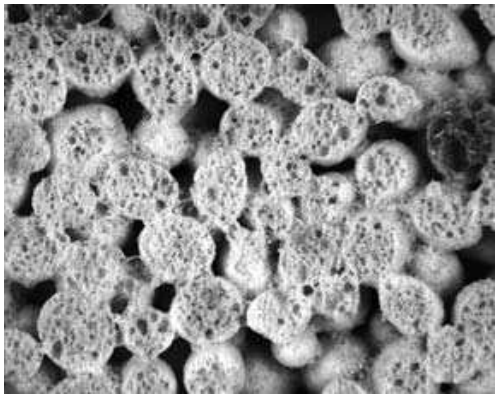

(a) Inorganic foam

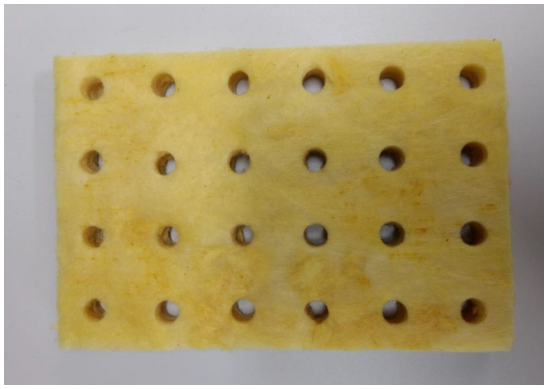

(b) Perforated glasswool

Figure 11 – Double porosity materials.
Reference: (a) Cox and D'Antonio (2009) and (b) author

- Mesoporosity (ϕ_p): defined as the ratio between the volume of the mesopores (larger pores) to the volume of the entire material;
- Microporosity (ϕ_m): defined as the ratio of the volume of micropores (smaller pores) to volume of the entire material, excluding the mesopores volume.

In this context, the porosity of the actual porous medium is given by (OLNY; BOUTIN, 2003):

$$\phi = \phi_p + (1 - \phi_p)\phi_m. \tag{2.33}$$

The general scheme of a double porosity material and the three geometric domains: macroscopic, mesoscopic and microscopic is described in Fig. 12, which is a generic representation of all types of double porosity materials. The two characteristic sizes of this type of material are l_p (mesoscopic) and l_m (microscopic). They represent one characteristic cell, which are representative volumes of one mesopore and one micropore, respectively. Also, the macroscopic size (L) is an elementary dimension representing a volume of the material containing a representative quantity of heterogeneities. However, L is frequency dependent, which is a result that come from single porosity wave propagation: it has to be smaller than the smallest wavelength of the frequency range of interest. Finally, the proper separation of scales between the three scales is given by the ratios ε and ε_0:

$$\varepsilon = \frac{l_p}{L}, \tag{2.34}$$

$$\varepsilon_0 = \frac{l_m}{l_p}. \tag{2.35}$$

To guarantee the condition for the homogenization technique, ε and ε_0 need to be much smaller than 1. The characteristic size of the phenomenon needs to be larger than the respective largest heterogeneities (OLNY; BOUTIN, 2003).

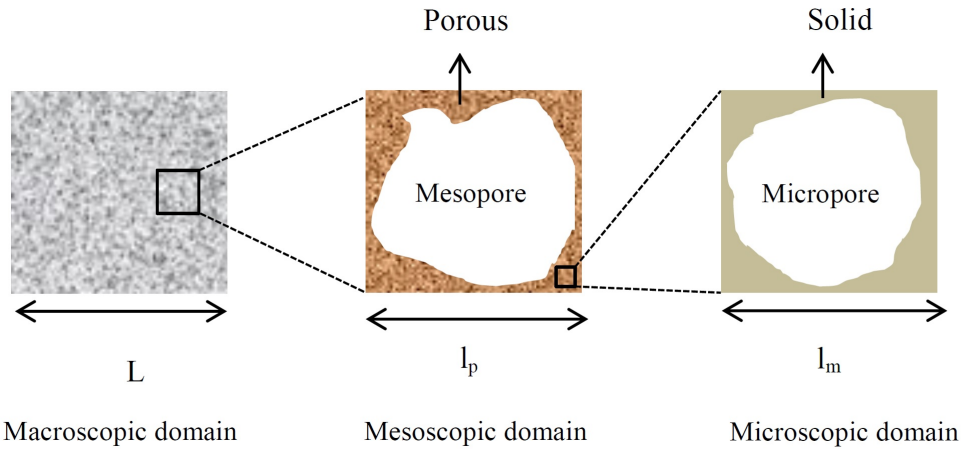

Figure 12 – Geometric scales at a generic double porosity material.
Reference: adapted from Olny and Boutin (2003)

Based on these facts, the development of a realistic double porosity material uses the proposed values: $l_p < 10^{-2}\ m$, to achieve the condition $\varepsilon << 1$ in the audible frequency range where the smaller wavelenghts are of the order of $10^{-2}\ m$; and $l_m \geq 10^{-5}\ m$, because the microporous medium should be pervious to acoustic waves.

Olny and Boutin (2003) studied two different situations: the low permeability contrast situation, where the ratio between l_p and l_m are low ($l_p = 10^{-3}\ m$ and $l_m = 10^{-4}\ m$); and the high permeability contrast situation, where the ratio between l_p and l_m are low ($l_p = 10^{-2}\ m$ and $l_m = 10^{-5}\ m$).

Considering that the wavelength of the sound wave in a double porosity material is different in the mesopores (λ_p) and in the micropores (λ_m), it is possible to define two viscous characteristics frequencies: ω_{vm}, for the micropores and ω_{vp}, for the mesopores. Additionally, the models of sound propagation for low and high frequencies present a different behavior and are represented by different expressions. In the work of Olny and Boutin (2003), values of the wavelengths were determinate for the two geometric domains, considering the behavior for low and high frequencies, and the range where it is not possible to use the homogenization theory, since the conditions of Eqs. 2.34 and 2.35 are not fulfilled. If the values of the wavelengths in the mesopores and in the micropores are plotted as a function of frequency, the intersection between the curves of the wavelengths in the mesopores for low and high frequencies cases defines ω_{vp}; and the intersection between the curves of mesopores wavelength and micropores wavelength defines ω_{vm} (OLNY; BOUTIN, 2003). Further details of the used models to calculate the wavelengths for low and high frequencies are presented in the study of Olny and Boutin (2003).

The interpretation of these characteristic frequencies is to divide the frequency range in cases with different physical behaviors, where the flows can be inertial (predominance of inertial effects) or can be viscous, (predominance of viscous effects). These cases are (OLNY; BOUTIN, 2003):

- First, low frequencies ($\omega << \omega_{vp}$): the waves are diffuse in mesopores and micropores and the difference between λ_p and λ_m is given in function of the separation of scales ε_0;
- Second, middle frequencies ($\omega_{vp} < \omega < \omega_{vm}$): the flow is viscous in micropores and is inertial in mesopores and the ratio between λ_m and λ_p is inversely to the viscous skin depth;
- Third, high frequencies ($\omega >> \omega_{vm}$): the viscous boundary layer thickness is much smaller than the mesopores, so the flow is totally inertial in both domains (mesopores and micropores). In this case, the wavelengths λ_m and λ_p are of the same order of magnitude.

In the case of the high contrast permeability, another characteristic frequency between the values of ω_{vp} and ω_{vm} is introduced: ω_d, the diffusion frequency. In the frequency range where the homogenization theory applies, the wavelength in the micropores remains smaller than in the pores, but the microscopic wavelength λ_m is of the same order as l_p.

It is possible to analyze the behavior of sound propagation in the three geometric scales (microscopic, mesoscopic and macroscopic), using ω_d. ω_d separates two frequency ranges:

- Low frequencies ($\omega << \omega_d$): the sound pressure is uniform in mesoscopic scale;
- High frequencies ($\omega >> \omega_d$): the micropores do not contribute to the macroscopic behavior of sound pressure.

The sound pressure of pores and micropores are of the same order around ω_d. However, the sound pressure at the microporous domains and the sound pressure in the mesopores present a difference in phase, which leads to a different sound dissipation that does not exist in a single porosity media. This effect only happens for diffuse waves and is known as pressure diffusion effect (OLNY; BOUTIN, 2003) and is responsible for an increase in sound absorption in double porosity materials.

2.5.2 Influence of double porosity in the sound absorption

Due to the pressure diffusion effect, the sound absorption is increased in the double porosity materials with a high permeability contrast. Around the diffusion frequency ω_d is noticed a peak in sound absorption, compared to the single porosity case.

In double porosity materials, the parameters related to shape and distribution of the mesopores also influences on the sound absorption.

Atalla *et al.* (2001) studied the influence of the size of the mesopores, the value of mesoporosity and other parameters for the specific case of perforated porous materials. They developed a numerical 3D model for a rectangular semi-infinite waveguide with a double porosity material rigidly backed by the end of the waveguide. They validated their model by measurements using a Kundt Tube of two different thickness double porosity materials with one unit cell of $Lc = 0.085\ m$, mesopore with radius, $R = 0.016\ m$ and mesoporosity, $\phi_p = 11\%$, as observed in Fig. 13.

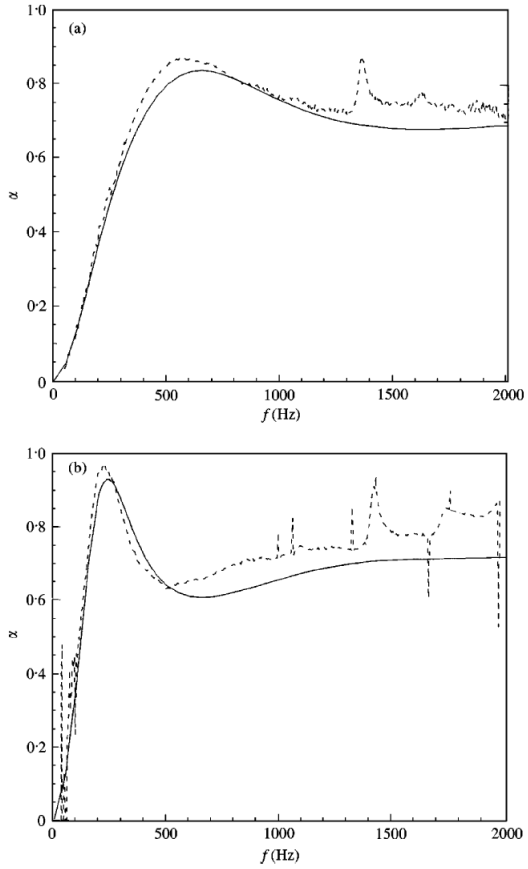

Figure 13 – Comparison between masurements (solid line) and numerical prediction (dashed line) for sound absorption of double porosity rockwoll with different thickness (e) (a) $e = 0.0575\ m$ and (b) $e = 0.115\ m$.
Reference: Atalla et al. (2001)

Additionally, using the numerical model, it was tested the influence of the hole size, the mesopores distribution, the value of mesoporosity and the influence of the flow resistivity

of the substrate material. The main results found in their study were:

- Testing one unit cell with a square hole of length of 0.0283 m and five different mesoporosities varying from ϕ_p = 0.04 to $\phi_p = 0.51$, the results showed that the peak of sound absorption increases until ϕ_p was increased from 0.04 until 0.18. For greater values this peak was damped;
- For the study of the influence of the size of the holes, the mesoporosity was kept constant at $\phi_p = 0.11$ and different hole size were tested: $a/4$, $a/2$, a and $2a$. The results showed that the position and the bandwidth of the peak increased with frequency, so the hole can be used to adjust the bandwidth;
- For the investigation of different mesopores distributions, it was tested some mesopores distributions concentrated on the center and some random distributions. For the centered distribution, results of absorption were better for low frequency and for random distributions the results of absorption presented better performance for high frequencies;
- The influence of flow resistivity was tested, calculating the sound absorption for five different values of flow resistivity. As the value of σ decreases, the frequency position of the peak increases, so for better results at low frequencies it is necessary a large flow resistivity.

Sgard *el al.* (2005) developed an analytical model for normal incidence sound absorption prediction based on the physical parameters of the double porosity material for the specific case of perforated porous materials with cells with mesopores placed on the cell center. Based on this models it is possible to define some practical rules for the design of a double porosity material. These models are explained in details in Section 2.5.3.

Gourdon and Seppi (2010) continued the experimental and analytical investigation of the influence of double porosity in sound absorption of porous material. In their study, they investigated the use of porous inclusion on the mesopores, i.e., a porous material with mesopores filled with another porous material. Their analytical model is based on the one developed by Sgard et al. (2005) and is valid for the same geometry of the samples. The motivation of using a porous inclusion was to obtain the pressure diffusion effect without losing performance in transmission loss, as the holes could decrease sound insulation when compared to the single porosity case.

To obtain good results at low frequencies, the two porous materials need to have very different values of flow resistivity. This is based on the result that a large flow resistivity leads to a gain of sound absorption at low frequencies, considering that the flow resistivity in a mesopore filled with air is almost zero. In this case, two characteristic lengths are introduced for the microporous domain, l_{m1} and l_{m2}, as in Fig. 14

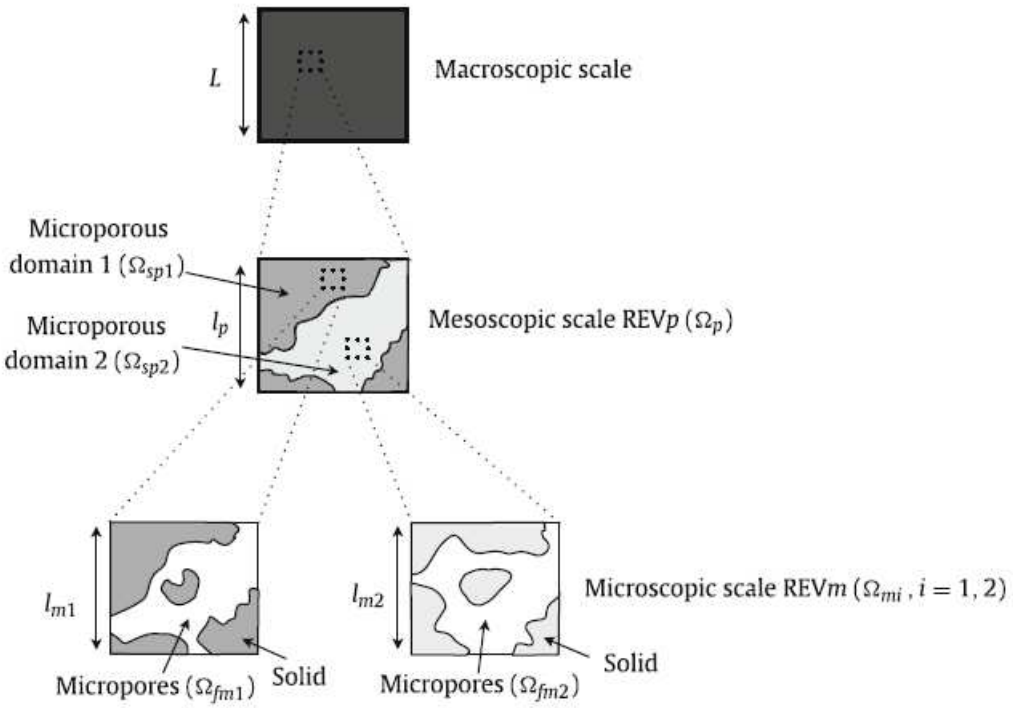

Figure 14 – Geometric scales in a generic double porosity material with porous inclusions.
Reference: Gourdon and Seppi (2010)

For the macroscopic, mesoscopic, and the two microporous domains, the proper separation of scales are given by:

$$\frac{l_p}{L} << 1; \tag{2.36}$$

$$\frac{l_{m1}}{l_p} << 1; \tag{2.37}$$

$$\frac{l_{m2}}{l_p} << 1. \tag{2.38}$$

The samples containing two porous materials were tested using three Kundt tubes, with the respective frequency ranges: Small (150 - 4300 Hz), Medium (150 - 2000 Hz) and Big (50 - 500 Hz). For the Small and the Medium tube, samples were tested with only one unit cell and for the Big Kundt Tube samples with 36 and 49 cells were tested (GOURDON; SEPPI, 2010).

They tested samples composed by melamine ($\sigma = 10000\ Ns/m^4$), u160 (a foam made of recycled materials), ($\sigma = 47700\ Ns/m^4$) and rockwool ($\sigma = 50000\ Ns/m^4$). Rockwool and u160 were used as frame materials and melamine to fill the perforations because of the contrast between the flow resistivity values. Also, in this study, the authors aimed to show that it is possible to obtain pressure diffusion effects with common materials, not only with the optimum conditions. They emphasized that the contrast of flow resistivity works in theory, but

in practice, this assumption is not robust, because of mounting conditions for the case where the mesopores were filled: the theoretical behavior does not work in the presence of a small air gap between the frame material and the material filling the mesopores (GOURDON; SEPPI, 2010).

The experimental results showed that the use of porous inclusions increased the sound absorption at low frequencies (400 - 600 *Hz*) compared with the use of double porosity with mesopores filled with air. In Fig. 15 this phenomena is observed for different mesoporosities configurations: A ($\phi_p = 0.056$), B ($\phi_p = 0.115$) and C ($\phi_p = 0.392$) at a test realized with the medium Kundt tube (GOURDON; SEPPI, 2010).

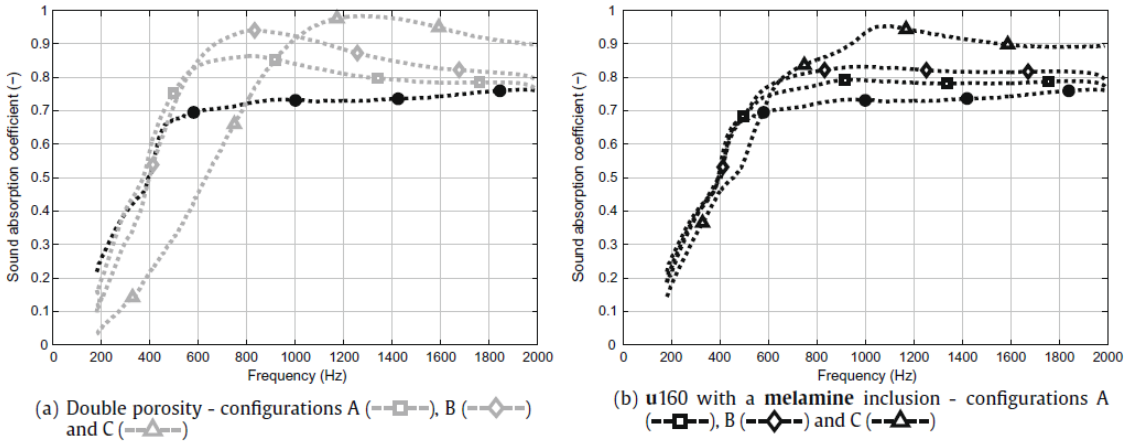

Figure 15 – Sound absorption for samples with mesopores not filled (a) and mesopores filled (b) for different configurations of mesoporosity compared to the single porosity case of u160 (—o—) for the Medium Kundt Tube.
Reference: Gourdon and Seppi (2010)

For the test with the Big Kundt Tube (50 - 500 *Hz*), is possible to observe the behavior for low frequencies specifically. Samples of rockwool frame and u160 frame were tested with inclusion of melamine and without inclusions. It was noted that for very low frequencies (50 - 200 *Hz*) the use of porous inclusion presented a better performance compared to single porosity case than the same samples without the use of inclusions compared to the single porosity case. In Fig. 16 this effect is showed for samples of u160 frame with 36 cells and $\phi_p = 0.360$ (GOURDON; SEPPI, 2010).

2.5.3 Analytical models for sound absorption of double porosity materials

In the study of Sgard *et al.* (2005), they developed an analytical model to predict the sound absorption in a double porosity material with mesopores not filled (filled with air) based on the expressions of sound propagation in double porosity media of previous works. Lately, Gourdon and Seppi (2010) developed an analytical model in a double porosity material with mesopores filled of another porous material, an adaptation of the model of Sgard *et al.* (2005). These models considered the incidence of plane waves in the material and calculate the surface impedance and sound absorption for the case when the material is rigidly backed. Also, they

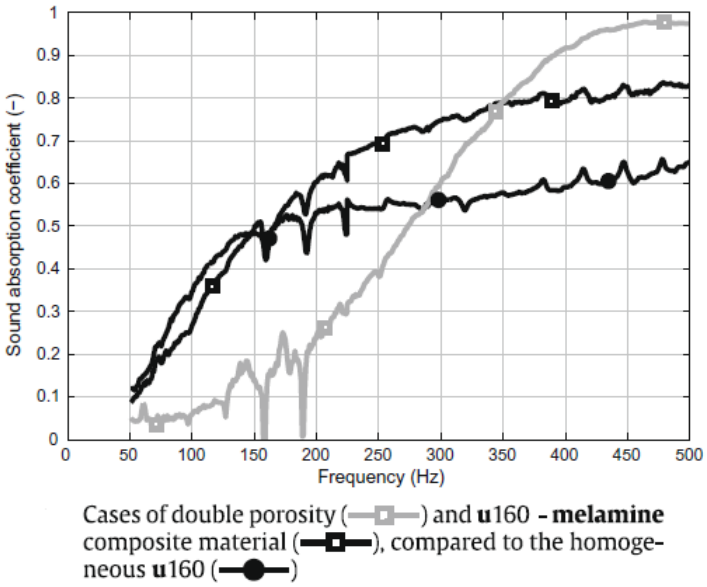

Figure 16 – Sound absorption for samples with mesopores not filled and mesopores filled compared to the single porosity case of u160 (—o—) for the Big Kundt Tube.
Reference: Gourdon and Seppi (2010)

considered that the medium is periodic, i.e., the mesopores are distributed periodically in the material: the material is divided in unit cells, which one containing one mesopore in its center.

Also, there is a model for double porosity sound absorption considering that the frame is deformable. It is based on the Biot theory of sound propagation for a single porosity material with a deformable frame, applied for the case of double porosity. It has the advantages of also representing the frame resonance effects on the values of sound absorption and of calculating sound absorption for the case where the material is not rigidly backed (DAZEL *et al.*, 2012). However, it has the disadvantage of using more physical parameters to calculated the surface impedance and sound absorption and using a more complicated mathematic formulation.

In this study, it was used only the models developed by Sgard *et al.* (2005) and Gourdon and Seppi (2010), which are based on the model of Johnson-Champoux-Allard-Lafarge, because of the ease of calculation and because they showed to be sufficient for the comparison with experimental data obtained by impedance tubes, where the sample is rigidly backed. These models, described in the next sections, were compared to the experimental data obtained.

2.5.3.1 Model for sound absorption of double porosity materials with mesopores not filled

For a double porosity material with mesopores not filled, the characteristic impedance (Z_c) and the wavenumber (k) are given by:

$$Z_c = \sqrt{\rho_{dp} K_{dp}}, \tag{2.39}$$

and

$$k = \omega\sqrt{\frac{\rho_{dp}}{K_{dp}}}, \tag{2.40}$$

respectively. K_{dp} is the dynamic Bulk modulus or compressibility modulus for the double porosity media, and ρ_{dp} the effective density in the case of double porosity media, given by:

$$\rho_{dp} = \frac{\eta}{j\omega\Pi_{dp}}, \tag{2.41}$$

where η is the air dynamic viscosity and Π_{dp} is the dynamic permeability of the double porosity media.

The surface impedance Z_{dp} of a double porosity material, with thickness e and backed by a material with impedance Z_s is given by (SGARD *et al.*, 2005):

$$Z_{dp} = Z_c\frac{Z_c - jZ_s cot(ke)}{Z_s - jZ_c cot(ke)}. \tag{2.42}$$

For the case of a rigid backing of just one layer of a double porosity material or another composite material, considering that Z_s is infinite (GOURDON; SEPPI, 2010), the Equation 2.42 is simplified, which leads to:

$$Z_{dp} = -jZ_c cot(ke). \tag{2.43}$$

Normal incidence absorption coefficient (α) is described by the equation:

$$\alpha = \frac{4\Re(z_{dp})}{(\Re(z_{dp})+1)^2\Im(z_{dp})^2}, \tag{2.44}$$

with $\Re$ and $\Im$, referring to the real and imaginary part of z_{dp}, which is the characteristic surface impedance, defined as:

$$z_{dp} = \frac{Z_{dp}}{\rho_0 c}, \tag{2.45}$$

where ρ_0 is air density and c the sound speed (SGARD *et al.*, 2005).

For the case of mesopores of circular cross section with constant radius R (circular cylindrical mesopores), Π_{dp}, the dynamic permeability of the double porosity media, is:

$$\Pi_{dp} = (1-\phi_p)\Pi_m + \Pi_p \tag{2.46}$$

with the index m corresponding to the microscopic scale and p to the mesoscopic scale.

Π_p is the dynamic permeability of a fictitious medium of the cylindrical pores replacing the microporous medium for an impervious medium and is calculated using Bessel functions of zero and first order, J_0 and J_1 (ZWIKKER; KOSTEN, 1949):

$$\Pi_p = \frac{\phi_p \delta_v^2}{j}\left(1 - \frac{2J_1(\mu\sqrt{-j})}{\mu\sqrt{-j}J_0(\mu\sqrt{-j})}\right), \tag{2.47}$$

where j is the imaginary unit, $\mu = R/\delta_v$ and δ_v is the viscous boundary layer thickness, given by:

$$\delta_v = \frac{\eta}{\rho_0 \omega}. \tag{2.48}$$

For the microporous medium, using the model of Johnson *et al.*, considering a single porosity medium, the dynamic permeability is

$$\Pi_m = \frac{\Pi_m(0)}{j\frac{\omega}{\omega_{vm}} + \sqrt{(1 + \frac{M}{2}\frac{\omega}{\omega_{vm}})}}, \tag{2.49}$$

where $\Pi_m(0)$ is the static permeability of a single porosity medium described as:

$$\Pi_m(0) = \frac{\eta}{\sigma_m}; \tag{2.50}$$

ω_{vm} is the viscous characteristic frequency of the microporous single porosity medium, given by (JOHNSON *et al.*, 1987):

$$\omega_{vm} = \frac{\sigma_m \phi_m}{\rho_0 \alpha_{\infty m}}; \tag{2.51}$$

and finally, dimensionless parameter M is defined as (SGARD *et al.*, 2005):

$$M = \frac{8\eta\alpha_\infty}{\sigma_m \phi_m \Lambda_m^2}. \tag{2.52}$$

According to Olny and Boutin (2003), the dynamic microscopic bulk modulus for a double porosity media is:

$$K_{dp} = \left[\frac{1}{K_p} + (1 - \phi_p)\frac{F_d(\omega\frac{P_0}{\phi_m K_m})}{K_m} \right]^{-1}. \tag{2.53}$$

K_p is the dynamic bulk moduli considering that the microporous part was substituted by an impervious material, where the mesopores constitutes the pores of a single porosity material. K_m could be calculated using Champoux or Lafarge's models.

The K_m of the Lafarge Model is given by:

$$K_m = \frac{\frac{\gamma P_0}{\phi_m}}{\gamma j(\gamma-1)\frac{\Theta_m}{\delta_t^2 \phi_m}}, \tag{2.54}$$

where P_0 is the static atmospheric pressure, γ is the ratio of the air specific heats (C_p/C_v), δ_t is the thermal boundary layer thickness, given by:

$$\delta_t = \sqrt{\frac{\kappa}{\rho_0 C_p \omega}}; \tag{2.55}$$

and Θ_m is the dynamic thermal permeability for microporous domain. This parameter is given by:

$$\Theta_m = \frac{\Theta_m(0)}{j\frac{\omega}{\omega_t} + \sqrt{1 + j\frac{M'}{2}\frac{\omega}{\omega_t}}}, \tag{2.56}$$

where $\Theta_m(0)$ is the static thermal permeability, obtained experimentally, ω_t is the thermal characteristic frequency, defined as

$$\omega_t = \frac{\kappa \phi_m}{\rho_0 C_p \Theta_m(0)}; \tag{2.57}$$

and M' is given by (LAFARGE *et al.*, 1997):

$$M' = \frac{8\Theta_m(0)}{\phi_m \Lambda_m'^2}. \tag{2.58}$$

The expression for K_p is obtained by Equation 2.54 changing index m for p, in all parameters, i.e., considering now the respective parameters of the mesoscopic media, so

$$K_p = \frac{\frac{\gamma P_0}{\phi_p}}{\gamma j(\gamma-1)\frac{\Theta_p}{\delta_t^2 \phi_p}}. \tag{2.59}$$

In this case,

$$\Theta_p = \frac{\phi_p \delta_t^2}{j}\left[\ 1 - \frac{2J_1(\mu\sqrt{-j})}{\mu\sqrt{-j}J_0(\mu\sqrt{-j})}\ \right]. \tag{2.60}$$

The frequency dependent function $F(\omega)$ was created to represent the ratio of the average pressure in the microporous domains to the pressure in the mesoscopic domain. This function is given by:

$$F(\omega) = 1 - j\frac{\omega}{\omega_d}\frac{D(\omega)}{D(0)} \tag{2.61}$$

where $D(\omega)$ is a function with similar properties with the function Θ_m, introduced by Lafarge et al (1997) and is given by

$$D(\omega) = \frac{D(0)}{j\frac{\omega}{\omega_d} + \sqrt{1 + j\frac{M_d}{2}\frac{\omega}{\omega_d}}}; \tag{2.62}$$

$D(0)$ is a geometric parameter related to the thermal permeability related to the size of one unit cell L_c, as in Fig. 17 and for a simple geometry, as a circular cross-section mesopore is given by:

$$D(0) = \frac{L_c}{4\pi}\left[\ ln(\tfrac{1}{\phi_p}) - \tfrac{3}{2} + 2\phi_p - \tfrac{\phi_p^2}{2}\ \right]; \tag{2.63}$$

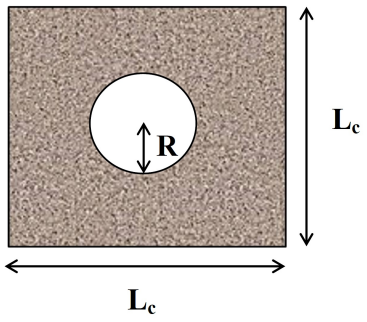

Figure 17 – Geometry of one unit cell using a circular cross section mesopore.
Reference: adapted from Sgard *et al.* (2005)

ω_d is the characteristic diffusion frequency, given by:

$$\omega_d = \frac{(1-\phi_p)P_0}{\phi_m \sigma_m D(0)}; \tag{2.64}$$

M_d is a shape factor, given by:

$$M_d = \frac{8}{\Lambda_d^2}\frac{D(0)}{1-\phi_p}, \tag{2.65}$$

with Λ_d representing a relationship between the surface area of the mesopore and the volume of microporous domain in one unit cell (SGARD *et al.*, 2005), i.e.,

$$\Lambda_d = \frac{2e(L_c^2 - \pi R^2)}{\pi Re + (L_c^2 - \pi R^2)}. \tag{2.66}$$

2.5.3.2 Model for sound absorption of double porosity materials with mesopores filled

Based on the model exposed in the previous subsection, a prediction model of sound absorption was developed by Gourdon and Seppi (2010) for the case where the mesopores are filled with another porous material. In this case, exists two microporous media.

The equations concerning the mesopore geometric parameters remain the same as shown in the previous case. The expressions concerning the microporous medium now consider the two types of porous materials. The previous knowledge of the physical parameters of each medium are necessary: σ_{mi}, ϕ_{mi}, $\alpha_{\infty mi}$, Λ_{mi}, Λ'_{mi} and $\Theta_{mi}(0)$ $(i = 1,2)$ for K_m calculation.

The expressions for the characteristic impedance Z_c, wavenumber k, effective density ρ_{dp}, surface impedance of the double porosity material Z_{dp}, characteristic surface impedance of the double porosity material z_{dp} and the expression for normal incidence sound absorption coefficient α remain the same as in Eqs. 2.39, 2.40, 2.41, 2.42, 2.43, 2.44.

The dynamic permeability is now given by the following expression, in function of the dynamic permeability of the two media (1 and 2):

$$\Pi_{dp} = (1 - \phi_p)\Pi_{m1} + \phi_p \Pi_{m2}. \tag{2.67}$$

The expressions of Π_{m1} and Π_{m2} are calculated using Eq. 2.49.

The macroscopic dynamic bulk modulus K_{dp} is given by (OLNY; BOUTIN, 2003):

$$K_{dp} = \left[\frac{\phi_p}{K_{m2}} + (1 - \phi_p)\frac{F_d(\omega)}{K_{m1}} \right]^{-1}, \tag{2.68}$$

where K_{m1} and K_{m2} are given by Eq. 2.54 (GOURDON; SEPPI, 2010).

For the case of mesopores filled, the diffusion frequency (ω_d) is calculated considering the physical parameters of medium 1, which is the frame material:

$$\omega_d = \frac{(1 - \phi_p)P_0}{\phi_{m1}\sigma_{m1}D(0)}. \tag{2.69}$$

The expressions for $F(\omega)$, $D(\omega)$, $D(0)$, M_d and Λ_d are given as functions of the mesopores geometry and the unit cell size, thus they remain the same as in Eqs. 2.61, 2.62, 2.63, 2.64 and 2.65, respectively.

Finally, for K_{m1} and K_{m2} it is necessary to calculate the dynamic thermal permeability for both media, Θ_{m1} and Θ_{m2} according to Equation 2.56 (GOURDON; SEPPI, 2010).

2.5.4 Influence of double porosity in the sound transmission loss

For the case of the transmission loss using double porosity material, there are few cases of study about transmission loss. Particularly, in the study of Sgard and Atalla (2001), a finite element model was developed to study the effects on transmission loss of a double porosity material inserted in an infinity rectangular waveguide. It was simulated the normal incidence transmission loss for a 37.5 *mm* thick and 100 *mm* wide square samples of a plastic foam with inclusions of polyestirene. The mesoporosity was 0.79 and four configurations were tested: one sample with single porosity; one sample with nine inclusions concentrated on the center; one sample with the nine inclusions equally distributed (creating 9 unit cells with one inclusion); and one sample with nine inclusions randomly distributed.

The results for sound transmission loss showed small gains only around 1000 *Hz* for all the samples with double porosity, although the different mesopores distribution, compared to the case of single porosity (ATALLA *et al.*, 2001). For the rest of the frequency range studied, the single porosity transmission loss is very similar to the curves of the double porosity samples.

In this study, the effect of double porosity is analyzed but for the case of porous material inclusions.

3 METHODOLOGY

In this study the materials of interest were characterized in terms of the acoustical parameters sound absorption and sound transmission loss by acoustic tests using impedance tubes. The physical parameters of porosity and tortuosity for single porosity rockwool and glasswool were determinated using X-ray microtomography (image method) and ultrasound measurements (acoustic method), respectively.

The materials used in this study to build the samples are glasswool panel, ISOVER manufacturer, nominal density of 20 kg/m^3 and rockwool panel, Rockfibras manufacturer, nominal density of 160 kg/m^3. The dimensions of both panels are 1200×600 mm and nominal thickness are $e = 25$ mm. The density difference between the two materials was chosen intentionally, because it was assumed that they could provide different flow resistivity values, a desired condition to build double porosity samples with porous inclusions (GOURDON; SEPPI, 2010).

3.1 Impedance tube tests

An alternative to perform the acoustic characterization of the materials is to test them using an impedance tube. The normal incidence absorption was measured by the proceedings established in ISO $10534-2:2001$, and the normal transmission loss by using the Transfer Matrix Method for an impedance tube (BOLTON *et al.*, 2007).

Different configurations are used for sound absorption and transmission loss tests when using an impedance tube. The impedance tube is divided into two parts: the first one contains the loudspeaker, and the second one is only a continuation of the tube. For absorption tests, it is used the first part of the tube and a sample holder is placed at the end. For sound transmission loss tests, both parts of the tube are used and the sample is placed at the beginning of the second tube.

Two different types of impedance tube were used in this study. One of circular cross-section and with a larger frequency range; and other with a rectangular cross-section and a narrower frequency range.

3.1.1 Sound absorption test using an impedance tube

For the sound absorption test, the proceedings of the ISO $10534-2:2001$ establishes the determination of the sound absorption of a sample by measuring the transfer functions between microphones and loudspeakers. It uses an impedance tube, two microphones, a loudspeaker and a digital frequency analyzer system. The sample is rigidly backed and located in a sample holder by the end of the tube and it is excited by plane sound waves coming from the

loudspeaker, located at the other end of the tube, as can be seen in Fig. 18. The decomposition of the interference field is calculated by measuring the sound pressure at both microphones at well-established positions (ISO10534-2, 2001).

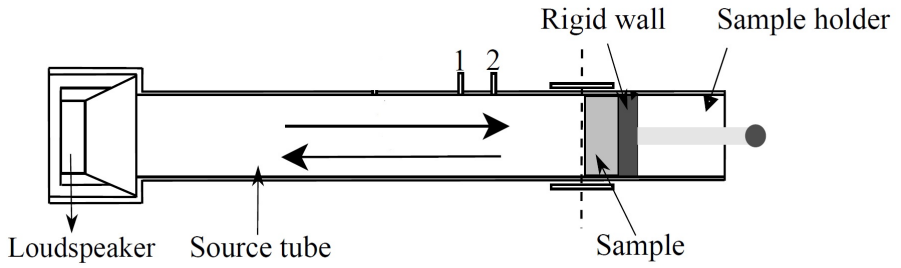

Figure 18 – Sound absorption test in a impedance tube.
Reference: Corredor-Bedoya (2016), adapted from Bolton (2007) and ISO 10534 – 2 : 2001

The measurement of the temperature of the room where the impedance tube is placed and the measurement of the transfer function between the two microphones and the loudspeaker enables to determine the sound absorption of the sample. First of all, the sound speed (c) is determined as a function of the temperature (T) in Celsius:

$$c = 343\sqrt{\frac{T}{293}}. \tag{3.1}$$

The wavenumber k is a function of c and the angular frequency, $\omega = 2\pi f$; and is given by:

$$k = \frac{\omega}{c}. \tag{3.2}$$

Considering the propagation of plane waves, the incident sound pressure is determined by a negative exponential (e^{-jkx}) and the reflected sound pressure is determined by a positive exponential (e^{jkx}), where x is the direction of propagation. The exponential complex function is used because it is the solution of the plane wave differential equation. Using the idea of the incident and the reflected field on the sample, it is possible to calculate the transfer functions between the microphones 1 and 2:

$$H_I = \frac{p_{2I}}{p_{1I}} = e^{-jk(x_1-x_2)} = e^{-jks}, \tag{3.3}$$

$$H_R = \frac{p_{2R}}{p_{1R}} = e^{jk(x_1-x_2)} = e^{jks}, \tag{3.4}$$

where H_I and H_R are the transfer functions between microphones 1 and 2 corresponding only to the incident and reflected waves, respectively; p_{1I} and p_{2I} are the sound pressures generated

by the incident wave at microphones 1 and 2, respectively; p_{1R} and p_{2R} are the sound pressures generated by the reflected wave at microphones 1 and 2, respectively; x_1 and x_2 are the positions of microphones 1 and 2; and s is the distance between microphones 1 and 2.

The transfer function, in terms of the sound reflection coefficient r, is given by:

$$H_{12} = \frac{p_2}{p_1} = \frac{e^{jkx_2} + re^{-jkx_2}}{e^{jkx_1} + re^{-jkx_1}}. \tag{3.5}$$

Isolating the variable r, it is possible to obtain (ISO10534-2, 2001):

$$r = \frac{H_{12} - H_I}{H_R - H_{12}} e^{2jkx_1}. \tag{3.6}$$

In this case, the incident wave is partially reflected and partially absorbed, so the sound absorption coefficient, α, is given by:

$$\alpha = 1 - |r|^2. \tag{3.7}$$

In the absorption test, α can be obtained by measuring the complex transfer function H_{12} using the signal recorded by the frequency digital analyzer system and by calculating H_I and H_r.

3.1.2 Transmission loss test using an impedance tube

The method for measuring the sound transmission loss uses four microphones positions and the two parts of the impedance tube with the sample at the beginning of the second tube. The Transfer Function method is used for the calculation of the sound transmission loss. This method is known as the four microphones method. Figure 19 shows the assemble of this test.

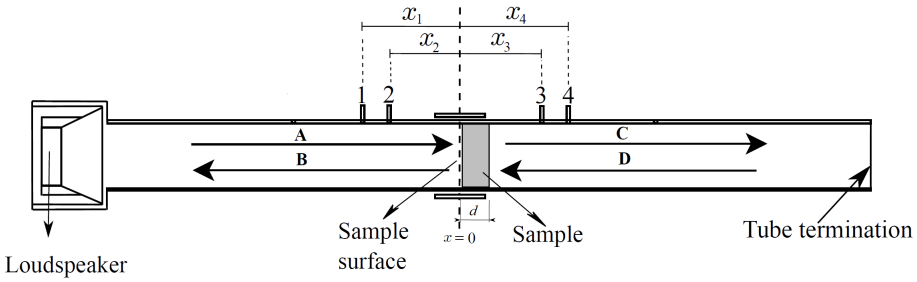

Figure 19 – Sound transmission loss test in a impedance tube.
Reference: Corredor-Bedoya (2016), adapted from Bolton (2007)

Considering plane waves propagation, the sound pressure field on the upstream and downstream of the sample is given as a function of positive and negative exponentials:

$$P_{up} = Ae^{-jkx} + Be^{jkx}, \tag{3.8}$$

$$P_{down} = Ce^{-jkx} + De^{jkx}, \tag{3.9}$$

where A, B, C, D are complex wave amplitudes. The signal of the exponential is related to the direction of propagation as in Eqs. 3.3 and 3.4.

Considering the position of the sample surface nearest to the loudspeaker as the referential origin of the problem ($x = 0$) and the position of the other sample surface ($x = d$), as in Fig. 19, the sound pressure and the particle velocity just before and just after the sample are given by:

$$P_{x_0} = A + B, \tag{3.10}$$

$$V_{x_0} = \frac{A - B}{\rho_0 c}, \tag{3.11}$$

$$P_{x_d} = Ce^{-jkd} + De^{jkd}, \tag{3.12}$$

$$V_{x_d} = \frac{Ce^{-jkd} - De^{jkd}}{\rho_0 c}. \tag{3.13}$$

In Eqs. 3.11 and 3.13, ρ_0 is dry-air density and is described as a function of temperature (T) and the atmospheric pressure (P_0) (ISO10534-2, 2001) according to

$$\rho_0 = 1.186 \frac{293 P_0}{101.325(T + 273.15)}. \tag{3.14}$$

The complex sound pressures at the four microphones locations are given by (BOLTON *et al.*, 2007):

$$P_1 = Ae^{-jkx_1} + Be^{jkx_1}, \tag{3.15}$$

$$P_2 = Ae^{-jkx_2} + Be^{jkx_2}, \tag{3.16}$$

$$P_3 = Ce^{-jkx_3} + De^{jkx_3}, \tag{3.17}$$

$$P_4 = Ce^{-jkx_4} + De^{jkx_4}. \tag{3.18}$$

The four complex pressure amplitudes can be described in terms of the measured microphones pressures:

$$A = \frac{j(P_1 e^{jkx_2} - P_2 e^{jkx_1})}{2sin(k(x_1 - x_2))}, \tag{3.19}$$

$$B = \frac{j(P_2 e^{-jkx_1} - P_1 e^{-jkx_2})}{2sin(k(x_1 - x_2))}, \tag{3.20}$$

$$C = \frac{j(P_3 e^{jkx_4} - P_4 e^{jkx_3})}{2sin(k(x_3 - x_4))}, \tag{3.21}$$

$$D = \frac{j(P_4 e^{-jkx_3} - P_3 e^{-jkx_4})}{2sin(k(x_3 - x_4))}. \tag{3.22}$$

Additionally, these equations can be written in terms of quantities that can be measured by the frequency analyzer: the complex transfer functions between the microphones with reference to the loudspeaker and the autospectrum of the loudspeaker. In this case, it is possible to obtain that:

$$A = \sqrt{Grr}\frac{j(H_{1r} e^{jkx_2} - H_{2r} e^{jkx_1})}{2sin(k(x_1 - x_2))}, \tag{3.23}$$

$$B = \sqrt{Grr}\frac{j(H_{2r} e^{-jkx_2} - H_{1r} e^{-jkx_1})}{2sin(k(x_1 - x_2))}, \tag{3.24}$$

$$C = \sqrt{Grr}\frac{j(H_{3r} e^{jkx_4} - H_{4r} e^{jkx_3})}{2sin(k(x_3 - x_4))}, \tag{3.25}$$

$$D = \sqrt{Grr}\frac{j(H_{4r} e^{-jkx_3} - H_{3r} e^{-jkx_4})}{2sin(k(x_3 - x_4))}, \tag{3.26}$$

where Grr is the loudspeaker autospectrum, H_{nr} is the transfer function of the microphone ($n = 1,2,3,4$) with reference of the loudspeaker (r), and x_n are the positions of the microphones ($n = 1,2,3,4$) .

The Transfer matrix method relates the sound pressure and the pressure particle velocity just before ($x = 0$) and just after ($x = d$) the sample (BOLTON *et al.*, 2007) according to

$$\begin{bmatrix} P \\ V \end{bmatrix}_{x=0} = \begin{bmatrix} T_{11} & T_{12} \\ T_{21} & T_{22} \end{bmatrix} \begin{bmatrix} P \\ V \end{bmatrix}_{x=d}. \tag{3.27}$$

The problem described above contains two equations and four unknown variables, leading to an undetermined system. If the sample is symmetrical, its sound transmission loss coefficient is the same for both sides of the sample. In the case of this study, all samples are symmetrical: the ones with macroperforations contains holes with a constant circular cross-section running through the thickness of the sample. In a case of symmetry, $T_{11} = T_{22}$ (BOLTON *et al.*, 2007). In addition, Equation 3.27 is valid for symmetrical systems and in this case:

$$T_{11}T_{22} - T_{12}T_{21} = 1. \tag{3.28}$$

The condition described in the Equation 3.28 is assumed in this work, although it could be tested experimentally for validation for the case of specific samples and materials.

The symmetry assumption gives two more equations for the system, so it becomes determined. Describing the unknown variables in function of the pressures and particle velocity, it is possible to obtain:

$$\begin{bmatrix} T_{11} & T_{12} \\ T_{21} & T_{22} \end{bmatrix} = \frac{1}{P_{x=0}V_{x=d} + P_{x=d}V_{x=0}} \begin{bmatrix} P_{x=d}V_{x=d} + P_{x=0}V_{x=0} & P_{x=d}^2 - P_{x=d}^2 \\ V_{x=d}^2 - V_{x=d}^2 & P_{x=d}V_{x=d} + P_{x=0}V_{x=0} \end{bmatrix}. \tag{3.29}$$

By the use of an anechoic termination at the end of the tube, it is considered that there are not reflection at the end of the tube, so the complex wave amplitude D is assumed to be zero. Matrix T can be described as a function of A, B, C and D by substituting Equations 3.10, 3.11, 3.12 and 3.13 in Equation 3.29. Also, the complex amplitudes A, B, C and D are described in terms of the loudspeaker autospectrum and the transfer function between the microphones and the loudspeaker. If these quantities are measured during experiments using a frequency analyzer, it is possible to determine the transfer function matrix.

The expression for the power transmission coefficient for normal incidence and an anechoically-terminated sample are found to be:

$$T_a = \frac{2e^{-jkd}}{T_{11} + \frac{T_{12}}{\rho_0 c} + \rho_0 c T_{21} + T_{22}}. \tag{3.30}$$

Finally, the normal transmission loss of the sample is given by (BOLTON *et al.*, 2007):

$$TL = 10log_{10}\left(\frac{1}{|T_a|^2}\right). \tag{3.31}$$

3.1.3 Impedance tube of circular cross section

The circular cross section impedance tube used in this work is a BSWA Tech impedance tube, model SW433. The tube is property of the Vibroacoustic Laboratory at the School of Mechanical Engineering at Unicamp and it was also used for researches about effects of air cavity backing porous materials in the impedance tube when using an indirect acoustical method (BANNWART *et al.*, 2016) and for acoustical characterization of materials, such as mortar and tire rubber composites (CORREDOR-BEDOYA, 2016).

The schematics of the impedance tube is shown in Fig. 20.

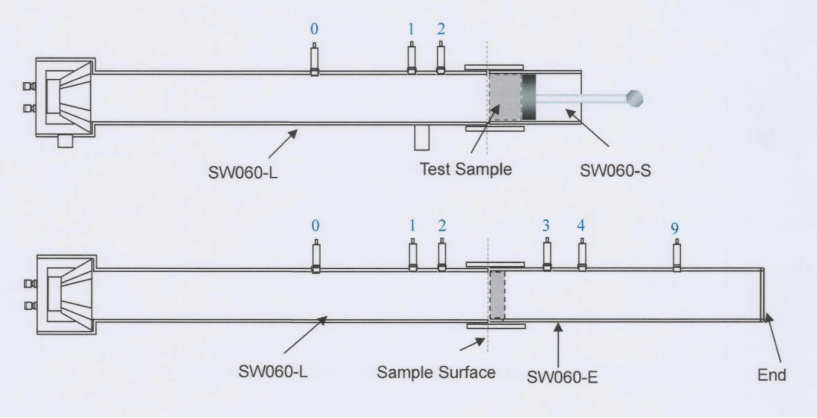

Figure 20 – Impedance tube scheme - absorption tests (above) and sound transmission loss tests (below).

Reference: BSWA Tech (2010)

This tube works in two different frequency ranges: 125 - 800 *Hz* and 400 - 2500 *Hz*. The frequency range depends on microphone positions. For sound absorption test positions 0 and 2 for 125 - 800 *Hz* and positions 1 and 2 for 400 - 2500 *Hz* are used. For sound transmission loss tests, positions 0, 2, 3, 9 for 125 - 800 *Hz* and positions 1, 2, 3, 4 for 400 - 2500 *Hz* are used.

The referential origin is at the sample surface nearest to microphone 2 or at the beginning of the second part of the tube.

For sound absorption tests, the position configuration of microphones and the sample are:

- Position of the microphone 0: 205 *mm*;

- Position of the microphone 1: 80 *mm*;
- Position of the microphone 2: 35 *mm*;
- Distance between microphones 0 and 2 (s): 170 *mm*;
- Distance between microphones 1 and 2 (s): 45 *mm*.

For sound transmission loss tests, the position configuration of microphones and the sample are:

- Position of the microphone 0: -205 *mm*;
- Position of the microphone 1: -80 *mm*;
- Position of the microphone 2: -35 *mm*;
- Position of the microphone 3: 100 *mm*;
- Position of the microphone 4: 135 *mm*;
- Position of the microphone 9: 270 *mm*.

3.1.4 Impedance tube of rectangular cross section

The rectangular cross section tube is used in this work for tests of larger samples than the ones compared with the circular tube. It works in the frequency range of 20 to 717 *Hz* (SIVIERO, 2011). The tube is made of medium-density fiberboard (MDF) with 25*mm* thickness and an its inner cross-section is 240 $\times$ 160 *mm*. The schematics for the sound absorption and transmission loss tests are presented in Fig. 21. This impedance tube was developed at the Vibroacoustic Laboratory at the School of Mechanical Engineering at Unicamp by Siviero (2011) for his doctoral research about hybrid acoustic control in souns transmission loss. For this study, a sample holder made also with MDF, was developed to perform sound absorption tests.

The referential origin is at the sample surface nearest to microphone 2 or at the beginning of the second part of the tube.

For sound absorption tests the position configuration of microphones and the sample are:

- Position of the microphone 1: 480 *mm*;
- Position of the microphone 2: 310 *mm*;
- Distance between microphones (s): 170 *mm*.

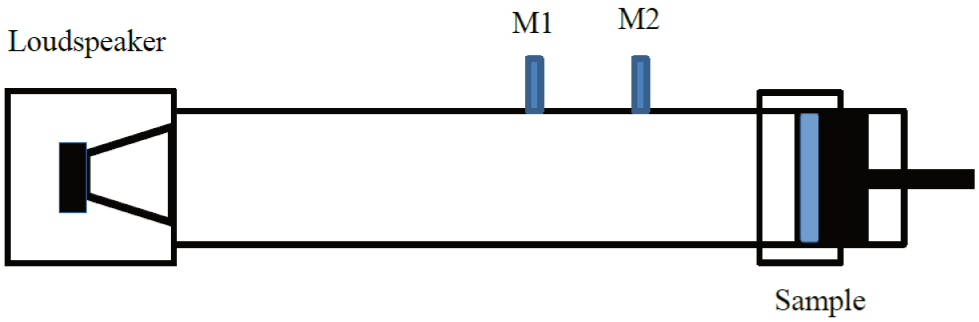

Figure 21 – Schematic of the Rectangular Impedance Tube - absorption tests - not scaled.
Reference: adapted from Siviero (2011)

3.1.5 Acoustical characterization data acquisition and instrumentation

For the tests using the two types of impedance tube, the frequency analyzer and signal generator LMS Scadas was utilized. In this equipment 32 input channels and two output channels are available. Also, for both tests, temperature was recorded using a digital termometer.

For the tests using the impedance tube of circular cross section, the following equipments with the respective work frequency range were used:

- Impedance tube: BSW 433 model, BSWA Tech manufacturer, 125 - 2500 *Hz*;
- Microphone: MPA 416 model, BSWA Tech manufacturer, 20 - 20000 *Hz* ;
- Loudspeaker: BSWA Tech manufacturer, 20 - 8000 *Hz* (BSWATECH, 2010);

The absorption and sound transmission loss test configurations using this tube can be observed at Figs. 22 and 23, respectively.

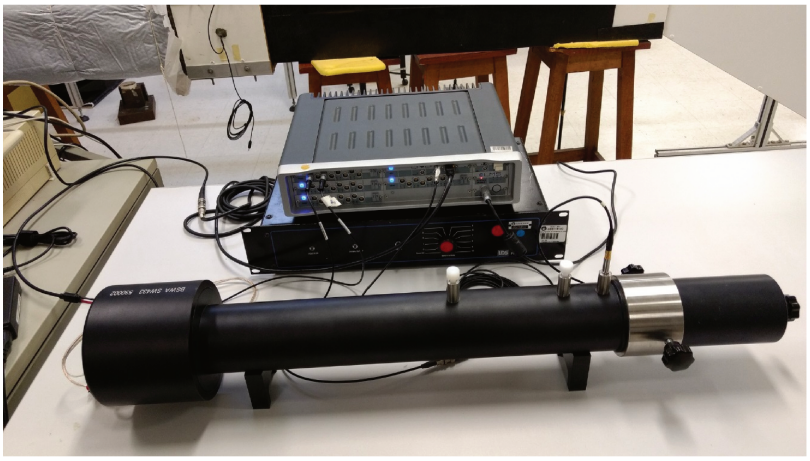

Figure 22 – Sound absorption test using the impedance tube of circular cross-section.

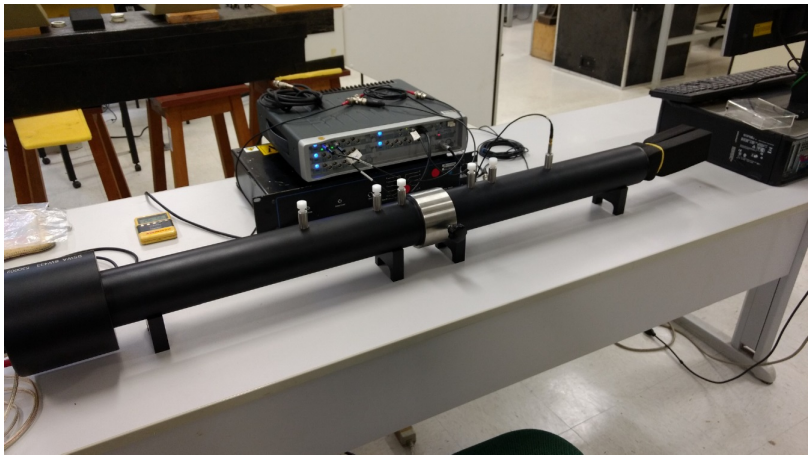

Figure 23 – Sound transmission loss test using the impedance tube of circular cross-section.

For the tests using the impedance tube of rectangular cross-section, the following equipments with the respective work frequency range were used:

- Impedance tube: 20 - 717 *Hz*;
- Microphone: 40 AD model, GRAS manufacturer, 3.15 - 10000 *Hz*;
- Loudspeaker: PMB-06 model, Bravox manufacturer, 20 - 717 *Hz* (SIVIERO, 2011);
- Calibrator: Cal 21 model, 01 dB manufacturer, 94 dB, 1000 *Hz*.

The absorption test configuration using this tube is observed in Fig. 24.

Figure 24 – Sound absorption test using the impedance tube of rectangular cross section.

The LMS Data acquisition and signal generator was used on the measurements for both impedance tubes. Figure 25 shows the representation of data acquisition and signal

processing during the measurement. On LMS Test Lab software, the parameters of the measurement were set, including the type of excitation signal, frequency range and types of sensors and transducers used. An analogical signal is used in the loudspeaker on the impedance tube. This signal was created by LMS Scadas by converting the computer signal from digital to analogical and by amplifying this analogical signal. On the microphone, the sound pressure signal is measured and the signal of the microphone is pre-amplified just inside the microphone. This analogical signal is received by the analogical input on LMS Scadas, filtered using one anti-alias filter to correct represent the frequency range of interest and finally the signal is converted to a digital one by an analogical to digital converter to be analyzed at the LMS Test Lab software on the computer (SIEMENS, 2015).

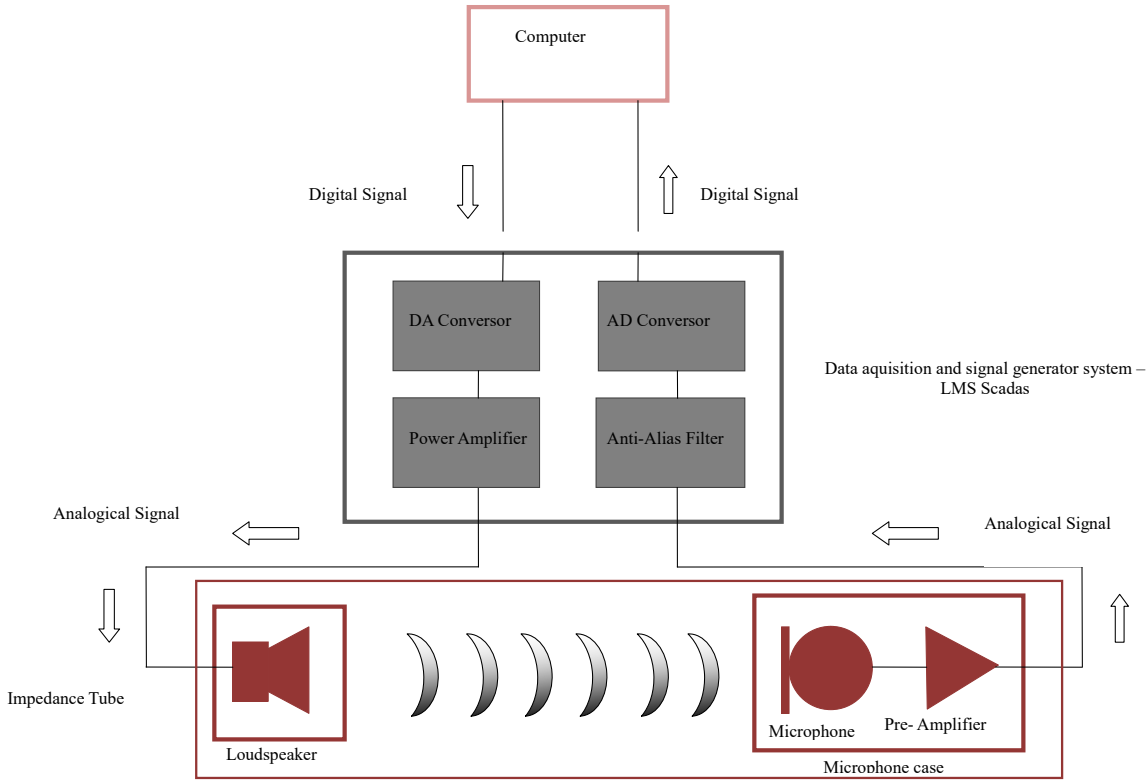

Figure 25 – Signal processing for impedance tube measurements.
Reference: adapted from Siemens (2015)

3.2 Porosity estimation using X-Ray microtomography

X-Ray microtomography has been used as one alternative way for the estimation of porosity and pore size distribution. For granular materials, it was shown that the X-Ray tomography led to very similar overall porosities, compared to the mercury porosimetry measurement. When using mercury porosimetry, the pore volume is determined directly from the insertion of mercury in the material at high pressures (FABER *et al.*, 2003). In 2016, Huallpa *et al.* and

Corredor-Bedoya used the X-Ray microtomography to estimate the porosity of coconut fiber and composites of mortar and tire rubber, respectively. In these cases, the materials were used for acoustical purposes. For mineral fibrous materials, as the ones studied in this research, it is possible to use X-ray Microtomography to estimate the porosity, as they have open pores structure and are composed of heavy molecules, leading to a good contrast at X-ray images. This method also has the advantages of using small samples and it is a non-destructive technique.

The X-Ray microtomography is a technique that allows obtaining 3D images of an object by its exposition to the X-Ray source and using a 2D detector. Also, images by the rotation of the object can be obtained. These images are pre-processed and form 2-D images of transversal cross-sections of the material. By the use of these 2D images, it is possible to reconstruct the 3D structure computationally.

The equipment used for this analysis was the Bruker X-Ray microtomograph 1272 Sky-Scan at the Brazilian Nanotechnology National Laboratory (LNNano). It has an X-Ray source of energy of 20 - 100 keV, resolution of 350 nm, and allows samples of maximum size of 75×70 mm of cross-section. In Fig. 26 it is possible to see the equipment with one sample of porous material inside (GOUVEIA, 2014).

The porosities were estimated by the use of Image-J free software. The 2D images of transversal cross sections of the material were converted from gray scale to binary scale and it was possible to estimate the porosity by the number of white and black pixels in these images (HUALLPA *et al.*, 2016). In this study it was used the *Default* method in Image-J for the binarization process. Black pixels correspond to the material structure and white pixels are empty spaces. This estimation was made for all the 2D images of the samples, leading to the following expression:

$$\phi = \frac{N_w}{N_t}, \tag{3.32}$$

where N_w is the number of white pixels in all the 2D-images and N_t is the number of total pixels in all the 2D images.

3.3 Tortuosity measurement using ultrasound measurements

The measurement of tortuosity can be done directly from an electrical conduction technique, where the conduction of the porous frame saturated by a fluid is compared to the conduction of the fluid itself. This fluid needs to be conductive and it is necessary an apparatus of electrodes, voltmeter, manometers, flowmeters and compressed air supply, because the saturation of fluid should be done with vacuum (VÉR; BERANEK, 2006). This technique has the disadvantages of damaging the cells of the porous frame and requires different types of instrumentation. An alternative technique is the use of ultrasonic wave speed measurements at

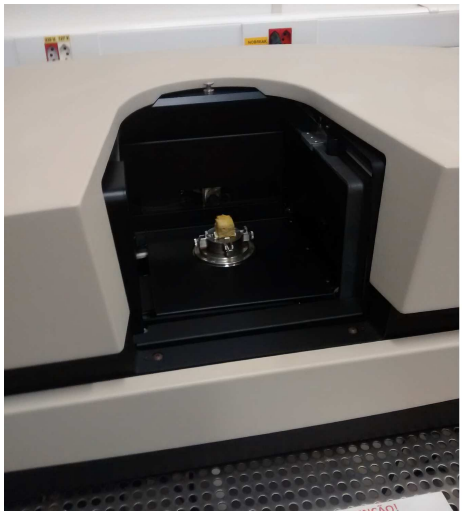

Figure 26 – X-ray microtomograph SkyScan 1272.

materials saturated by air. Using the hypothesis of the rigid frame, tortuosity is related to the velocity of acoustic waves, for an inviscid fluid, given by (ALLARD; LAURIKS, 1994):

$$\alpha_\infty = \frac{C_i^2}{C_{is}^2}, \tag{3.33}$$

where C_i is the wave speed in the fluid and C_{is} is the wave speed in the same fluid when it saturates the frame. For air, there are also losses related to viscous and thermal exchanges. In this case, tortuosity is a function of the frequency, the characteristics viscous and thermal lengths, the Prandtl number, the air density, and the viscosity. This lead to a correction at Equation 3.33 produced by the damping from the ultrasonic pulse, when measuring the ultrasonic pulse through the sample. Considering that not all the physical parameters are known and the correction from damping only provides a small correction, an estimative using Equation 3.33 can be considered sufficient (ALLARD; LAURIKS, 1994).

For this type of measurement, it is necessary an ultrasonic transducer operating at the order of *kHz*. Higher frequencies have a great attenuation in a porous material because of pore size.

The measurement procedure consists of measuring the time that the ultrasonic pulse propagates between the sending and receiving transducers with and without the sample of porous material (MAREZE, 2013). The distance between the transducers needs to be fixed. Considering the time that the wave travels from one transducer to another, it is possible to measuring tortuosity by calculating C_i and C_{is} and using Equation 3.33 (ALLARD; LAURIKS, 1994).

In this work, the tests with ultrasound were performed at the Non-destructive Tests Laboratory at the School of Agricultural Engineering at Unicamp.

4 RESULTS

Double porosity materials were tested to have their acoustic properties, sound absorption and sound transmission loss, determined. Also, the porosity and the tortuosity of single porosity (pure) rockwool and glasswool were experimentally determined. The diffusion frequency of the double porosity samples tested was estimated using the values of porosity and tortuosity obtained in the experiments and flow resistivity values in the Literature. The analytical models for double porosity materials were analyzed using the results of sound absorption tests, experimental values of porosity and tortuosity and a curve fitting for the analytical model to the experimental data.

4.1 Experimental acoustical characterization

Two types of samples were tested: single porosity rockwool and glasswool, and double porosity rockwool and glaswool. Single porosity samples were used as references samples to analyze the effects of double porosity. Double porosity samples were also divided into two other types: samples with mesopores not filled and samples with mesopores filled. The samples with mesopores filled are: samples with rockwool substrate with mesopores filled by glasswool and samples with glasswool substrate with mesopores filled by rockwool. Replicas of the same sample were taken from different parts of the material, as recommended by the standard of sound absorption tests (ISO10534-2, 2001). The same type of samples and respective replicas were used for transmission loss tests.

4.1.1 Results of sound absorption tests

Sound absorption tests were made in the impedance tube of circular cross-section and also in the impedance tube of rectangular cross-section.

4.1.1.1 Circular cross-section impedance tube

The samples consisted of one unit cell: a circular sample with one circular hole. The mesoporosity values chosen were similar to those that led to good results in the work of Atalla *et al.*, (2001). Also, samples of higher mesoporosity (ϕ_p above 0.15) are difficult to be experimentally built, leading to failure on the borders of the sample. The hole diameter was calculated according to the desired mesoporosity and sample size. Figure 27 shows some samples with filled mesoporosities.

Pure rockwool and pure glasswool samples are denoted as R and G, respectively. Rn and Gn initials (n=1,...,6) are used for samples with mesopores not filled and RPn and GPn (n=1,...,6) for samples with filled mesopores. Table 3 shows samples configurations that were

Figure 27 – Samples with mesopores filled: glasswool substrate filled with rockwool (above) and rockwool substrate filled with glasswool (below).

tested as a function of the mesopore diameter and mesoporosity, which is the ratio of mesopore area to the sample area.

Table 3 – Configurations of the tested samples at the circular impedance tube.

Samples	Sample Diameter (mm)	Hole Diameter (mm)	Mesoporosity
R, G	60	-	-
R1, RP1, G1, GP1	60	6.4	0.01
R2, RP2, G2, GP2	60	9.5	0.03
R3, RP3, G3, GP3	60	12.5	0.04
R4, RP4, G4, GP4	60	17.5	0.08
R5, RP5, G5, GP5	60	20.2	0.11
R6, RP6, G6, GP6	60	22.3	0.14

Two different ranges of frequencies were measured using this impedance tube: 125 - 800 Hz and 400 - 2500 *Hz*, this comes from the experimental setup as explained in Section 3.1.3 and implies in two measured curves for each sample. To facilitate comparison between curves of different samples, in the intersection range, 400 - 800 *Hz*, the mean value of sound absorption from the two curves were taken. Also, the samples described in Tab. 3 were physically replicated, 3 replicas of each (A, B and C). The curves Rn, Gn, RPn and GPn represent the mean values of the replicas for the same type of sample in the next sections.

Figures 28 shows the value of sound absorption for the modified samples of rockwool with mesopores not filled in comparison with the pure case. Figure 29 shows sound absorption for the case of mesopores filled with glasswool. Considering both pictures, it is possible to notice that double porosity creates gains in absorption above the frequency of 1000 *Hz* and the results are similar for the double porosity materials with mesopores filled and not.

Figures 28 and 29 shows ripples for the Rn and RPn curves between 500 - 1000 *Hz*. The presence of these ripples are explained in the following. For example, in the RP1 curve, for each of the three replicas, two curves were measured on the impedance tube, one

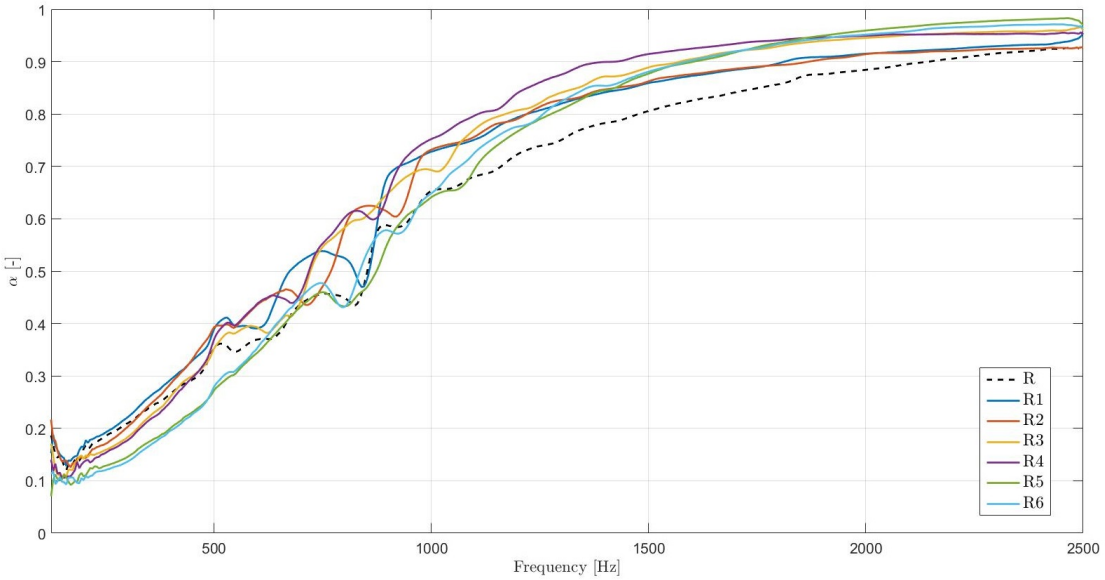

Figure 28 – Sound absorption for pure case and samples with mesopores not filled - rockwool substrate - circular samples.

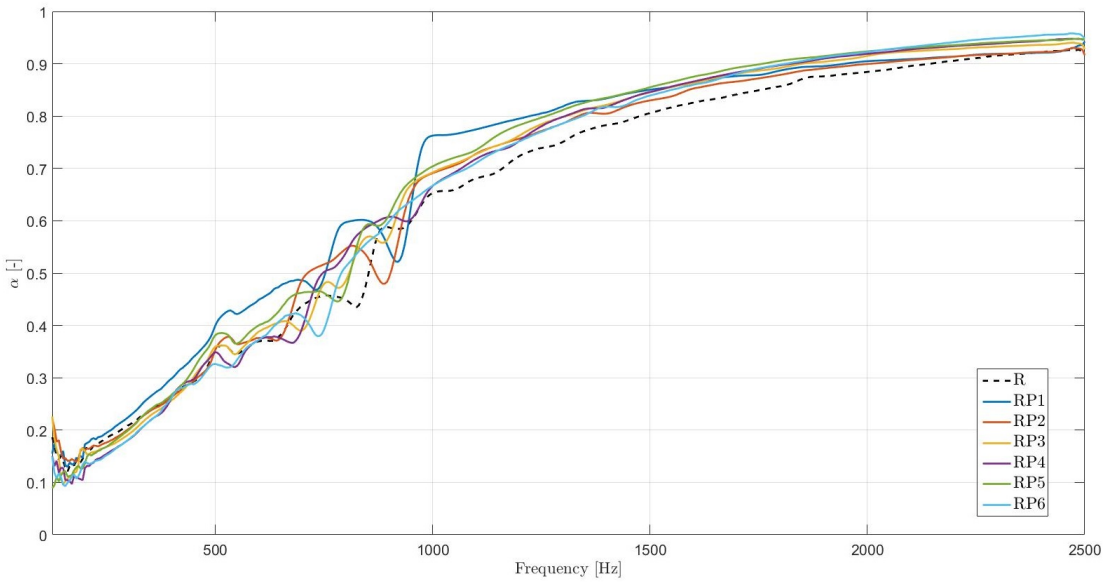

Figure 29 – Sound absorption for pure case and samples with mesopores filled - rockwool substrate - circular samples.

in the interval of 125 - 800 Hz and another of 400 - 2500 Hz. In Fig. 30, the curves for each replicas are presented without taking the mean value on the frequency intersection range 400 - 800 Hz, and an axis zoom between 300 - 1000 Hz was taken to facilitate the observation. In the intersection range, it is noticed that the two curves of the same replica are similar, but not identical. Figure 31 presents the sound absorption separately for R1 (replicas A, B and C) after the mean value was taken. It is observed that the position of the minimum region of sound absorption is different between each replica. The minimum region is related to the structural resonance of the sample (HONORATO, 2013), so the differences between each replica are

probably cause by the material heterogeneities. The final curve R1, presented in Fig. 28, is the mean value of the three curves presented in Fig. 31. The ripples presented in the final curve are a result of the two computed means and a closer attention is need when analyzing the results in the ripples region.

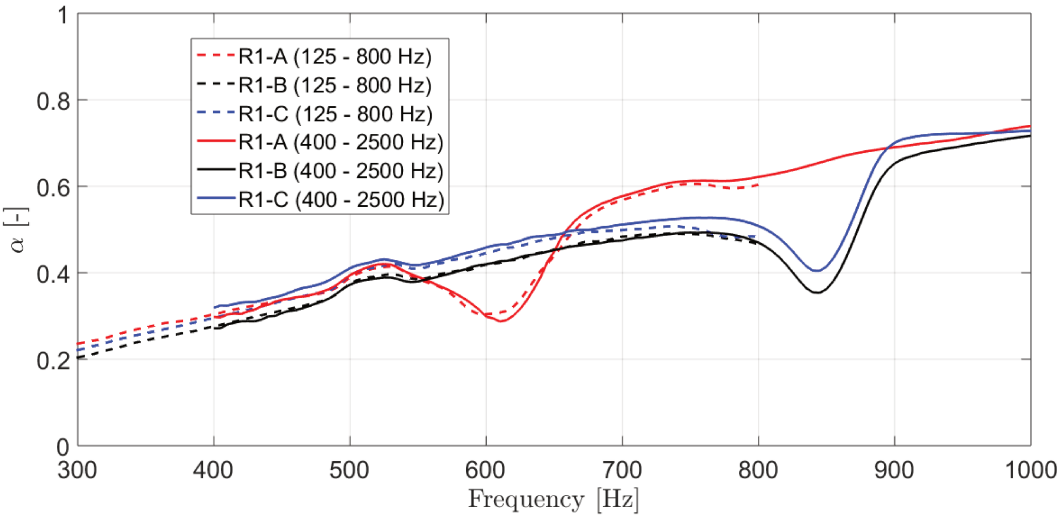

Figure 30 – Sound absorption in separated frequency ranges for samples R1, replicas A, B and C - rockwool substrate - circular samples.

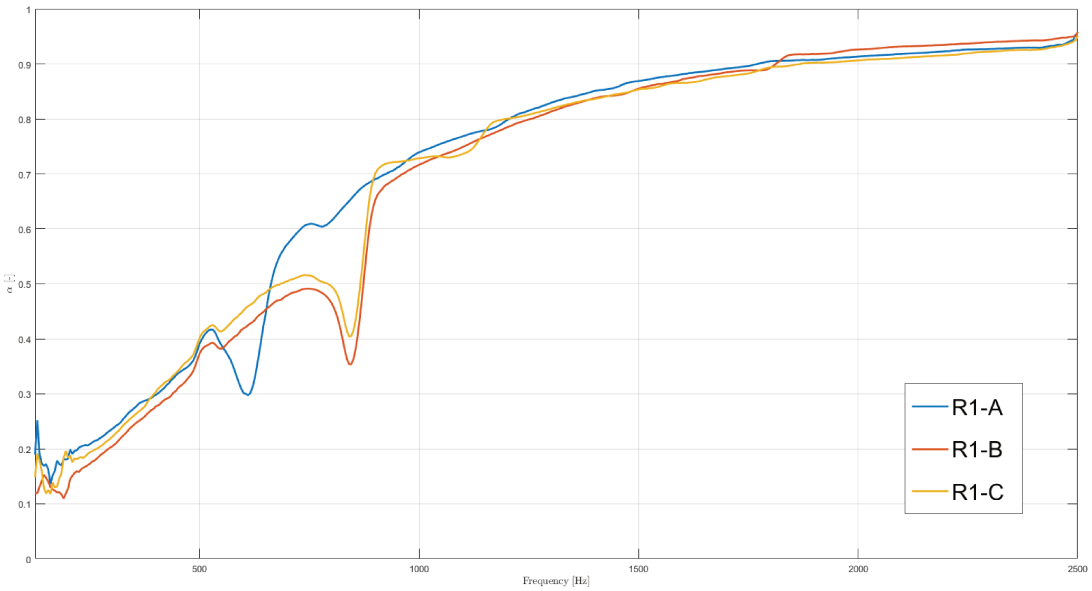

Figure 31 – Sound absorption for samples R1, replicas A, B and C - rockwool substrate - circular samples.

For a detailed analysis of the gains in sound absorption considering the double porosity samples in comparison with pure rockwool, Table 4 shows the sound absorption coefficient at 250, 500, 1000 and 2000 Hz for each sample. The absolute gain is expressed by the symbol (Δ) and is given by the difference between sound absorption coefficient for each modified samples curve and the pure curve (R), for each frequency. The percentage gain (%) expresses

the same difference, but in percentage in respect to the pure curve (R), for each frequency. Gains in sound absorption are expressed as positive values and losses in sound absorption as negative values.

In a general way, for higher frequencies, the modifications lead to gains in absorption. Especially for RP1 curve at 1000 Hz, the gain is about 17%. In the frequency of 2000 Hz, all the double porosity samples provided gains, but with a small percentage. In lower frequencies (for example 250 Hz), there are losses in absorption for all curves, except for R1 and RP1. Considering the sound absorption values for this four specific frequencies, it was not possible to establish a direct relationship between the increasing values of mesoporosity and gains in sound absorption coefficient.

Table 4 – Sound absorption coefficient for rockwool samples and absolute (Δ) and percentage (%) gains at 250, 500, 1000 and 2000 *Hz* obtained by the modified rockwool samples compared to the pure case (R) - circular samples.

Sample	**Frequency (*Hz*)**											
	250	Δ_{250}	$\%_{250}$	500	Δ_{500}	$\%_{500}$	1000	Δ_{1000}	$\%_{1000}$	2000	Δ_{2000}	$\%_{2000}$
R	0.1847	0.0000	0.0	0.3525	0.0000	0.0	0.653	0.0000	0.0	0.8845	0.0000	0.0
R1	0.1919	0.0072	3.9%	0.3891	0.0366	10.4%	0.7281	0,0751	11.5%	0.9152	0.0307	3.5%
R2	0.1704	-0.0143	-7.7%	0.3929	0.0404	11.5%	0.732	0.079	12.1%	0.9142	-0.001	-0.1%
R3	0.1588	-0.0259	-14.0%	0.3522	-0.0003	-0.1%	0.6932	0.0402	6.2%	0.9453	0.0311	3.5%
R4	0.1529	-0.0318	-17.2%	0.3697	0.0172	4.9%	0.7523	0.0993	15.2%	0.9494	0.0041	0.5%
R5	0.1285	-0.0562	-30.4%	0.2724	-0.0801	-22.7%	0.6413	-0.0117	-1.8%	0.9594	0.0100	1.1%
R6	0.1203	-0.0644	-34.9%	0.2796	-0.0729	-20.7%	0.6486	-0.0044	-0.7%	0.9517	-0.0077	-0.9%
RP1	0.1949	0.0102	5.5%	0.3998	0.0473	13.4%	0.7628	0.1098	16.8%	0.9049	0.0204	2.3%
RP2	0.1763	-0.0084	-4.5%	0.3533	0.0008	0.2%	0.6911	0.0381	5.8%	0.8996	0.0151	1.7%
RP3	0.1683	-0.0164	-8.9%	0.3595	0.0070	2.0%	0.6924	0.0394	6.0%	0.9151	0.0306	3.5%
RP4	0.1546	-0.0301	-16.3%	0.3489	-0.0036	-1.0%	0.6665	0.0135	2.1%	0.9190	0.0345	3.9%
RP5	0.1680	-0.0167	-9.0%	0.3814	0.0289	8.2%	0.704	0.0510	7.8%	0.9237	0.0392	4.4%
RP6	0.1520	-0.0327	-17.7%	0.3265	-0.0260	-7.4%	0.667	0.0140	2.1%	0.9226	0.0381	4.3%

Figures 32 and 33 show sound absorption coefficient for glasswool samples with mesopores not filled and filled with rockwool, respectively. For the case of double porosity samples with mesopores not filled, the curves are similar or above the reference curve G, except for G5 and G6. Although the values of mesoporosity for G5 and G6 are 0.11 and 0.14 respectively, there was no gain in absorption. In the study of Atalla *et al.* (2001), for the case of similar mesoporosity values (ϕ_p = 0.11 and 0.18), gains in absorption for the frequency range of 100 - 2000 *Hz* were reported when compared to the single porosity case. However, in the study of Atalla *et al.* (2001) the results were based in a numerical approach.

Figure 33 presents the results for the case of samples with mesopores filled. The values of sound absorption are similar to the reference curve for GP1 curve and above for GP2, GP3, GP4, GP5 and GP6.

In the case of glasswool double porosity samples curves, it is noticed that the modified samples curves are offset in comparison to the reference curve (G), but maintaining the same shape of the reference curve. The gain absorption when presented, it is observed in all the interval of frequencies for the same sample. This effect was not observed in the case of rockwool samples, where the behavior of the same curve varies in frequency compared to the reference curve.

In the case of the curves of the glasswool samples with mesopores not filled, the best performance was obtained for G4 curve. The absorption increased as mesoporosity increased for the case of the curves G1 and G2; decreased for G3; reached a maximum value in G4 and decreased for G5 and G6. From the literature, it was found numerically that mesoporosity has an interval that produces better results for sound absorption (ATALLA *et al.*, 2001). As showed in Section 2.5.2, the sound absorption increases with the mesoporosity increasing until it reaches a maximum. However, the same situation it is not found in Fig. 32, where an interval of mesoporosity which guarantees better results is not defined. On the other hand, an interesting situation found is that G4 curve presented the better performance for sound absorption in the interval range of 1000 - 1500 *Hz*, similarly to the rockwool curve R4 in Fig. 28. This samples have in common the same mesoporosity $\phi_p = 0.08$ and the mesopores not filled.

For the case of mesopores not filled, Fig. 33 shows that the mesopores filled contributed to enhance to sound absorption (except for G1), however this is not direct related to the value of mesoporosity because the curve GP2 compared to GP3 and curve GP5 compared to GP6 are similar besides the different values of mesoporosity.

Table 5 shows the value of sound absorption coefficient for each double porosity glasswool samples and single porosity glasswool. The absolute percentage gain of the glasswool double porosity samples compared to the G curve at 250, 500, 1000 and 2000 *Hz* are also presented. For samples with mesopores not filled (Gn), samples with higher mesoporosity (larger holes) presented reductions in absorption at these specific four frequencies.

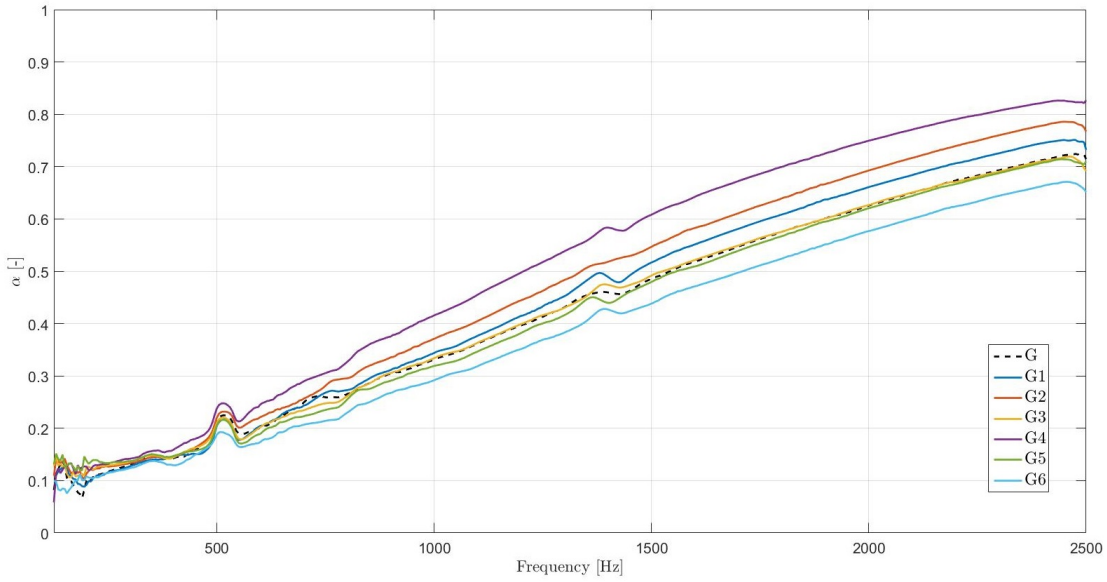

Figure 32 – Sound absorption for pure case and samples with mesopores not filled - glasswool substrate - circular samples.

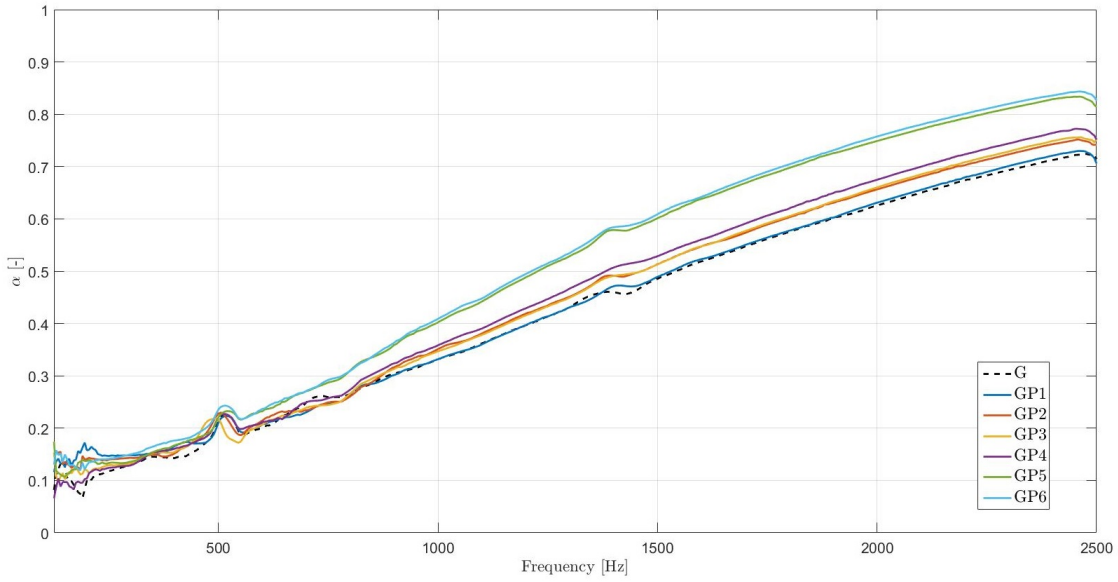

Figure 33 – Sound absorption for pure case and samples with mesopores filled - glasswool substrate - circular samples.

For samples with mesopores filled with rockwool, (GPn) samples, the results presented in Tab. 5 can give the idea that filling mesopores with rockwoll can enhance absorption in a general way. The only negative value of gain is 2.1% for the GP1 sample at 500 *Hz*. But, considering the GP1 curve in Fig. 33, the conclusion can be considered different, i.e., there is almost no gain for this curve compared to the pure case, (G), as discussed above.

In the case of the glasswool double porosity samples, analyzing the values in Tab. 5 is not possible to obtain a direct relationship between the gain in sound absorption and the increase of mesoporosity.

Table 5 – Sound absorption coefficient for glasswool samples and absolute (Δ) and percentage (%) gains at 250, 500, 1000 and 2000 *Hz* obtained by the modified glasswool samples compared to the pure case (G) - circular samples.

Sample	**Frequency (*Hz*)**											
	250	Δ_{250}	$\%_{250}$	500	Δ_{500}	$\%_{500}$	1000	Δ_{1000}	$\%_{1000}$	2000	Δ_{2000}	$\%_{2000}$
G	0.1181	0.0000	0.0	0.2156	0.0000	0.0	0,3316	0.0000	0.0	0.6254	0.0000	0.0
G1	0.1160	-0.0021	-1.8%	0.2051	-0.0105	-4.9%	0.3441	0.0125	3.8%	0.6609	0.0355	5.7%
G2	0.1266	0.0085	7.2%	0.2208	0.0052	2.4%	0.3711	0.0395	11.9%	0,6927	0.0673	10.8%
G3	0.1293	0.0112	9.5%	0.2109	-0.0047	-2.2%	0.3339	0.0023	0.7%	0.6266	0.0012	0.2%
G4	0.1322	0.0141	11.9%	0.2382	0.0226	10.5%	0.4159	0.0843	25.4%	0.7496	0.1242	19.9%
G5	0.1335	0.0154	13.0%	0.2062	-0.0094	-4.4%	0.3192	-0.0124	-3.7%	0.6205	-0.0049	-0.8%
G6	0.1145	-0.0036	-3.0%	0.1881	-0.0275	-12.8%	0.2918	-0.0398	-12.0%	0.5769	-0.0485	-7.8%
GP1	0.1467	0.0286	24.2%	0.2110	-0.0046	-2,1%	0.3318	0.0002	0.1%	0.6310	0.0056	0.9%
GP2	0.1399	0.0218	18.5%	0.2280	0.0124	5.8%	0.3513	0.0197	5.9%	0.6563	0.0309	4.9%
GP3	0.1292	0.0111	9.4%	0.2171	0.0015	0.7%	0.3468	0.0152	4.6%	0.6603	0.0349	5.6%
GP4	0.1242	0.0061	5.2%	0.2211	0.0055	2.6%	0.3583	0.0267	8.1%	0.6748	0.0494	7.9%
GP5	0.1335	0.0154	13.0%	0.2212	0.0056	2.6%	0.4024	0.0708	21.4%	0.7489	0.1235	19.7%
GP6	0.1413	0.0232	19.6%	0.2361	0.0205	9.5%	0.4091	0.0775	23.4%	0.7575	0.1321	21.1%

4.1.1.2 Sample repositioning effect in the circular cross-section impedance tube

During the experiments to obtain the curves of Figs. 28, 29, 32 and 33, it was noticed that removing and repositioning the same sample on the sample holder have affected the final result.

Because of this effect, repeatability tests were performed for both materials. These tests constituted in placing and removing the same sample from the impedance tube and repeating the measurement of interest. The repositioning were carried out 10 times to one sample of pure glasswool (G) and one sample of pure rockwool (R).

Almost no effects were noticed on the final results of sound absorption for the rockwool samples. However, for the glasswool samples, in the absorption tests, it was noticed differences between the results for the same sample. Figure 34 shows the sound absorption coefficient for one sample of glasswool which was replaced 9 times into the impedance tube. The glasswool used on the samples is very soft and easy to compress. A piston in the sample holder (Fig. 19) is used to adjust samples with different thickness into the impedance tube. When the piston is moved by the user to fit the specimen on the sample holder to avoid an air gap behind it, the user can unintentionally compress the sample in a different way in each different repositioning. In this case, the sound absorption behavior can be more affected by the sample repositioning for the glasswool samples in the circular impedance tube.

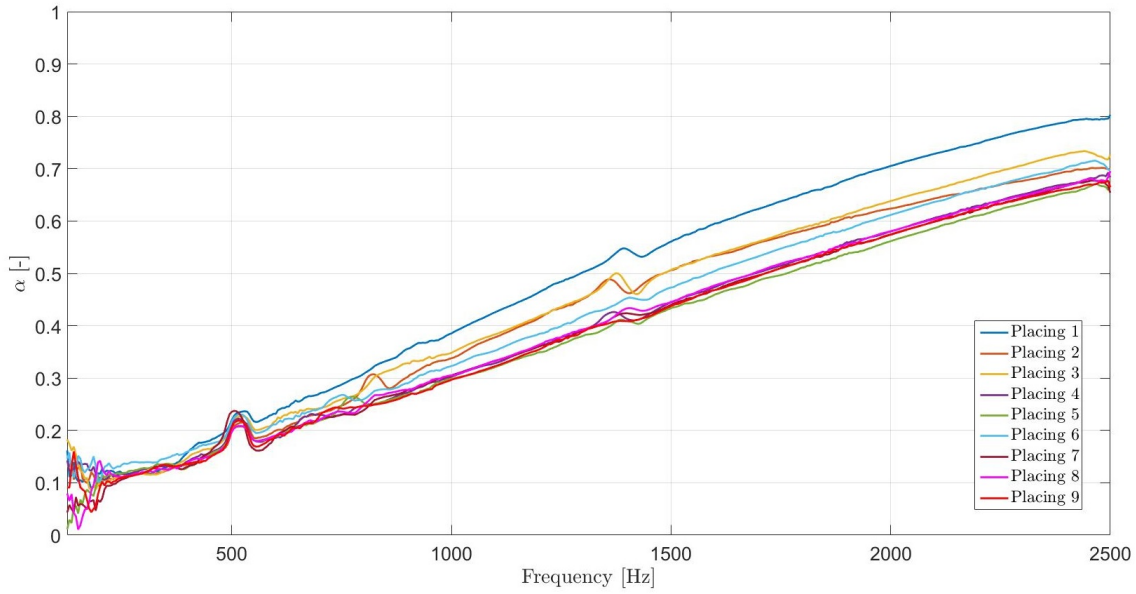

Figure 34 – Variation in the absorption of a glasswool pure sample by repositioning it 9 times on the sample holder - circular samples.

Table 6 shows the values of sound absorption coefficient obtained at these 9 placings of the sample. To verify the differences between the curves of Fig. 34, the mean values of sound absorption and the standard deviation were calculated for the frequencies of 250, 500, 1000 and 2000 *Hz*.

Table 6 – Sound absorption coefficient at 250, 500, 1000 and 2000 *Hz*, mean value of the curves and respective standard deviation for the glasswool pure sample placed 9 times into the sample holder - circular samples.

Placing	**Frequency (*Hz*)**			
	250	**500**	**1000**	**2000**
Placing 1	0.1186	0.2202	0.3559	0.7053
Placing 2	0.1104	0.1996	0.3020	0.6239
Placing 3	0.1102	0.2125	0.3284	0.6382
Placing 4	0.1170	0.2116	0.2720	0.5801
Placing 5	0.1185	0.1986	0.2685	0.5616
Placing 6	0.1348	0.2177	0.2900	0.6116
Placing 7	0.1067	0.2359	0.2770	0.5739
Placing 8	0.1112	0.1979	0.2774	0.5807
Placing 9	0.1101	0.2073	0.2667	0.5745
Mean Value	0.1153	0.2112	0.2931	0.6055
Standard Deviation	0.0085	0.0123	0.0307	0.0455

The values of standard deviation presented the same order of magnitude or even a higher order of magnitude than several absolute gains in absorption showed in Tab. 5. The gains in sound absorption greater than the standard deviation occurred for the samples G3, G4, G5, GP1, GP2, GP3, GP5 and GP6 at 250 *Hz* and for samples G4, GP5 and GP6 at 2000 *Hz*.

4.1.1.3 Rectangular cross-section impedance tube

In the case of the rectangular cross-section tube, the samples contain 6 or 24 unit cells, so it is possible to study the effect of periodicity. These number of cells were chosen in order to fill completely the cross-section of the tube. The characteristics of the tested samples are presented in Tab. 7 and some samples that were tested are shown in Figs. 35 and 36.

The mesoporosities chosen were approximately 0.08 or 0.09 and 0.24 or 0.25 to analyze the influence of smaller and greater mesoporosities. Samples of higher mesoporosity are difficult to be experimentally built (above 0.25), leading to failure on the borders of the sample. Also, it was evaluated if a higher number of cells influenced the acoustical parameters: samples of very similar mesoporosities were tested with 6 and 24 cells.

All of the samples had physical replicas, 3 of each. The results showed in this section are the mean values of the replicas for each type of sample. The initials RR and GR are used for pure rockwool and pure glasswool samples, respectively. The initials RRn and GRn (n=$1,\ldots,6$) are used for samples with not filled mesopores and the initials RRnP and GRnP (n=$1,\ldots,6$) for samples with filled mesopores.

For the rockwool samples, the sound absorption for the modified samples are presented in Figs. 37 and 38.

The rockwool samples with mesopores not filled did not show absorption gains

Table 7 – Configurations of the tested samples at the rectangular impedance tube.

Samples	Size of cell (mm)	Hole Diameter (mm)	Mesoporosity (ϕ_p)
RR, GR	240 × 160*	-	-
RR1, GR1, RR1P, GR1P	80 × 80**	45.2	0.25
RR2, GR2, RR2P, GR2P	80 × 80**	26.6	0.09
RR3, GR3, RR3P, GR3P	40 × 40***	22.3	0.24
RR4, GR4, RR4P, GR4P	40 × 40***	12.5	0.08

* 1 cell, ** 6 cells, *** 24 cells

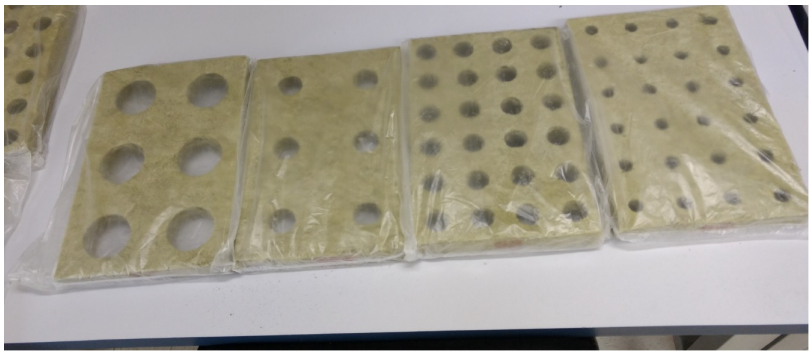

Figure 35 – Rockwool substrate samples with mesopores not filled.

Figure 36 – Glasswool substrate samples with mesopores filled with rockwool.

except for the RR4 curve around 250 *Hz* and RR3 and RR4 curves at approximately 20 *Hz*. RR2 and RR4 curves, with similar mesoporosities $\phi_p = 0.09$ and $\phi_p = 0.08$, respectively, presented the greatest values of sound absorption considering the full frequency range of this impedance tube.

The rockwool samples with mesopores filled presented better absorption with gains around 250 *Hz*, and for the RR4P little gains between 250 to 400 *Hz* and around 700 *Hz*. The RR2P and RR4P curves, with mesoporosities $\phi_p = 0.09$ and $\phi_p = 0.08$, respectively, presented the greatest values of sound absorption, similar to the case of rockwool samples with mesopores not filled. These results, for rockwool samples, shows that the number of cells does not influence on sound absorption but the mesoporosity does.

Table 8 shows values of the sound absorption coefficient and the absolute and percentage absorption gains for the frequencies of 125, 250 and 500 *Hz*, for the rockwool samples. It was noticed that for this specific frequencies, there were only gains for the samples RR4,

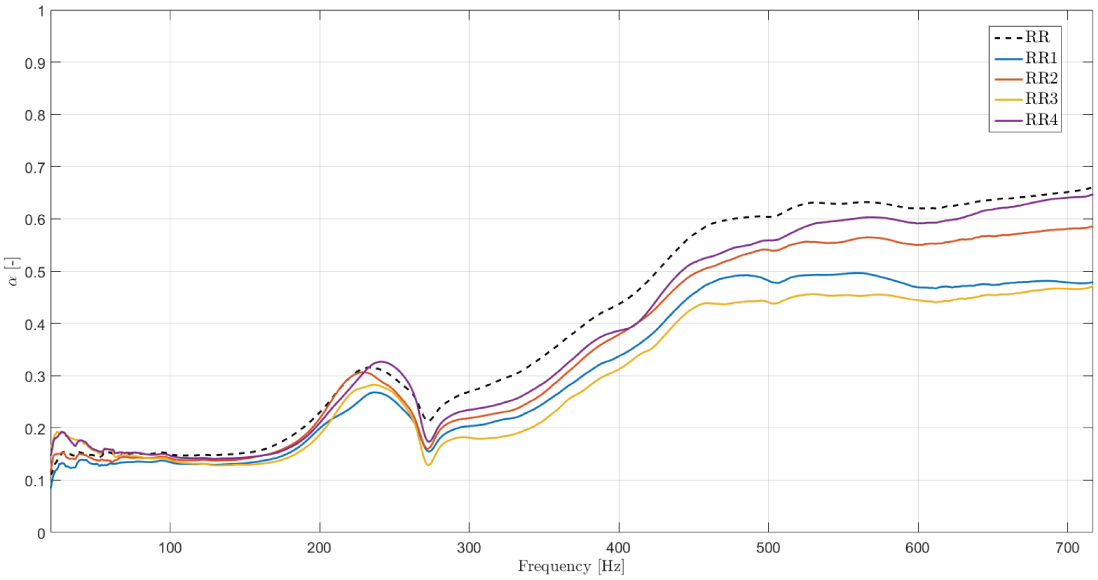

Figure 37 – Sound absorption for pure case and samples with mesopores not filled - rockwool substrate - rectangular samples.

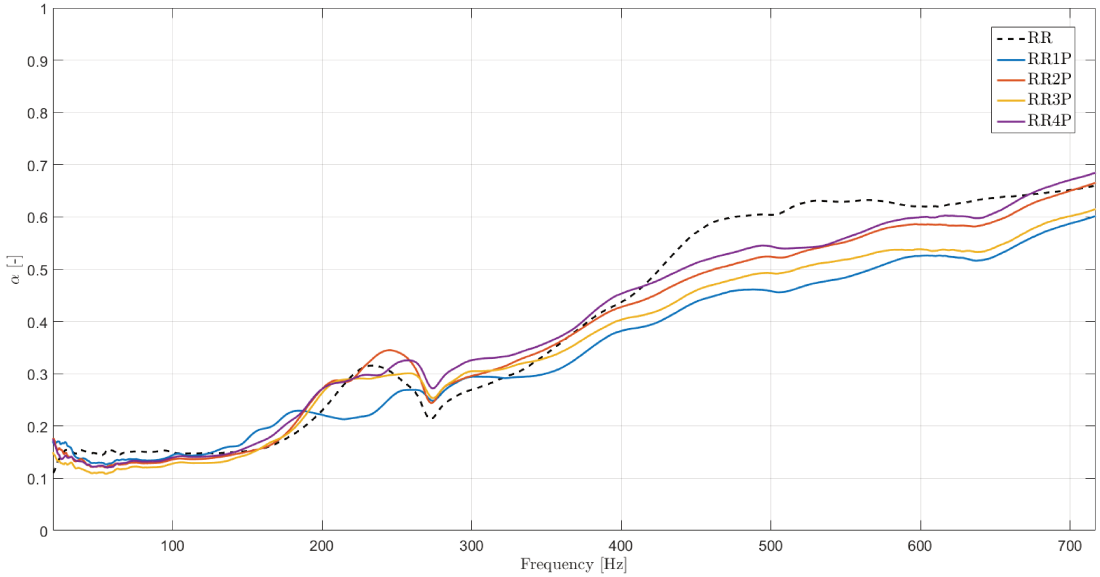

Figure 38 – Sound absorption for pure case and samples with mesopores filled - rockwool substrate - rectangular samples.

RR2P, RR3P and RR4P at 250 Hz. Analyzing Tab. 8 and Fig. 38, it is noticed the influence of the porous inclusion in the region around 250 Hz, compared to the pure case (RR). Also, the values on the table confirm that for higher mesoporosity ($\phi_p = 0.24/0.25$), there are more losses than in the case of $\phi_p = 0.08/0.09$, independently of the number of the cells.

Figure 39 shows the absorption of the modified glasswool samples with mesopores not filled. GR4 and GR2 curves present a small gain in the frequency range of 250 to 450 Hz, although the other curves are very similar to the pure case (GR). In the interval between 500

Table 8 – Sound absorption coefficient for rockwool samples and absolute (Δ) and percentage (%) gains at 125, 250 and 500 *Hz* obtained by the modified rockwool samples compared to the pure case (R) - rectangular samples.

Sample	**Frequency (*Hz*)**								
	125	Δ_{125}	$\%_{125}$	**250**	Δ_{250}	$\%_{250}$	**500**	Δ_{500}	$\%_{500}$
RR	0.1482	0.0000	0.0%	0.2948	0.0000	0.0%	0.6039	0.0000	0.0%
RR1	0.1305	-0.0177	-11.9%	0.2510	-0.0438	-14.8%	0.4817	-0.1222	-20.2%
RR2	0.1385	-0.0098	-6.6%	0.2708	-0.0240	-8.1%	0.5406	-0.0633	-10.5%
RR3	0.1303	-0.0180	-12.1%	0.2650	-0.0298	-10.1%	0.4401	-0.1637	-27.1%
RR4	0.1418	-0.0064	-4,3%	0.3165	0.0217	7.4%	0.5589	-0.0450	-7.5%
RR1P	0.1484	0.0001	0,1%	0.2638	-0.0310	-10.5%	0.4580	-0.1459	-24.2%
RR2P	0.1383	-0.0100	-6,7%	0.3421	0.0473	16.0%	0.5240	-0.0799	-13.2%
RR3P	0.1295	-0.0187	-12.6%	0.2987	0.0040	1.3%	0.4925	-0.1114	-18.4%
RR4P	0.1422	-0.0060	-4.1%	0.3206	0.0258	8.8%	0.5436	-0.0602	-10.0%

and 700 *Hz*, samples with smaller mesoporosity, GR2 and GR4, presented greater values of absorption than the samples with higher mesoporosity, GR1 e GR3.

Figure 40 shows the results for the glasswool samples with filled mesopores. It is noticed that the modified samples have a decrease in absorption around approximately 240 *Hz* and an increase between 350 to 500 *Hz* compared to the pure case (GR). In this case, it is not possible to visualize a relationship between mesoporosity and sound absorption because all curves of the double porosity samples are very similar.

Table 9 presents the absorption gains for the frequencies of 125, 250 and 500 *Hz*, for the glasswool modified samples. There are gains especially for the samples with mesopores filled. However, in the case of glasswool, the gains are concentrated at 500 *Hz*, with a maximum value of 7.4% for the GR4P sample.

In general, it was not possible to notice an influence of the number of the cells for samples with rockwool or glasswool substrate. The performances for the modified samples were similar for samples with the same mesoporosity, the same type of mesopores (filled or not) and different number of cells, for the case of the frequencies 125, 250 and 500 *Hz*.

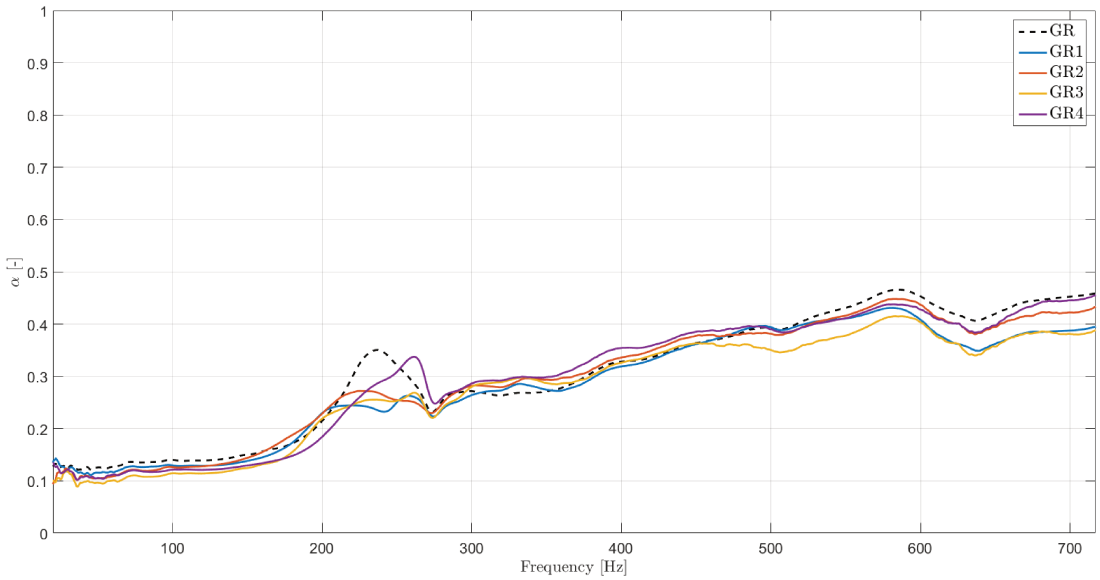

Figure 39 – Sound absorption for pure case and samples with mesopores not filled - glasswool substrate - rectangular samples.

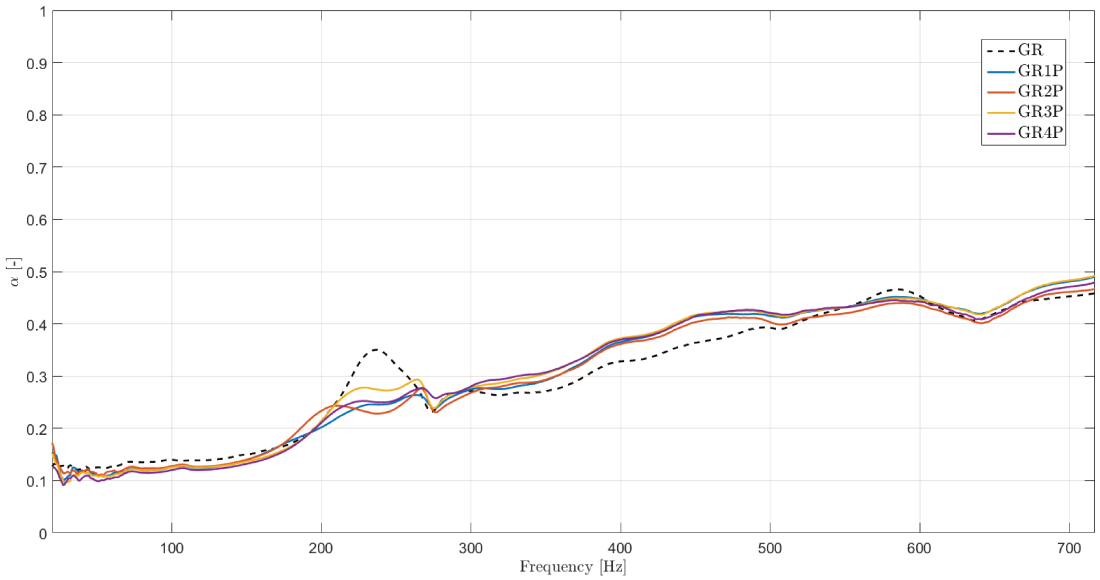

Figure 40 – Sound absorption for pure case and samples with mesopores filled - glasswool substrate - rectangular samples.

Table 9 – Sound absorption coefficient for glasswool samples and absolute (Δ) and percentage (%) gains at 125, 250 and 500 *Hz* obtained by the modified glasswool samples compared to the pure case (G) - rectangular samples.

Sample	**Frequency (*Hz*)**								
	125	Δ_{125}	$\%_{125}$	**250**	Δ_{250}	$\%_{250}$	**500**	Δ_{500}	$\%_{500}$
GR	0.1395	0	0.0%	0.3207	0.0000	0.0%	0.3920	0.0000	0.0%
GR1	0.1290	-0.0105	-7.5%	0.2505	-0.0703	-21.9%	0.3940	0.0020	0.5%
GR2	0.1291	-0.0104	-7.4%	0.2544	-0.0664	-20.7%	0.3814	-0.0106	-2.7%
GR3	0.1147	-0.0248	-17.8%	0.2530	-0.0677	-21.1%	0.3502	-0.0418	-10.7%
GR4	0.1214	-0.0181	-13.0%	0.3086	-0.0121	-3.8%	0.3899	-0.0020	-0.5%
GR1P	0.1255	-0.0140	-10.0%	0.2511	-0.0697	-21.7%	0.4150	0.0230	5.9%
GR2P	0.1275	-0.0119	-8.6%	0.2388	-0.0820	-25.6%	0.4031	0.0111	2.8%
GR3P	0.1263	-0.0132	-9.5%	0.2751	-0.0457	-14.2%	0.4186	0.0266	6.8%
GR4P	0.1212	-0.0182	-13.1%	0.2546	-0.0662	-20.6%	0.4209	0.0290	7.4%

4.1.1.4 Sample repositioning effect in the rectangular cross-section impedance tube

It was also investigated the influence of the samples repositioning in the impedance tube of rectangular cross-section. For both rockwool and glasswool samples, there is an influence of repositioning the same sample at absorption tests. Figures 41 and 42 show this situation for one sample of pure rockwool (RR) and glasswool (GR).

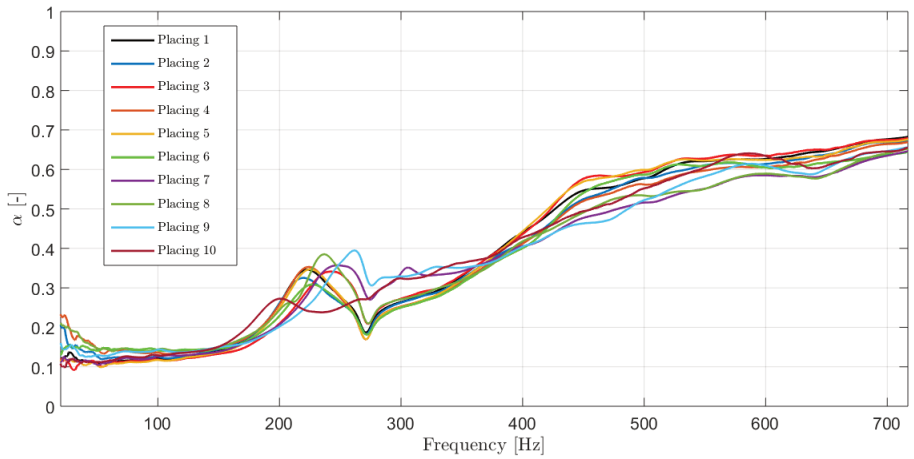

Figure 41 – Variation in the absorption of a rockwool pure sample by repositioning it 10 times on the sample holder - rectangular samples.

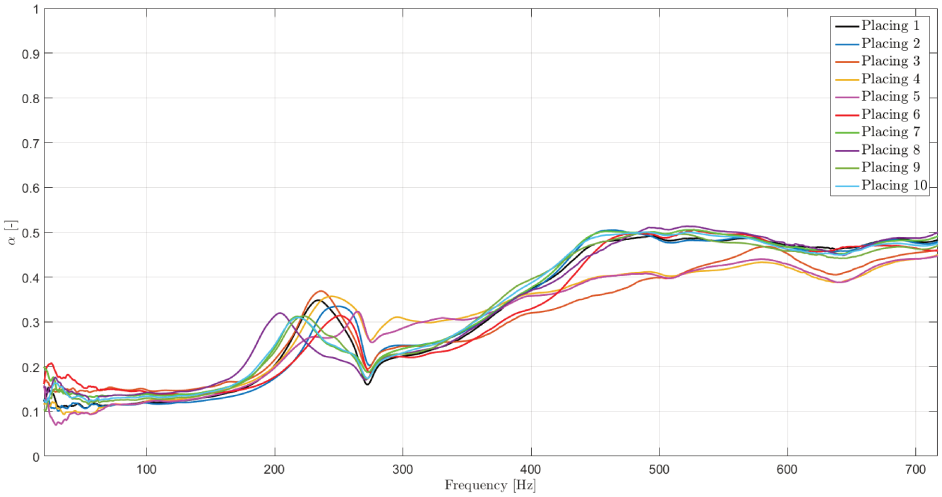

Figure 42 – Variation in the absorption of a glasswool pure sample by repositioning it 10 times on the sample holder - rectangular samples.

Tables 10 and 11 present the absorption coefficient for the tests of repositioning the same sample many times, for rockwool an glasswool, respectively. In the case of rectangular samples, both materials showed differences on the values of sound absorption. When using the rectangular samples, the samples are larger than the circular one and is difficult to align all the borders of the sample in the sample holder, because the sample is not perfectly flat, leading to variations on the results.

Also, the mean value of sound absorption coefficient and the respective standard deviation of each sample are presented in Tabs. 10 and 11. The values of the standard deviation presented in these tables are higher than several of the values of absolute gain or losses, especially on the frequencies of 250 and 500 *Hz* in Tabs. 8 and 9.

Table 10 – Sound absorption coefficient at 125, 250, 500 *Hz*, mean value of the curves and respective standard deviation for the rockwool pure sample placed 10 times into the sample holder - rectangular samples.

Placing	**Frequency (*Hz*)**		
	125	**250**	**500**
1	0.1280	0.2782	0.5776
2	0.1295	0.2618	0.5786
3	0.1224	0.3357	0.5933
4	0.1387	0.2750	0.5618
5	0.1242	0.2803	0.5989
6	0.1433	0.2650	0.5865
7	0.1297	0.3566	0.5161
8	0.1397	0.3420	0.5339
9	0.1376	0.3627	0.5221
10	0.1363	0.2498	0.5520
Mean Value	0.1329	0.3007	0.5621
Standard Deviation	0.0071	0.0433	0.0299

Table 11 – Sound absorption coefficient at 125, 250, 500 *Hz*, mean value of the curves and respective standard deviation for the glaswool pure sample placed 10 times into the sample holder - rectangular samples.

Placing	**Frequency (*Hz*)**		
	125	**250**	**500**
1	0.1243	0.3032	0.4869
2	0.1199	0.3347	0.4826
3	0.1466	0.3220	0.3981
4	0.1270	0.3535	0.4073
5	0.1235	0.2722	0.4016
6	0.1385	0.3137	0.4897
7	0.1380	0.2380	0.4982
8	0.1441	0.2154	0.5090
9	0.1311	0.2568	0.4968
10	0.1352	0.2414	0.4956
Mean Value	0.1328	0.2851	0.4666
Standard Deviation	0.0091	0.0467	0.0450

For the cases of gains (positive values) observed in Tabs. 8 and 9, the values are of the same order of magnitude than the respective standard deviation for each material.

It is possible to verify that for the samples RR1, RR3, RR2P and RR3P at 125 Hz, and for the samples RR1, RR3, RR1P and RR3P at 500 Hz, the losses in absorption (negative

values) are one order of magnitude higher than the standard deviation. This also occurs for all samples of glasswool in the frequency of 125 Hz.

4.1.1.5 Comparing results obtained at the two impedance tubes

The sound absorption at two different frequency ranges were evaluated considering the tests of the two impedance tubes. For the circular samples, representing the frequency range of 125 - 2500 Hz, there were gains at sound absorption above 1000 Hz for rockwool samples with mesopores not filled and filled with glasswool. For the glasswool circular samples, these samples presented the higher gains: at 250 Hz for samples G3 ($\phi_p = 0.04$), G4 ($\phi_p = 0.08$), G5 ($\phi_p = 0.11$), GP2 ($\phi_p = 0.03$), GP3 ($\phi_p = 0.04$), GP5 ($\phi_p = 0.11$) and GP6 ($\phi_p = 0.14$); and at 2000 Hz for glasswool samples G4 ($\phi_p = 0.08$), GP5 ($\phi_p = 0.11$) and GP6 ($\phi_p = 0.14$).

In addition, for the majority of the samples tested in the impedance tube of rectangular cross-section, for both rockwool and glasswoll, there were small losses at absorption. For the case of specific bandwidths there were gains in sound absorption (around 250 Hz for glasswool and around 500 Hz for rockwool).

Considering the results of the two impedance tubes, the gains in absorption produced by double porosity for rockwool were found concentrated at higher frequencies (1000 - 2000 Hz) for circular samples and at 250 Hz for rectangular samples. For the double porosity glasswool samples, gains were presented around 250 Hz for the circular samples with mesopores filled (especially samples with greater mesoporosity, cases GP5 and GP6), and also at500 Hz for rectangular samples.

For both impedance tubes, it was not noticed gains in absorption when comparing the sample with mesopores filled with the same sample with mesopores not filled when considering the same type of sample (same mesoporosity and cell size). This result was noticed in the work of Gourdon and Seppi (2010) and was explained in Sec. 2.5.2. Two circular rockwool samples with same mesoporosity were compared in Fig. 43 to verify this situation.

As it can be seen in Fig. 43, samples with mesopores filled and not filled presented insignificant differences for the same mesoporosity in the interval of frequencies 125 to 200 Hz.

In studies of Atalla et al. (2001), Sgard et al. (2005) and Gourdon and Seppi (2010), high percentual gains of sound absorption at low frequencies comparing double porosity samples to the correspondent single porosity sample were verified. The diffusion frequency (ω_d), described in Equation 2.33, can be calculated for the samples of the rockwool and glasswool used in this study. The diffusion frequency describes the region in frequency where gains in absorption for double porosity materials are expected. This analysis is made in Section 4.3.

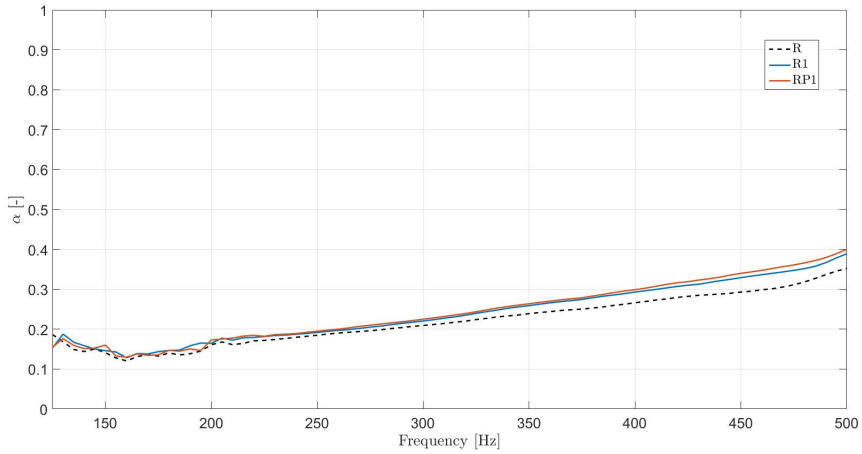

Figure 43 – Variation of absorption for circular samples R, R1 (mesopores not filled) and RP1 (mesopores filled with glasswool).

4.1.2 Results of sound transmission loss tests

The influence of double porosity was also investigated for sound transmission loss (TL) for the samples of the impedance tube of circular cross-section. The samples were the same used for sound absorption tests and are described in Tab.3 in Section 4.1.1.1. In this case it was only tested the samples with mesopores filled.

For rockwool samples with mesopores filled with glasswool, TL is presented in Fig. 44. In this case, only RP1 and RP2 showed higher values of TL when compared to the pure case R. The better performance in insulation appeared in the samples with the lowest values of mesoporosity. This can be probably caused due to the lower value for the insulation of glasswool itself, which can be observed in Fig. 45.

For glasswool samples with mesopores filled with rockwool all the samples, except GP5, presented similar results, as presented in Figure 45. Only curve GP5 can be highlighted from the others in all frequencies.

Double porosity glasswool and rockwool curves showed ripples in the regions of 125 - 500 Hz and 500 - 1000 Hz, respectively, as verified in Figs. 44 and 45. In this cases, the presence of the ripples is due to the mean values of the replicas as described in Section 4.1.1.1. When processing the mean values of the three replicas it was noticed that the minimum values of TL varied for each replica and also for the two different frequency ranges related to the operation of the impedance tube.

Considering the mean values of the replicas for each sample it is noticed that for rockwool, the value of the TL minimum region in frequency is increased in frequency by the use of the mesopores with glasswool. The opposite is observed for the glasswool samples with double porosity, i.e., the value of TL minimum region decreased in frequency. This effect is caused by the changes between the pure sample and the double porosity samples.

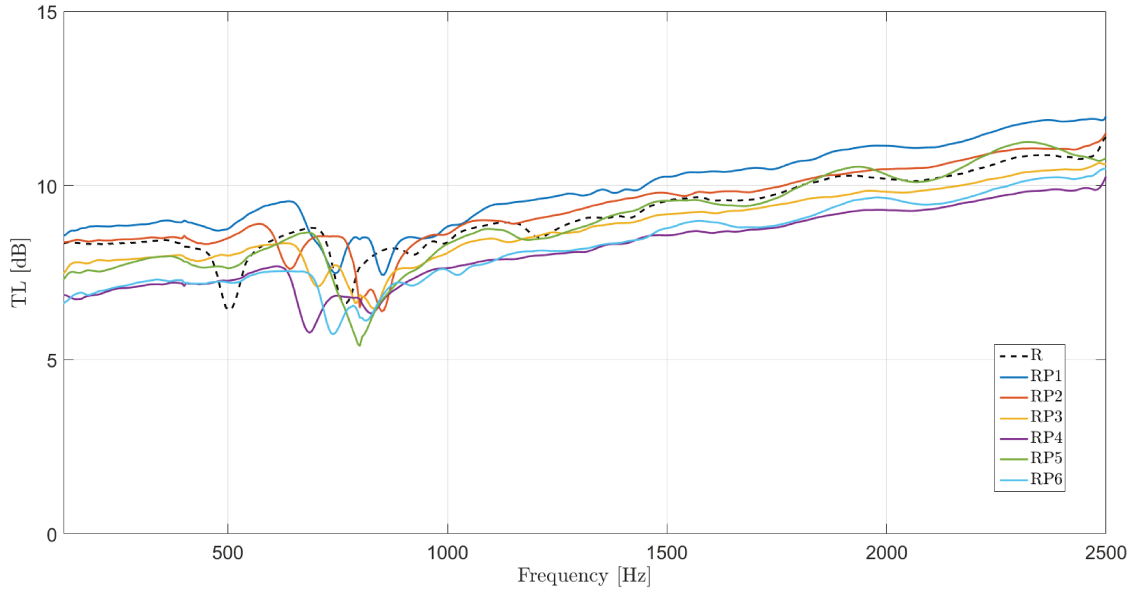

Figure 44 – Sound transmission loss for pure sample and samples with mesopores filled - rockwool substract - circular samples.

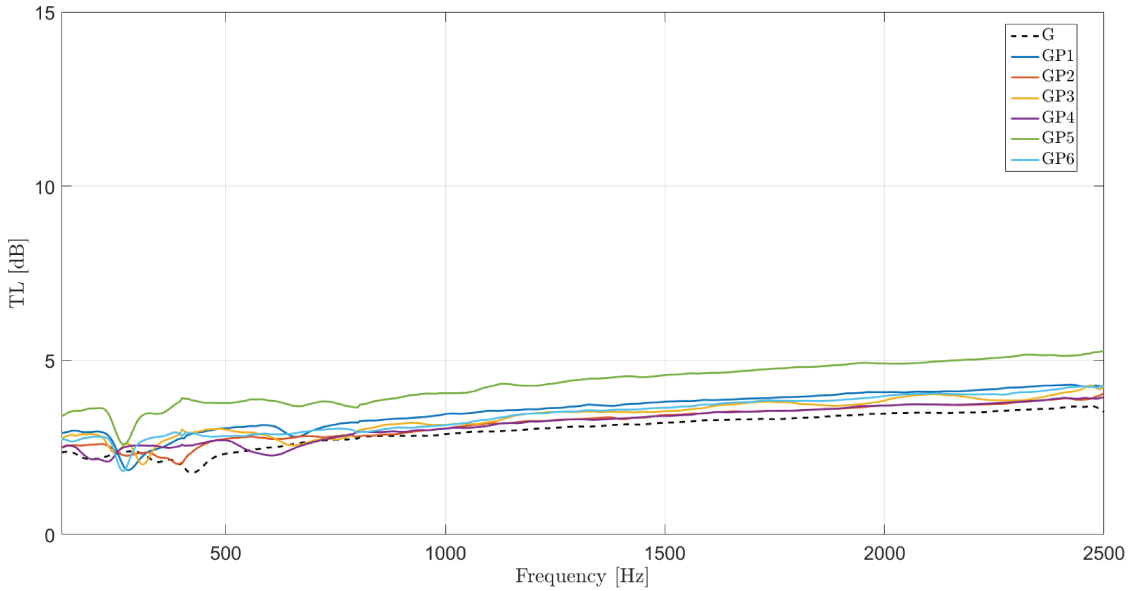

Figure 45 – Sound transmission loss for pure sample and samples with mesopores filled - glasswool substract - circular samples

Table 12 shows TL values for each sample and the absolute gain (Δ) in decibel scale at frequencies 250, 500, 1000 and 2000 Hz. It is noticed that the gains are concentrated around 500 Hz. The minimum region for pure glasswool is around 400 Hz and for rockwool 500 Hz, so the double porosity samples provided gains specially in 500 Hz.

The percentage gains for TL, are presented at Tab. 13. However, in this case, the analysis is made using the transmission coefficient (τ), as it was defined by Equation 2.4, because TL is defined on a logarithmic scale and τ uses a linear scale. This conversion can be

Table 12 – Sound transmission loss values for samples and absolute gains, at 250, 500, 1000 and 2000 *Hz* obtained by the modified rockwool (RPn) and glasswool (GPn) samples compared to the pure cases (R and G) - circular samples

Sample TL (dB)	**Frequency (*Hz*)**							
	250	Δ_{250}	**500**	Δ_{500}	**1000**	Δ_{1000}	**2000**	Δ_{2000}
R	8.3	0.0	6.4	0.0	8.4	0.0	10.2	0.0
RP1	8.9	0.5	8.8	2.3	8.8	0.5	11.1	1.0
RP2	8.4	0.1	8.5	2.1	8.6	0.2	10.5	0.3
RP3	7.9	-0.5	8.0	1.6	8.1	-0.3	9.8	-0.4
RP4	7.0	-1.3	7.3	0.8	7.6	-0.7	9.3	-0.9
RP5	7.7	-0.7	7.6	1.2	8.3	0,0	10.3	0.1
RP6	7.1	-1.2	7.2	0.8	7.6	-0.8	9.6	-0.6
G	2.3	0,0	2.3	0.0	2.9	0.0	3.5	0,0
GP1	2.4	0.1	3.1	0.7	3.5	0.6	4.1	0.6
GP2	2.4	0.1	2.7	0.4	3.0	0.2	3.7	0.2
GP3	2.3	0.0	3.0	0.7	3.1	0.3	3.8	0.4
GP4	2.3	0.0	2.7	0.4	3.0	0.2	3.7	0.2
GP5	2.9	0.6	3.8	1.5	4.1	1.2	4.9	1.4
GP6	2.2	-0.1	2.8	0.5	3.1	0.3	4.0	0.5

considered suitable for a percentage analysis.

The experimental values of TL were obtained in decibel scale and could be converted to linear scale by Equation 2.5. This leads to the following expression:

$$\tau = \frac{1}{10^{\frac{TL}{10}}} \tag{4.1}$$

In this case, the percentage gain in sound insulation, is expressed as:

$$\%_\tau = 100\frac{\tau_{pure} - \tau_{modified}}{\tau_{pure}} \tag{4.2}$$

where τ_{pure} is the transmission coefficient for pure samples R and G, and $\tau_{modified}$ is the transmission coefficient for modified samples Rn, RPn, Gn and GPn. Using Eq. 4.2, gains in insulation or losses in transmission coefficient, are represented by positive values.

Analyzing Tab. 13, it is noticed a maximum gain of 23% for the curve RP1 at 500 *Hz* and also a great loss of 16% for the curve RP4 at 250 *Hz*, for rockwool samples. For glasswool samples, the maximum gain (15%) in insulation occurs for GP5 curve at 500 and 2000 *Hz* and the only situation of loss is for GP6 curve at 250*Hz*. These tables shows that the modified samples provided considerable gains restricted to some frequencies and some samples.

For transmission loss, using double porosity samples, the curves were offseted in the entire frequency range studied compared to the respective single porosity case, as it was noticed in Figs 44 and 45. In the study of Sgard and Atalla (2000), described in Section 2.5.4,

Table 13 – Transmission coefficient values (τ) for all samples and percentage gains, at 250, 500, 1000 and 2000 Hz obtained by the modified rockwool (RPn) and glasswool (GPn) samples compared to the pure cases (R and G) - circular samples

Sample	**Frequency (Hz)**							
	250	$\%_{250}$	**500**	$\%_{500}$	**1000**	$\%_{1000}$	**2000**	$\%_{2000}$
R	0.3830	0.0%	0.4767	0.0%	0.3815	0.0%	0.3095	0.0%
RP1	0.3610	5.7%	0.3650	23.4%	0.3621	5.1%	0.2774	10.4%
RP2	0.3782	1.2%	0.3763	21.1%	0.3711	2.7%	0.2997	3.2%
RP3	0.4043	-5.6%	0.3987	16.4%	0.3951	-3.6%	0.3229	-4.3%
RP4	0.4445	-16.1%	0.4335	9.1%	0.4156	-8.9%	0.3431	-10.9%
RP5	0.4132	-7.9%	0.4158	12.8%	0.3835	-0.5%	0.3052	1.4%
RP6	0.4419	-15.4%	0.4357	8.6%	0.4185	-9.7%	0.3298	-6.6%
G	0.7659	0.0%	0.7659	0.0%	0.7175	0.0%	0.6708	0.0%
GP1	0.7543	1.5%	0.7034	8.2%	0.6715	6.4%	0.6249	6.8%
GP2	0.7599	0.8%	0.7289	4.8%	0.7047	1.8%	0.6528	2.7%
GP3	0.7642	0.2%	0.7069	7.7%	0.6961	3.0%	0.6423	4.3%
GP4	0.7653	0.1%	0.7328	4.3%	0.7046	1.8%	0.6530	2.7%
GP5	0.7150	6.6%	0.6476	15.4%	0.6269	12.6%	0.5683	15.3%
GP6	0.7764	-1.4%	0.7220	5.7%	0.6970	2.9%	0.6327	5.7%

it was only found gains in *TL* in a specific frequency, 1000 Hz, probably linked to the type of inclusion utilized, in their case a polyestirene inclusion.

For sound transmission loss tests the same repeatability test was done as in the case of sound absorption. Replacements were carried out 10 times to one sample of pure glasswool (G) and one sample of pure rockwool (R) and the effect of positioning the samples was not significant for TL.

4.2 Experimental determination of physical parameters of porous materials

4.2.1 Values obtained for porosity using X-ray microtomography

The porosity estimation of pure rockwool and pure glasswool was done by the use of the X-ray microtomography technique. The obtained 2D images were converted to binary representation and the estimation was made according to the number of white pixels compared to the global number of pixels with the use of Image J software.

The following test configurations were used for both materials and all samples: resolution of 7.5 μm (pixel length) and X-ray source voltage of 60 kV. Samples used in this test were taken from different positions on the same panel to verify if there are porosity variations at the same panel.

4.2.1.1 Glasswool

Four samples of glasswool were tested and the porosity estimation was made for each one. Table 14 shows the values obtained for each sample, the mean value and the standard deviation.

Table 14 – Porosity values for glasswool using X-ray microtomography.

Samples	**Porosity**
Sample A	0.9812
Sample B	0.9764
Sample C	0.9649
Sample D	0.9627
Mean Value	0.9713
Standard Deviation	0.0089

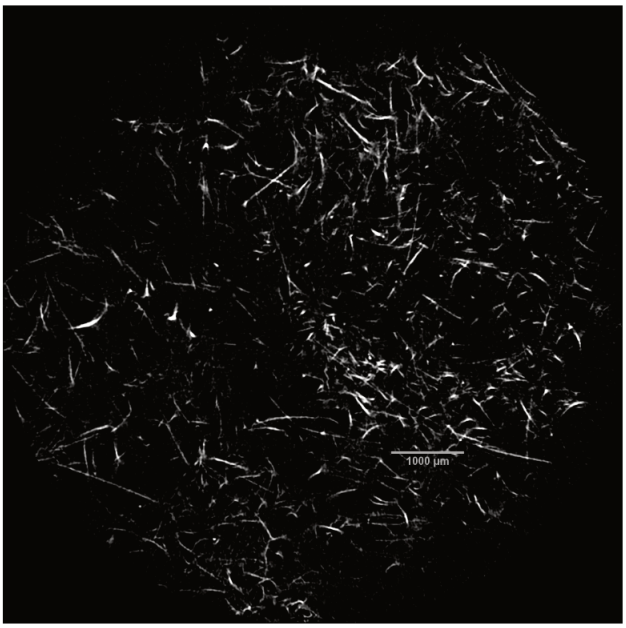

Figure 46 – 2D image of one cross section of glasswool obtained using X-ray microtomography.

The value of porosity for glasswool can be assumed as 97%, because usually porosity is presented with only two significant digits, as in the studies of Atalla *et al.* (2001), Sgard *et al.*(2005) and Gourdon and Seppi (2010). The value of standard deviation shows a good agreement between samples. In Figs. 46 and 47 it is noticed that there is no preferential direction of the fibers of glasswool.

4.2.1.2 Rockwool

Four samples of rockwool were tested and the porosity estimation was made for each one. Table 15 shows the values obtained for each sample, the mean value and the standard deviation. Figure 48 shows one cross section obtained with microtomography for one of the

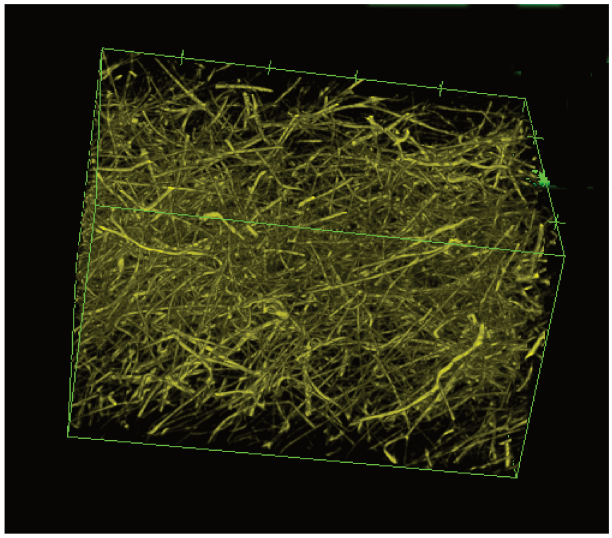

Figure 47 – 3D view of glasswool obtained using X-ray microtomography - each division corresponds to 1000 μm.

rockwool samples. Also, Fig. 49 shows the 3D reconstruction of a rockwool piece done at Image-J software.

Table 15 – Porosity values for rockwool using X-ray microtomography.

Samples	**Porosity**
Sample A	0.9641
Sample B	0.9690
Sample C	0.9689
Sample D	0.9733
Mean Value	0.9688
Standard Deviation	0.0037

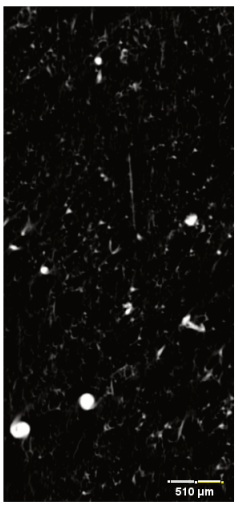

Figure 48 – 2D image of one cross section of glasswool obtained using X-ray microtomography.

The value of porosity for rockwool can be assumed as 97%. The mean and the standard deviation values implies that porosity is very similar between these samples. From

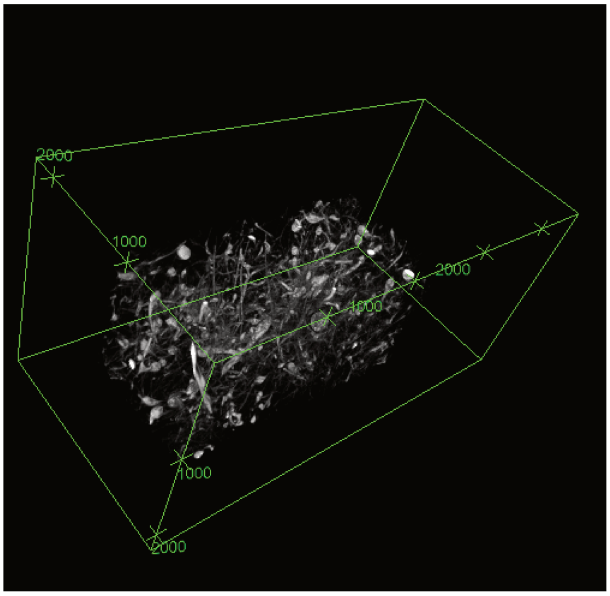

Figure 49 – 3D view of rockwool obtained using X-ray microtomography - units in μm.

figures 48 and 49, it is observed that there is no preferential direction to the fiber orientation. However, it is noticed the presence of small particles in the structure of rockwool, probably with different density from the fibers. The pixels related to this particles are lighter in color, indicating higher density at the X-ray image. Some of these particles can be visualized at naked eye, which can be seen in Fig. 50.

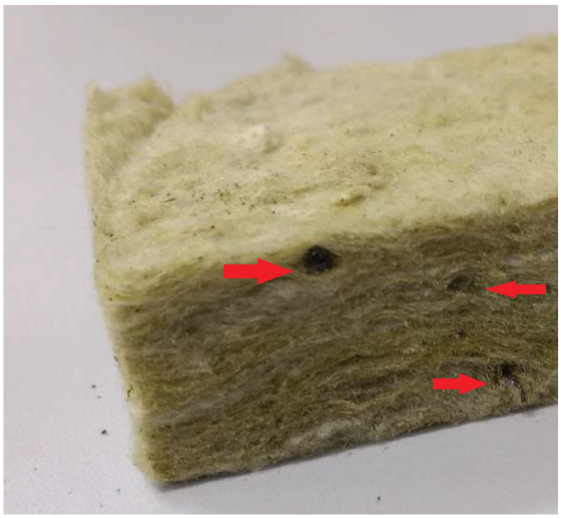

Figure 50 – Rockwool with small dark particles.

4.2.2 Values obtained for tortuosity using ultrasound measurements

Using the experimental methodology described in Section 3.3, values of tortuosity were measured for six samples of pure rockwool and pure glasswool. The samples were taken from two panels at different positions on the same panel. The samples were circular with 60 *mm* diameter and the panel thickness was preserved in the samples. The equipment used was an

Agricer US Lab ultrasound pulse/receiver and an apparatus that was developed in order to hold the sample and to maintained the transducers in the same position during the measurement. The ultrasound equipment and the apparatus are indicated in Fig. 51. The working frequency of the Pulser was 25 kHz.

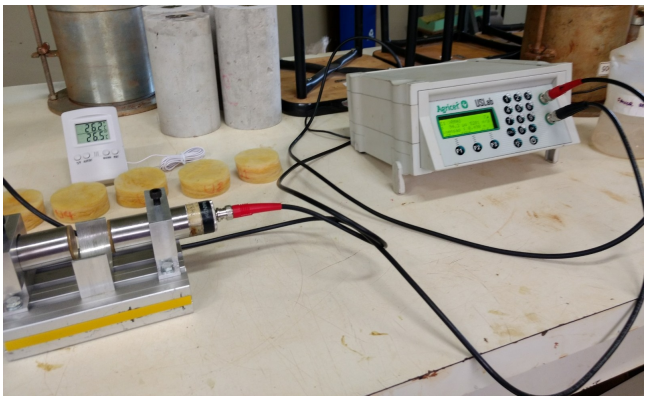

Figure 51 – Ultrasound equipment and measurement apparatus for tortuosity measurement.

Six different samples for each material were measured in the following way: the sample was placed in the sample holder between the two transducers, the pulser and the receiver, and the time for the wave to propagate through the sample was recorded. After, the sample was removed from the middle of the transducers and the separation between them was maintained, and the time of the ultrasound wave to propagate in air were recorded. This procedure was repeated three times for each sample (RP1, RP2, RP3), with RP referring to repetition. The rockwool samples were named as UR1,..., UR6 and the glasswool samples were named as UG1,..., UG6.

Figure 52 shows a measurement procedure of a glasswool sample. Table 16 and Tab. 17 shows the results for the time of the ultrasound wave propagating between the transducers with and without the samples. The separation of transducers are also presented, which corresponds to the thickness of the samples used.

Table 16 – Time of ultrasound waves propagating between transducer with and without samples for rockwool samples.

Sample	**Transducer separation (mm)**	**Time with sample (μs)**				**Time without sample (μs)**			
		RP1	**RP2**	**RP3**	**Mean**	**RP1**	**RP2**	**RP3**	**Mean**
UR1	24.9	113.5	113.3	113.1	113.3	86.3	85.9	86.2	86.1
UR2	26.4	113.5	113.6	113.4	113.5	88.8	89.2	89.1	89.0
UR3	26.2	112.4	112.4	112.5	112.4	88.5	89.5	89.3	89.1
UR4	27.7	110.2	110.3	110.4	110.3	93.5	93.8	93.7	93.7
UR5	27.9	110.4	110.3	110.5	110.4	93.9	94.4	93.8	94.0
UR6	28.3	111.9	112.1	111.9	112.0	94.5	94.2	94.9	94.5

First, it was calculated the velocity of propagation of the ultrasonic wave by the expression: $C = \Delta(x)/time$, where $\Delta(x)$ is the separation of the transducers, which was maintained

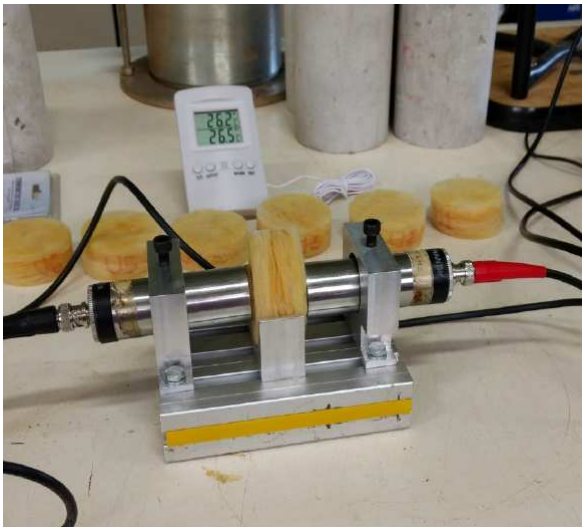

Figure 52 – Tortuosity measurement using ultrasound measurement for a glasswool sample.

Table 17 – Time of ultrasound waves propagating between transducer with and without samples for glasswool samples.

Sample	**Transducer separation (mm)**	**Time with sample (μs)**				**Time without sample (μs)**			
		RP1	**RP2**	**RP3**	**Mean**	**RP1**	**RP2**	**RP3**	**Mean**
UG1	29.3	114.8	114.4	114.3	114.5	94.5	94.3	94.3	94.4
UG2	26	115.5	115.7	115.5	115.6	88.7	88.6	88.4	88.6
UG3	25.9	116	116.3	116.5	116.3	89	88.6	88.4	88.7
UG4	23.2	114.2	114.2	114.2	114.2	81.3	81.5	81.8	81.6
UG5	26.8	116.2	116.5	116.4	116.4	90	90.7	90.2	90.3
UG6	28.3	113.5	114.3	113.9	114.0	94.3	94.5	93.9	94.2

constant at the measurements with and without sample; and time is the mean time of the ultrasound wave to propagate between transducers. This calculation was done for the cases with and without the sample, leading to the values of C_{is} and C_i, respectively, presented in Section 3.3. Finally, using Equation 3.33 the tortuosity of each sample was calculated. Results of tortuosity are presented in Tabs. 18 and 19.

Table 18 – Values of tortuosity for each sample of glasswool, mean value and standard deviation of the samples.

Sample	**Tortuosity**
UG1	1.7303
UG2	1.6251
UG3	1.5923
UG4	1.3867
UG5	1.3784
UG6	1.4028
Mean Value	1.5193
Standard Deviation	0.1497

The results obtained for rockwool and glasswool tortuosity are similar, with the

Table 19 – Values of tortuosity for each sample of rockwool, mean value and standard deviation of the samples.

Sample	**Tortuosity**
UR1	1.4722
UR2	1.7026
UR3	1.7195
UR4	1.9618
UR5	1.6607
UR6	1.4610
Mean Value	1.6630
Standard Deviation	0.1815

value of rockwool a slightly higher than for glasswool. The values of tortuosity are expressed with one decimal digit because of the resolution of the equipment utilized in the measurement, so α_∞ = 1.7 for rockwool and α_∞ = 1.5 for glasswool. Considering the images obtained from the Scanning electron microscopy analysis (presented in Appendix B), it is possible to see the similarity of the structures of the pores in both materials, especially the distribution of the fibers on the materials. This contributes to similar values of tortuosity, which is a parameter linked to the geometry of the pores.

The results of tortuosity of fibrous porous materials are on the interval of 1 - 1.06 according to Cox and D'Antonio (2009). For rockwool, values of tortuosity found in articles are α_∞ = 2.1 (higher density rockwool) in Sgard et al. (2005) and Atalla *et al.* (2001); and α_∞ = 1.07 (lower density rockwool) in Gourdon and Seppi (2010). Additionally, for glasswoool only, α_∞ = 1 in Atalla *et al.* (2001). It is possible to verify some differences between the obtained values compared to the values obtained in the references. Also, it is possible to verify differences between the reported values of the references. This can be due to different techniques of measurements and even due to differences in the materials.

4.3 Diffusion frequency estimation

Considering the experimental results obtained in Sec. 4.1.1 and the sound propagation in the double porosity described in Sec. 2.5.1, it is possible to compare the experimental results with what was predicted by the double porosity sound propagation theory by the estimation of the diffusion frequency, which is the frequency region where the sound absorption increases for a double porosity, due to the pressure diffusion effect.

To verify the diffusion frequency value for each sample, calculations were made using the values of porosity and tortuosity given in Secs. 4.2.1 and 4.2.2. Also, values of flow resistivity of glasswool and rockwool are necessary. According to Sgard et al. (2005), the value of flow resistivity for rockwool is σ= 135000 Ns/m^4, and according to Vigran (2008) the value of flow resistivity for glasswool is σ= 9000 Ns/m^4. These values were selected considering

materials with densities similar to the densities of the rockwool and glasswool of the samples.

The diffusion frequency can be calculated using Eqs. 2.64 and 2.69. The value of ω_d only depends on the physical parameters of the substrate material, even in the case where the mesopores were filled. Considering the values of mesoporosity and hole radius for the circular and rectangular samples given in Tabs. 3 and 7, the values of diffusion frequency were calculated and are presented in Tabs. 20 and 21 for circular samples and in Tabs. 22 and 23 for rectangular samples. In the case of the circular samples, the size of the squared cell (L_c) utilized was the one that provides the same area of a circle of 60 *mm* radius, i.e, $L_c = 0.106\ m$.

Table 20 – Diffusion frequency for circular rockwool samples.

Sample	ω_d ***(rad/s)***	f_d ***(Hz)***
R1, RP1	257	41
R2, RP2	381	60
R3, RP3	433	68
R4, RP4	631	100
R5, RP5	784	125
R6, RP6	948	151

Table 21 – Diffusion frequency for circular glasswool samples.

Sample	ω_d ***(rad/s)***	f_d ***(Hz)***
G1, GP1	3855	613
G2, GP2	5714	909
G3, GP3	6498	1034
G4, GP4	9464	1507
G5,GP5	11758	1871
G6, GP6	14215	2262

In the case of circular samples, because there is only one unit cell, it is not possible to assure that the diffusion frequency is correctly estimated, since the analytical model supposes periodicity of the medium. However, the values are presented to verify if it is possible to establish a relationship between the diffusion frequency and the experimental results for circular samples.

Considering the circular samples, it is noticed that for rockwool, the frequency of diffusion was below the measurement range (125 - 2500 *Hz*), except for samples R6 and RP6. However, these two samples did not present gains around 151 *Hz* compared to the pure case *R*, as showed in Figs. 28 and 29. In the case of glasswool samples, only the samples G2, GP2, G4, GP4, GP5 and GP6 presented gains in absorption around their respective diffusion frequency, as indicated in Figs. 32 and 33.

It was not perceived a peak in sound absorption around the diffusion frequencies. The curve was displaced in some frequency range, depending on the sample, compared to the

pure case. In this case, it was not possible to establish a relationship with the circular samples and the diffusion frequency.

Table 22 – Diffusion frequency for rectangular rockwool samples.

Sample	ω_d *(rad/s)*	f_d *(Hz)*
RR1, RR1P	3009	479
RR2, RR2P	1196	190
RR3, RR3P	11446	1821
RR4, RR4P	4433	706

Table 23 – Diffusion frequency for rectangular glasswool samples.

Sample	ω_d *(rad/s)*	f_d *(Hz)*
GR1, GR1P	45140	7184
GR2, GR2P	1794	2855
GR3, GR3P	17170	27326
GR4, GR4P	6649	10583

Tables 20 and 21 show that the diffusion frequency of the samples RR3P and RR3 and all glasswool samples are beyond the measurement frequency range of the impedance tube of rectangular cross-section (20 - 717 *Hz*). For the rockwool samples RR1, RR1P, RR2, RR2P, RR4 and RR4P, there was not any gain in absorption at the region of the respective diffusion frequencies, even if these values are between 20 - 717 *Hz*.

It is noticed that there was not an agreement between the diffusion frequency values and the regions were the gains were identified for some samples.

4.4 Analytical model analysis

The analytical models described in Sec. 2.5.3 were utilized to verify the adherence of the model to the experimental data. Only the samples measured at the impedance tube of rectangular cross-section were utilized in this analysis, because they have periodical mesopores, and these models are based on the assumption of a periodic medium.

Considering the experimental data, an adjustment of the curve was made using the non-linear least-squares curve fitting on Matlab software (*lsqcurvefit* command). In this case, the least-squares method were used to adjust the prediction model to the experimental data. The purpose of this adjustment is to verify if the experimental curve presents a good correlation to the experimental data. A brief explanation of how the adjustment is made using the least-squares method is presented in Appendix C.

The values of mesoporosity (ϕ_p), cell size (L_c), hole radius (R), microporosity (ϕ_m) and tortuosity ($\alpha_{\infty m}$) of each sample are the input variables of the problem (known parameters). Also, the air properties used on the analytical model were: $P_0 = 945\ hPa$, $\eta = 1.846 \times 10^5\ kg/ms$

, $\kappa = 2.26\times10^{-2}\ W/mK$ and ρ_0 was calculated using the previous parameters according to Eq.3.14. These paramaters were based on the temperature of 27^oC or 300 K.

The input variables are described in Tabs. 24 and 25 for the samples that were analyzed. Samples of same mesoporosity and size of cell were chosen, variating the frame material and if mesopores are filled or not.

Table 24 – Input parameters for the adjust of curves of samples with mesopores not filled.

Input Parameter	Sample	
	RR1	GR1
ϕ_p	0.25	0.25
R (mm)	22.6	22.6
L_c (mm)	80	80
ϕ_m	0.97	0.97
$\alpha_{\infty m}$	1.7	1.5

Table 25 – Input parameters for the adjust of curves of samples with mesopores filled.

Input Parameter	Sample	
	RR1P	GR1P
ϕ_p	0.25	0.25
R (mm)	22.6	22.6
L_c (mm)	80	80
ϕ_{m1}	0.97	0.97
$\alpha_{\infty m1}$	1.7	1.5
ϕ_{m2}	0.97	0.97
$\alpha_{\infty m2}$	1.5	1.7

The estimated values of flow resistivity σ_m, viscous characteristic length (Λ_m), thermal characteristic length (Λ'_m) and the static thermal permeability ($\Theta_m(0)$) (unknown parameters) are given as the output of the curve fitting, however, a dependency between the variables were assumed. The expression of Microscopic Viscous Dynamic Permeability (Φ_m) used at the double porosity models, comes from the work of Champoux and Allard (1991) and is given by:

$$\Lambda = b\sqrt{\frac{8\alpha_\infty\eta}{\sigma\phi}}, \tag{4.3}$$

where b is a coefficient that lies between 0.25 to 1 for porous materials (CHAMPOUX; ALLARD, 1991). The value adopted for b was b= 0.78 for glasswool and b= 0.99 for rockwool (KINO; UENO, 2007). As the values of ϕ and α_∞ are given as input parameters, the output parameters Λ and σ are linked.

The values of the estimated parameters are static, so they are frequency independent as defined in Sec. 2.4.

The output variables received lower and upper limits to the solution of the least-squares non linear curve fitting. The values used were: $10^3 \leq \sigma \leq 10^6$; $100 \times 10^6 \leq \Lambda' \leq 200 \times 10^6$; $10^{-10} \leq \Theta_m(0) \leq 10^{-8}$ (SGARD *et al.*, 2005)(GOURDON; SEPPI, 2010)(JAOUEN, 2018). Λ was calculated according to the σ output value, so it was not directly constrained.

The termination tolerance for the objective function variation was 10^{-6} and the termination tolerance of output parameters variation was 10^{-12}.

The initial point is described as X_0=[$\sigma, \Lambda', \Theta_m(0)$]. For rockwool it was used X_0 =[$135000, 100 \times 10^{-6}, 3.3 \times 10^{-9}$] and for glasswool X_0 =[$9000, 100 \times 10^{-6}, 3.3 \times 10^{-9}$]. These initial values were based on the values presented on the articles of Atalla *et al.*(2001), Sgard *et al.* (2005), Gourdon and Seppi (2010) and in the book of Vigran (2008).

The curve fitting for the rockwool sample with mesopores not filled is presented in Fig. 53 and the output values obtained in this adjustment are presented in Tab. 26. In this figure it is possible to see that the experimental data and the adjusted curve have a different behavior. However, in this case, the experimental data curve is influenced by the absorption of the empty impedance tube, discussed in Appendix A, which have complicated the curve adjustment.

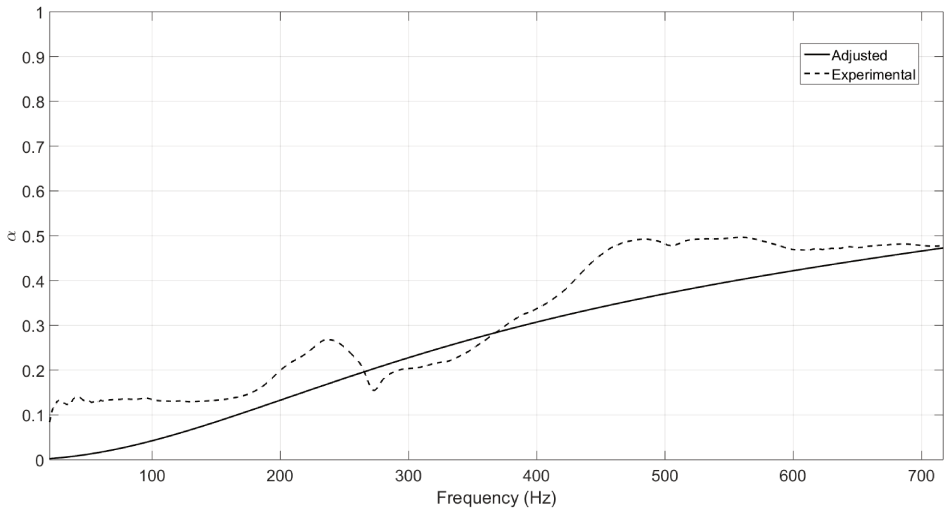

Figure 53 – Comparison between experimental curve data and analytical model curve fitting for sample R1.

Figure 54 shows the curve fitting for the glasswool sample GR1, with mesopores not filled. Table 26 presents the output values of this adjustment. In this case, the experimental data followed the behavior of the adjusted curve.

To quantify the differences from the experimental data and in the curve fitting, Tab. 27 and Tab. 28 shows the sound absorption coefficient at 125, 250 and 500 *Hz* for the samples RR1 and GR1, respectively. Δ represent the difference between the adjusted sound absorption coefficient to the experimental one and % the percentage difference.

Considering here that a good agreement between the experimental data and the

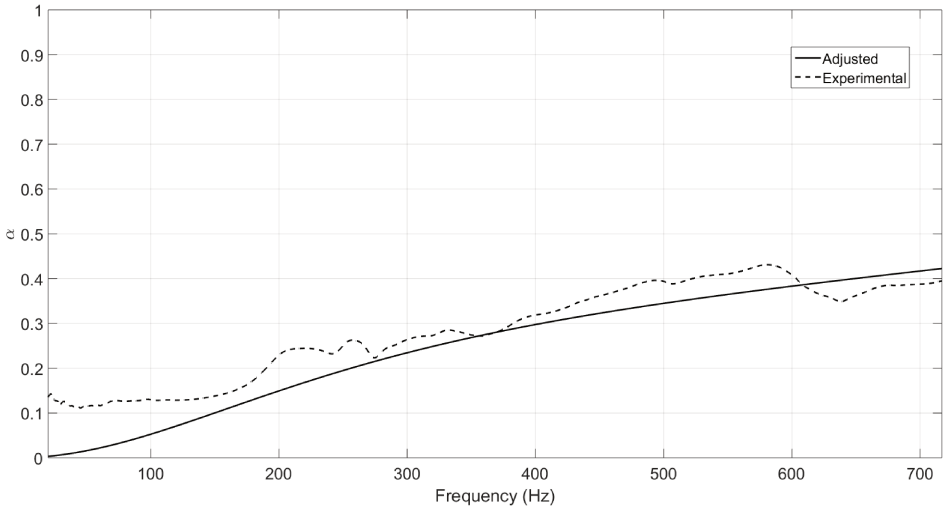

Figure 54 – Comparison between experimental curve data and analytical model curve fitting for sample G1.

Table 26 – Output parameters for the adjustment of samples with mesopores not filled.

Output Parameter	**Sample**	
	RR1	GR1
σ_m (Ns/m^4)	131339.4	168643.1
Λ_m (m)	43.9×10^{-6}	30.6×10^{-6}
Λ'_m (m)	110.9×10^{-6}	198.2×10^{-6}
$\Theta_m(0)$ (m^2)	0.8×10^{-9}	2.7×10^{-9}

Table 27 – Experimental and adjusted sound absorption coefficient at 125, 250 and 500 *Hz* - RR1 sample.

RR1 / Frequency (*Hz*)	**125**	**250**	**500**
α experimental	0.1305	0.251	0.4817
α curve fitting	0.0625	0.1816	0.3705
Δ	-0.068	-0.0694	-0.1112
%	-52%	-28%	-23%

Table 28 – Experimental and adjusted sound absorption coefficient at 125, 250 and 500 *Hz* - GR1 sample.

GR1/ Frequency (*Hz*)	**125**	**250**	**500**
α experimental	0.129	0.2525	0.394
α curve fitting	0.0758	0.1949	0.3448
Δ	-0.0532	-0.0576	-0.0492
%	-41%	-23%	-12%

adjusted curve would be given by a $\Delta \leq 0.05$ for each evaluated frequency, the adjustment of the RR1 data was not satisfactory, considering 125, 250 and 500 Hz. In the case of the GR1, considering the differences obtained at 125, 250 and 500 Hz, the adjustment can be considered satisfactory only at 500 Hz. For both cases, the adjustment for frequencies below 100 Hz do not

satisfies $\Delta \leq 0.05$ as can be visualized in Figs. 53 and 54.

Figures 55 and 56 shows the curve adjustments for the rockwool sample with mesopores filled with glasswool and the glasswool sample with mesopores filled with glasswool, respectively. It is noticed that in the case of the rockwool, the model could not fit very well to the experimental data. On the other hand, the fitting was visually satisfactory for the glasswool sample GR1P.

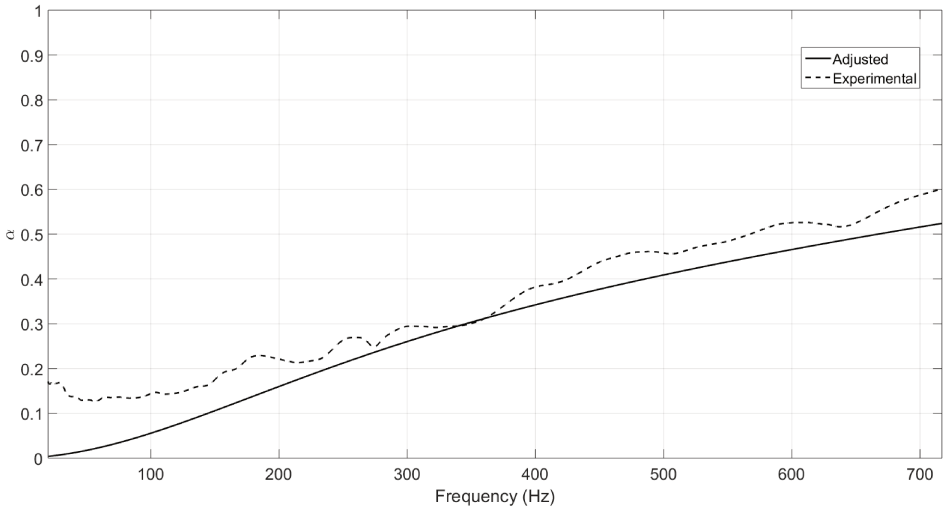

Figure 55 – Comparison between experimental curve data and analytical model curve fitting for sample RR1P.

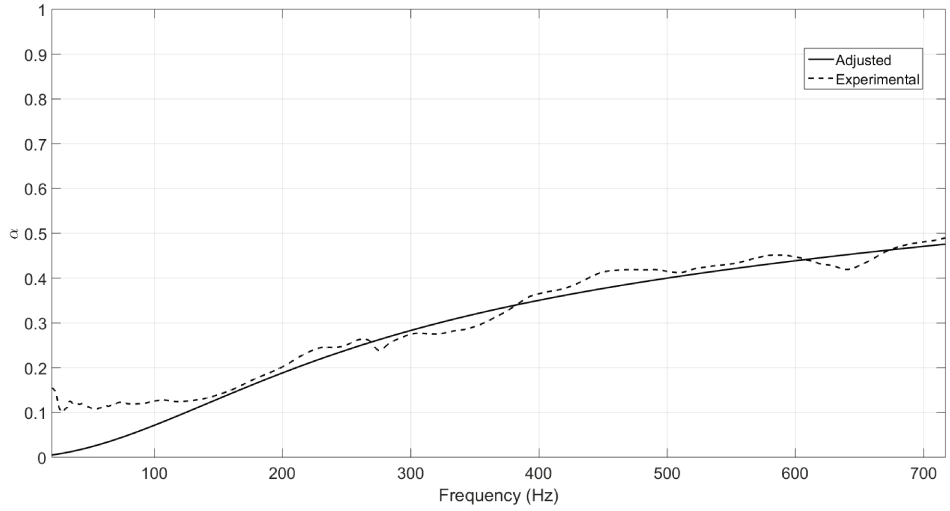

Figure 56 – Comparison between experimental curve data and analytical model curve fitting for sample GR1P.

Tables 27 and 28 shows the sound absorption coefficient at 125, 250 and 500 *Hz* and the differences obtained for the samples RR1P and GR1P, respectively. Analyzing the results given by these tables, it is noticed that for the RR1P sample, the adjustment was satisfactory only at 500 *Hz*, and for the GR1P sample, the adjustment was satisfactory for the three frequen-

Table 29 – Output parameters for the adjustment of samples with mesopores filled.

Output Parameter	**Sample**	
	RR1	GR1
σ_{m1} (Ns/m^4)	122152.0	115595.6
Λ_{m1} (m)	45.6×10^{-6}	34.7×10^{-6}
Λ'_{m1} (m)	199×10^{-6}	171×10^{-6}
$\Theta_{m1}(0)$ (m^2)	7.8×10^{-9}	9.9×10^{-9}
σ_{m2} (Ns/m^4)	14419.0	100000
Λ_{m2} (m)	98.0×10^{-6}	50.3×10^{-6}
Λ'_{m2} (m)	170.0×10^{-6}	199×10^{-6}
$\Theta_{m2}(0)$ (m^2)	9.9×10^{-9}	9.9×10^{-9}

cies analyzed. In this case, below 80 Hz the difference between curves do not satisfies $\Delta \leq 0.05$ as can be visualized in Figs. 55 and 56.

Table 30 – Experimental and adjusted sound absorption coefficient at 125, 250 and 500 Hz - RR1P sample.

RR1P / Frequency (Hz)	**125**	**250**	**500**
α experimental	0.1484	0.2638	0.458
α curve fitting	0.0798	0.2123	0.4089
Δ	-0.0686	-0.0515	-0.0491
%	-46%	-20%	-11%

Table 31 – Experimental and adjusted sound absorption coefficient at 125, 250 and 500 Hz - GR1P sample.

GR1P / Frequency (Hz)	**125**	**250**	**500**
α experimental	0.1255	0.2511	0.415
α curve fitting	0.1007	0.2347	0.3999
Δ	-0.0248	-0.0164	-0.0151
%	-20%	-7%	-4%

Another way to quantify the agreement between the data and the adjusted curves is to determinate $\hat{Q}$ and $\hat{\sigma}$, the value of the residue and the residual standard deviation, respectively (presented in Appendix C). They describe how far the adjusted curve is from the data. Considering a maximum value of $\Delta = 0.05$, the respective values of $\hat{Q}$ and $\hat{\sigma}$ would be $\hat{Q} = 2.235$ (considering the 984 different frequencies where the sound absorption was measured) and $\hat{\sigma} = 0.048$. Table 32 show the values of $\hat{Q}$ and $\hat{\sigma}$ for each curve fitting.

The curve fitting in the case of GR1P, provided the lowest values of $\hat{Q}$ and $\hat{\sigma}$, and this is the only case with $\hat{Q} \leq 2.235$ and $\hat{\sigma} \leq 0.048$. The curve fitting in the case of RR1, provided the highest values of $\hat{Q}$ and $\hat{\sigma}$. These results agree with which was observed in the figures of the curve adjustment.

Table 32 – Values of the residue and the residual standard deviation for each adjustment.

Sample adjustment	$\hat{Q}$	$\hat{\sigma}$
RR1	5.0006	0.0749
GR1	2.4572	0.05251
RR1P	3.5450	0.0630
GR1P	1.1207	0.0355

Comparing the four curves adjustments presented in Figs. 53, 54, 55 and 56, the results presented in Tabs. 27, 28, 30 and 31 and the values presented in Tab. 32, the best curve fitting were provided by the GR1P sample.

Considering the parameters given as output of the samples in Tabs. 23 and 29 , it is noticed that the rockwool σ and λ values are similar for the adjustment of samples RR1, RR1P and GRP1. For rockwool Λ' and $\Theta(0)$ varied between the lower and upper limits of the restrictions. For the samples with glasswool substrate, especially for σ values, there are higher differences between values of flow resistivity for each adjustment.

5 CONCLUSIONS

In this study, double porosity materials made of rockwool and glasswool were tested experimentally in terms of sound absorption and sound transmission loss. Important physical parameters of the materials were measured: tortuosity and porosity, which were used as input for the analytical model used to predict sound absorption and to calculate the diffusion frequency.

The porosity estimation using X-ray Microtomography, led to similar values for both materials. Using X-ray Microtomography and Scanning electron microscopy images, the last one presented in Appendix B, it was noticed that rockwool and glasswool fibers are randomly oriented.

Tortuosity for glasswool and rockwool were estimated by ultrasound measurements, leading to $\alpha_{\infty m}$= 1.5 and $\alpha_{\infty m}$= 1.7, respectively. These results are related to the fact that the pore geometry of both materials are similar, although the rockwool fibers are non uniform as visualized in the SEM images.

For the acoustic characterization, rockwool and glasswool single and double porosity samples were used, with mesopores not filled and mesopores filled. These samples were built to be used in two impedance tubes with different frequency ranges and with different cross-sections: circular and rectangular.

The sound transmission loss tests of the acoustical characterization were realized only for the circular samples. For both double porosity configurations it seems that the *TL* values of each material contributed separately to the TL values of the double porosity sample, according to the sample's mesoporosity. The single porosity rockwool has a higher *TL* than the single porosity glasswool *TL*, i.e. double porosity samples with great amount of rockwool are the ones which provided more insulation. However, the best result for sound transmission loss of the glasswool samples with mesopores filled with rockwool was for GP5 curve, which is not the curve with the samples of higher amount of rockwool. For this case, it is possible that the rockwool used in the mesopores of the 3 replicas presented an individual greater value of TL, due to the heterogeneities of the material. This indicates that the heterogeneities of rockwool could influenced the final results of all curves. It was not observed a effect in TL direct linked to the double porosity, as the TL of glasswool and rockwool contributed individually for the the gains obtained.

Regarding the effects of double porosity in sound absorption, it was noticed that higher gains in absorption were found at high frequencies and smaller gains at low frequencies. For the circular samples, gains in sound absorption were found for all rockwool samples with mesopores not filled and filled above 1000 *Hz*; and for the glasswool circular samples, gains were found for eight types of samples (mesopores filled and not) at 250 *Hz* and for three types

of samples (two with mesopores filled) at 2000 *Hz*. These conclusions considered the glasswool samples that were not affected by the positioning effects of the samples, i.e., the samples with the highest gain values, gains which are one order of magnitude higher than the respective standard deviation due to sample positioning effect. For the rectangular samples, gains were found for four (two with mesopores filled) types of rockwool samples at 250 *Hz* and for the eight types of glasswool samples at 500 *Hz*. However, this gains are of the same order of magnitude of the standard deviation due to the sample positioning effect.

With respect to the sample positioning effect, it is necessary to evaluate the errors caused by this effect by using a statistical approach to better quantify these values. Another aspect is the reduction of this error by determining the samples conditions that reduces these errors, for example, ensuring no additional compression in the samples and using a more precise boundary contact conditions of the sample in the tube.

The double porosity samples are conceptually easy to be manufactured, but in practice some difficulties were found at the cut and assemble of the samples. Especially for the cases of mesopores filled, it is difficult to assure that the porous material completely fills the mesopores or that is not compressed or stretched on the mounting process. This aspect can be one source of results variability.

With reference to the rectangular samples, it was investigated the influence of the number of periodic cells. Using samples with different number of cells but similar mesoporosities, for the rockwool samples with mesopores filled or not and for the glasswool samples with mesopores not filled, it was found that the number of cells did not influenced the final result, but mesoporosity did. This was an expected result, because the analytical model does not consider the number of cells, but assume periodicity. However, in this study, this fact was verified experimentally.

The diffusion frequency was also estimated to be compared with the experimental results of sound absorption of the acoustical characterization. In this case it was noticed that for some circular samples, around the respective diffusion frequency there were gains in absorption. However, for the rectangular samples these gains were not found at the diffusion frequencies. Considering this, the adopted values of flow resistivity used in the calculation of the diffusion frequency could be different from the real ones or the sample repositioning effect can be affecting the final results of sound absorption in the rectangular samples. However, it was not possible to confirm these two hypothesis.

Considering the adjustment of the analytical model of double porosity materials sound absorption to the experimental data, it was only observed a good agreement between the model prediction using the non-linear curve fitting and the experimental data for glasswool sample with mesopores filled, GR1, considering the entire frequency range. However, the value of glasswool flow resistivity estimative given in this case is far from the presented value on the literature reference for glasswool with similar density. This fact enhances the importance of

the previous knowledge of this parameter, which plays an important function on the analytical model.

For future works, important measurements and analysis can be performed:

- Measure porosity with a direct technique to compare the results with the estimate presented in this work;
- Study the influence of other types of mesopores (dead-end pores, irregular cross-sections, etc) and other types of porous inclusion or elastic inclusions, with respect both of sound and transmission loss;
- Apply a methodology to estimate the errors of positioning the sample;
- Develop a methodology or adopt a methodology to calculate the sound absorption and sound transmission loss in the intersection range of the impedance tube of circular cross-section;
- Process MEV images (Appendix B) with advanced techniques to obtain mean fiber diameter, index of orientation and determine the size of the pores and connection regions between pores. This data can be used for a estimation of the two characteristic lengths for fibrous materials (ALLARD; ATALLA, 2009).

BIBLIOGRAPHY

ALLARD, J.; ATALLA, N. **Propagation of sound in porous media: modelling sound absorbing materials**. Second edition. [S.l.]: John Wiley & Sons, 2009.

ALLARD, J. F.; LAURIKS, W. Evaluation of tortuosity in acoustic porous materials satured by air. **Review of Scientific Instruments**, v. 65, n. 3, p. 754 – 755, mar. 1994.

ATALLA, N. *et al.* Acoustic absorption of macro-perforated porous materials. **Journal of Sound and Vibration**, v. 243, n. 4, p. 659 – 678, 2001.

AURIALT, J. L.; BOUTIN, C. Deformable media with double porosity - iii: Acoustics. **Trannsport in porous media**, v. 14, n. 2, p. 143–162, 1994.

BANNWART, F. C. *et al.* On the effects of air cavity backing porous materials for its characterization by the three-microphone method. In: **Proceedings of ISMA 2016 including USD 2016**. [S.l.: s.n.], 2016.

BIES, D. A.; HANSEN, C. H. **Engineering noise control: theory and practice**. Third edition. [S.l.]: Spon Press, 2003.

BOLTON, J. S.; YOO, T.; OLIVIERI, O. Measurement of normal incidence transmission loss and other acoustical properties of materials placed in a standing wave tube. **Bruel and Kjaer Sound & Vibration Measurement A/S**, 2007.

BOUTIN, C.; GEINDREAU, C. Estimates and bounds of dynamic permeability of granular media. **The Journal of the Acoustical Society of America**, v. 124, n. 6, p. 3576–3593, 2008.

BOUTIN, C.; ROYER, P.; AURIAULT, J. L. Acoustic absorption of porous surfacing with dual porosity. **International Journal of Solids Structures**, v. 35, p. 4709–4737, 1998.

BSWATECH. **User's Manual: Impedance Tube Test System**. [S.l.], 2010.

CHAMPOUX, Y.; ALLARD, J. Dynamic tortuosity and bulk modulus in air-saturated porous media. **Journal of Applied Physics**, 1991.

CORREDOR-BEDOYA, A. C. **Acoustic characterization of mortar and tire rubber composites for noise insulation**. Dissertação (Mestrado) — Universidade Estadual de Campinas, 2016.

COX, T. J.; D'ANTONIO, P. **Acoustic absorbers and diffusers: theory, design and application**. Second edition. [S.l.]: Taylor & Francis, 2009.

DAZEL, O.; XBÉCOT, F.; JAOUEN, L. Biot effects for sound absorbing double porosity materials. **Acta Acustica united with Acustica**, v. 98, n. 4, p. 567–576, 2012.

DEDAVID, B. A.; GOMES, C. I.; MACHADO, G. **Microscopia eletrônica de varredura: aplicações e preparação de amostras**. [S.l.]: EDIPUCRS, 2007.

EN13162. **EN 13162:2012+A1:2015 - Thermal insulation products for buildings — Factory made mineral wool (MW) products — Specification**. 2015.

EN826. **EN 826:2013 - Thermal insulating procucts for building applications - Determination of compression behaviour**. 2013.

FABER, L.; TARDOS, G.; MICHAELS, J. N. Use of x-ray tomography to study the porosity and morphology of the granules. **Powder Technology**, v. 132, p. 57–63, 2003.

FAHY, F.; GARDONIO, P. **Sound and structural vibration: radiation, transmission and response**. Second edition. [S.l.]: Academic Press, 2007.

GERGES, S. **Ruído: Fundamentos e Controle**. [S.l.]: NR Editora, 1992.

GOURDON, E.; SEPPI, M. On the use of porous inclusions to improve the acoustical response of porous materials: Analytical model and experimental verification. **Applied Acoustics**, v. 71, p. 283–298, 2010.

GOUVEIA, R. **Microtomografia de raios-X**. 2014. Internet. Https://pt.slideshare.net/CNPEM/microtomografia-de-raios-x.

HAFNER, B. **Scanning Electron Microscopy Primer**. [S.l.], 2007.

HONORATO, A. M. B. **Avaliação de modelos analíticos para a determinação de absorção sonora de materiais poroelásticos**. Dissertação (Mestrado) — Universidade Federal de Santa Catarina, 2013.

HUALLPA, B. N. *et al.* Post-processing of x-ray tomographic images of an acoustic fibrous material and possible use of numerical methods such as fem and lbm to determine biot's porous technical parameters. In: **XI Congresso Nacional de Engenharia Mecânica (CONEM)**. [S.l.: s.n.], 2016.

HUMANS, I. W. G. on the Evaluation of Carcinogenic Risks to. **IARC Monograph on the evaluation on carcinogen risk to humans**. [S.l.]: World Health Organization, 1988. v. 43.

ISO10534-2. **EN ISO 10534-2, Determination of sound absorption coefficient and impedance in impedance tubes - Part** 2**: Transfer-function methode**. 2001.

JAOUEN, L. **Acoustic porous materials reciepes**. 2018. Internet. Www.apmr.matelys.com.

JOHNSON, D.; KOPLIK, J.; DASHEW, R. Theory of dynamic permeability and tortuosity in fluid-saturated porous media. **Journal of Fluid Mechanics**, 1987.

KINO, N.; UENO, T. Experimental determination of the micro-and macrostructural parameters influencing the acoustical performance of fibrous media. **Applied Acoustics**, v. 68, n. 11-12, p. 1439–1458, 2007.

KUTRUFF, H. **Room acoustics**. Fourth edition. [S.l.]: Spon Press, 2000.

LAFARGE, D. *et al.* Dynamic compressibility of air in porous structures at audible frequencies. **Journal of the Acoustical Society of America**, v. 102, n. 4, p. 1995–2006, 1997.

MAREZE, P. H. **Análise da influência da microgeometria na absorção sonora de materiais porosos de estrutura rígida**. Tese (Doutorado) — Universidade Federal de Santa Catarina, 2013.

NIST/SEMATECH. **e-Handbook of Statistical Methods**. 2018. Internet. Http://www.itl.nist.gov/div898/handbook/.

OLNY, X.; BOUTIN, C. The influence of pressure diffusion effects on absorbing properties of porous media with double porosity. In: **INTER-NOISE and NOISE-CON Congress and Conference Proceedings**. [S.l.: s.n.], 2000. v. 2000, n. 5, p. 2909–2913.

OLNY, X.; BOUTIN, C. Acoustic wave propagation in double porosity media. **The Journal of the Acoustical Society of America**, v. 114, n. 1, p. 73 – 89, 2003.

RAICHEL, D. R. **The science and applications of acoustics**. Second edition. [S.l.]: Springer, 2006.

SGARD, F. C.; ATALLA, N. Transmission loss through barriers lined with heterogeneous porous materials. **Canadian Acoustic**, v. 28, n. 3, p. 92 – 93, 2000.

SGARD, F. C. *et al.* On the use of perforations to improve the sound absorption of porous materials. **Applied Acoustics**, v. 66, n. 6, p. 625–651, 2005.

SIEMENS. **User's Manual - LMS Scadas Mobile and Recorder - Version 2.1**. [S.l.], 2015.

SIVIERO, D. A. **Controle acústico híbrido da perda de transmissão sonora**. Tese (Doutorado) — Universidade Estadual de Campinas, 2011.

VÉR, I. L.; BERANEK, L. L. **Noise and vibration control enginnering - principles and applications**. Second edition. [S.l.]: John Wiley & Sons, 2006.

VIGRAN, T. E. **Building acoustics**. First edition. [S.l.]: Taylor & Francis, 2008.

WILLIAMS, M.; MCCLURE, P. R. **Toxicological profile for synthetic vitreous fibers**. [S.l.]: U. S Departament for Health and Human Services, 1994.

ZWIKKER, C.; KOSTEN, C. **Sound absorbing materials**. [S.l.]: Elselvier, 1949.

APPENDIX A – EMPTY IMPEDANCE TUBE SOUND ABSORPTION

The rectangular impedance tube used in this study was characterized in terms of sound absorption when empty, i.e., without samples. It is possible to notice that the impedance tube and the sample holder developed had some absorption and this influenced the curves of the samples tested, especially at a drop around 270 *Hz*. In Figure 57 it is observed the curve for the empty tube and the curves for the mean values of the samples RR and GR, pure rockwool and glasswool, respectively. At very low frequencies, the value of sound absorption is greater for the empty tube than for the absorptive materials and this probably caused by external variations of the measurement.

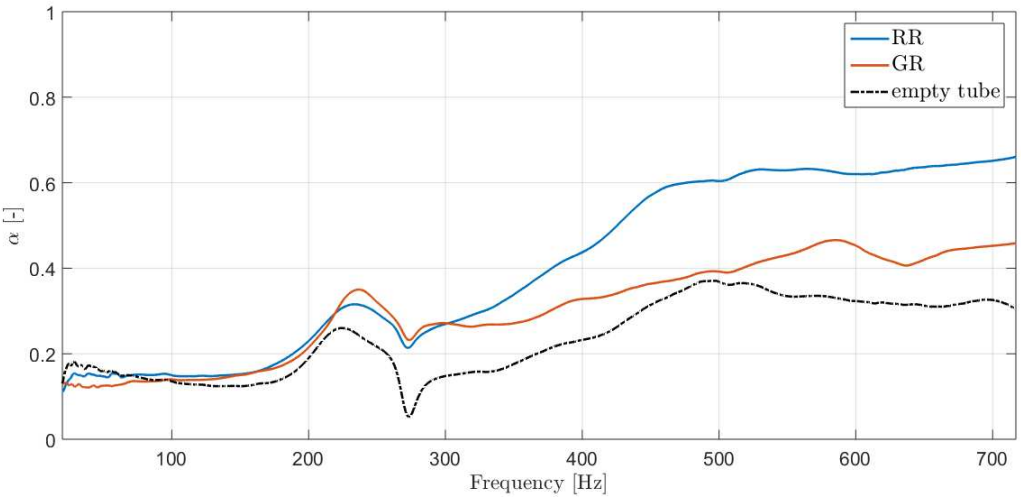

Figure 57 – Sound absorption for the empty tube, pure rockwool (RR) and pure glaswool (GR).

Additionally, the same characterization was done for the impedance tube of circular-cross section, for the case of empty tube only. Figure 58 shows the absorption for this tube when empty. It is possible to see that in this case the absorption is smaller than 0.1 in all frequency range and around 500 *Hz* there is a increase in absorption, exceeding the value of 0.1.

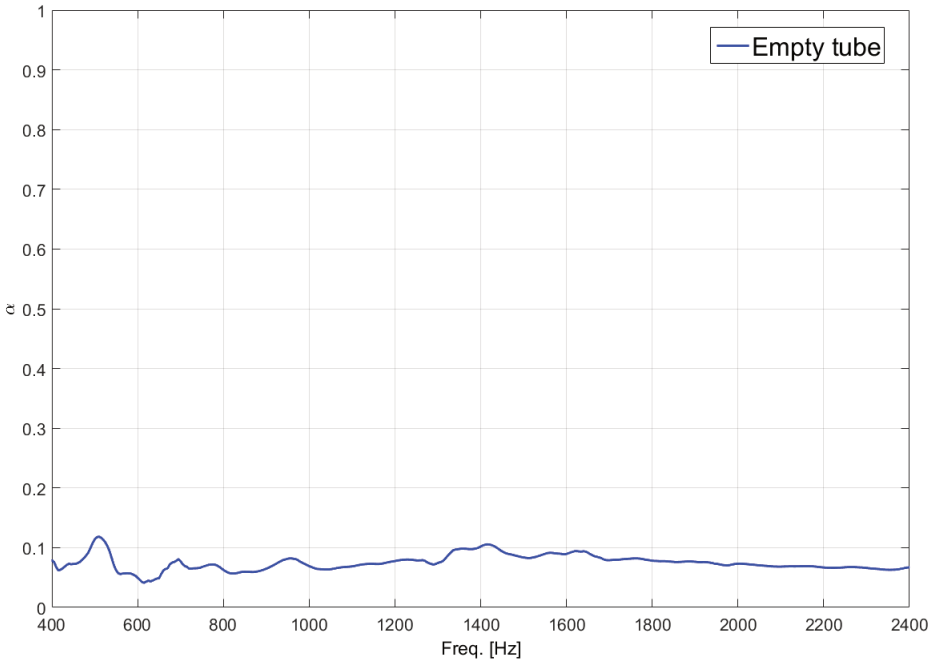

Figure 58 – Sound absorption for the empty tube.

APPENDIX B – SCANNING ELECTRON MICROSCOPY (SEM)

Scanning electron microscopy (SEM) was utilized in order to obtain images from the fibrous porous materials to study their microscopical geometry, size of the fibers and chemical composition.

In a Scanning electron microscopy, a electron beam generated by an electron gun is accelerated down the column until it reaches the sample on the bottom part. In this column, there are condenser and objective lenses utilized to focus and control the size of the beam on the specimen, appertures which affects the properties of the beam and deflection coils, which are responsible for rastering the beam across the sample surface. On the bottom part, where the sample is placed, there are detectors for the signals emitted from the sample (HAFNER, 2007).

The interaction between the sample and the electron beam can produce different signals: backscattered electrons, secondary electrons, X- rays and others (DEDAVID *et al.*, 2007).

Two types of tests were realized using Scanning Electron Microscopy. First, images were generated using the secondary electrons (SE) and backscattered electrons (BSE) radiations for rockwool and glasswool samples coated with gold. These signals offer information from the topography of the sample. Second, an analysis using the X-rays emitted from the samples and detected by an energy dispersion (EDS) detector was used to identify the chemical components for rockwool and glasswool samples coated with carbon. Because of the non-conductive nature of the samples, the coating on the samples is necessary to obtain SEM images and chemical data.

In this study, the samples were analyzed at the Brazilian National Nanotechnology Laboratory (LNNano) using an FEI Quanta 650 FEG Scanning Electron Microscope. For the analysis using an EDS detector the XEDS Oxford X-Max SDD 80 mm^2 accessory was used. The coating (metallization process) with gold and carbon used the equipment Bal-Tec SCD 050.

B.0.1 Images obtained by SE and BSE

Images were obtained using SE and BSE radiation. For the case of mineral fibers the best images, with better resolution and contrast, were obtained using SE. Figure 59 shows the image for a rockwool sample using SE, with a magnification of 100 times. It was noticed that the fibers are randomly distributed and there are narrower and thicker fibers, and also the formation of some particles with a much greater thickness than the others fibers. Additionally, the sample of rockwool is showed with a magnification of 250 times in Fig. 60, where a circular particle is presented.

For the glasswool sample, an image of the same magnification (100 times) was

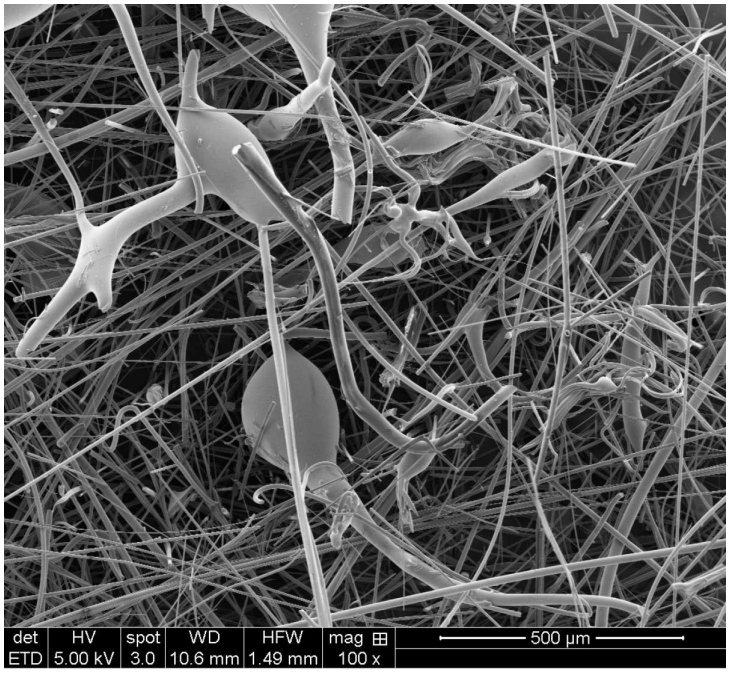

Figure 59 – Image of rockwool sample using SEM, 100 times magnification.

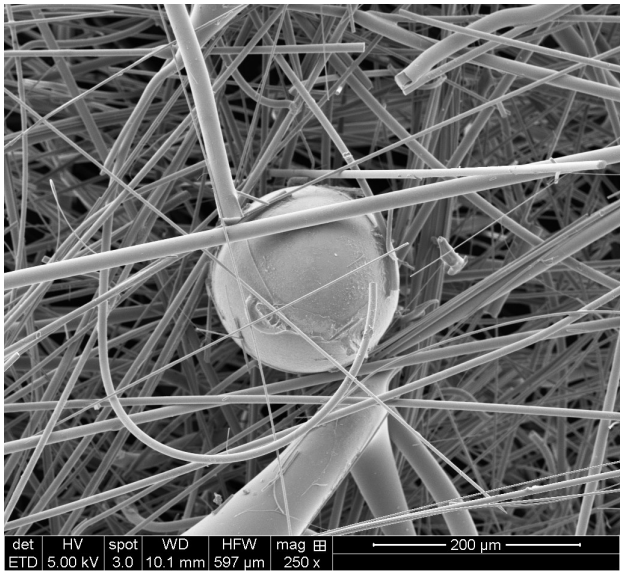

Figure 60 – Image of rockwool sample using SEM , 250 times magnification.

taken to be compared with Fig. 59. It is also noticed that for glasswool samples there is no preferential orientation of the fibers, however, the thickness of the fibers are similar between each other. Visually, the narrower fibers of rockwool are similar in diameter to the fiber of glasswool.

B.0.2 Chemical composition using EDS detector for X-rays

Using this technique, it was possible to represent the chemical components of the material over the images taken at the electron microscopy. Figure 62 shows the main image of the rockwool sample in black and white at the upper part of the figure. Below, the same figure

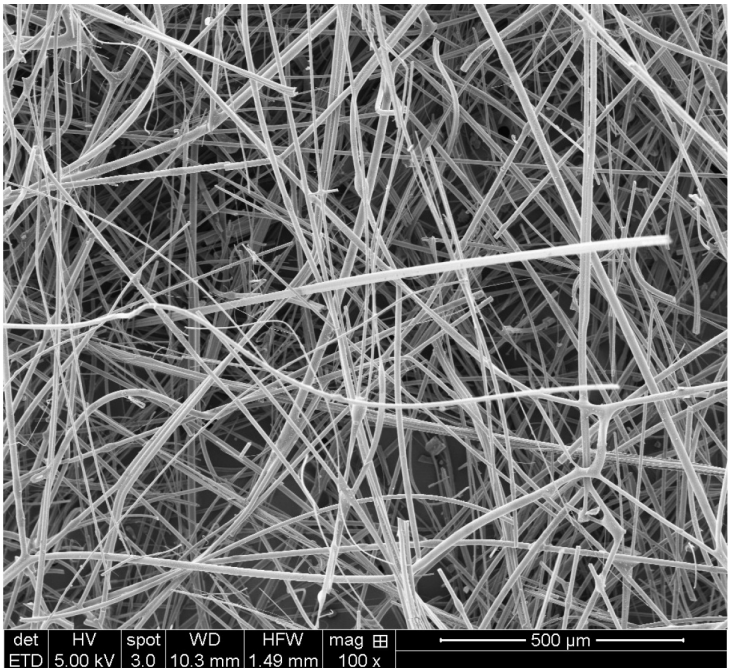

Figure 61 – Image of glasswool sample using SEM, 100 times magnification.

was repeated and pictures were colored according to the presence of each chemical component on the sample. The higher is the color intensity, the most this substance composes the material.

Also, using a spectrogram it was possible to quantify the percentage of each chemical component on the sample, as in Fig. 64 for rockwool. A peak of carbon is presented on the spectrum, however, due to the coating utilized on the sample. The main components of rockwool are Oxigen (O), because of the presence of different oxides, calcium (Ca) and silicon (Si).

Figure 63 represents the same analysis of chemical components for a glasswool sample. The spectrum of the percentual quantity of chemical components is given in Fig. 65. In this case the main components are Oxigen (O), due the presence of different oxides, silicon (Si), sodium (Na) and calcium (Ca).

Considering the chemical composition, the difference between these two material are concentrated on the presence of a greater percentage of Na in glasswool (11.1%), a greater percentage of Ca in rockwool (19.9%) and a small difference in the percentual values of magnesium (Mg), 1.1% for glasswool and 4.0% for rockwool. The samples are rich in oxides, silicon and the glasswool have a greater percentage of Na, as it was shown in Section 2.3.1.

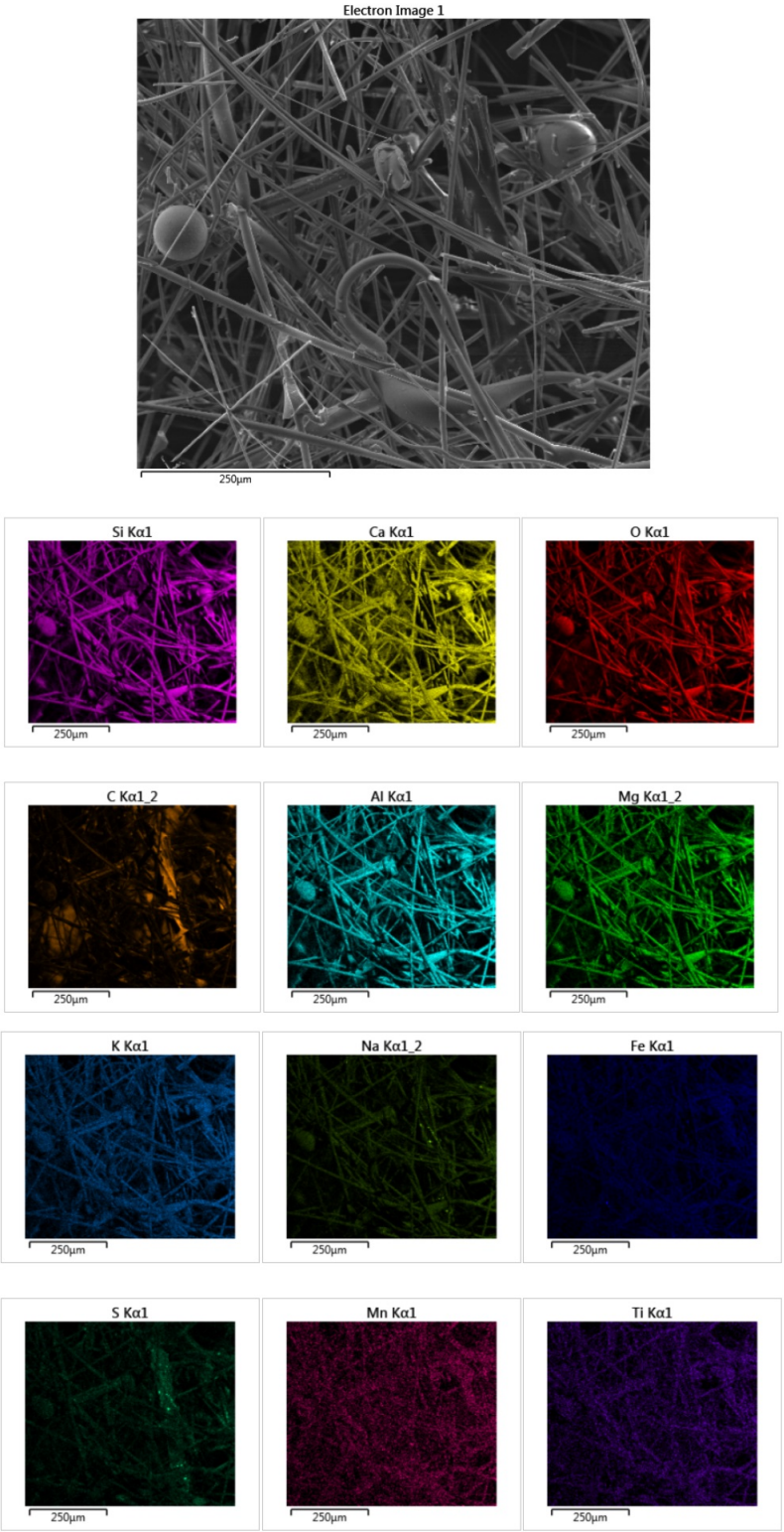

Figure 62 – EDS analysis for rockwool.

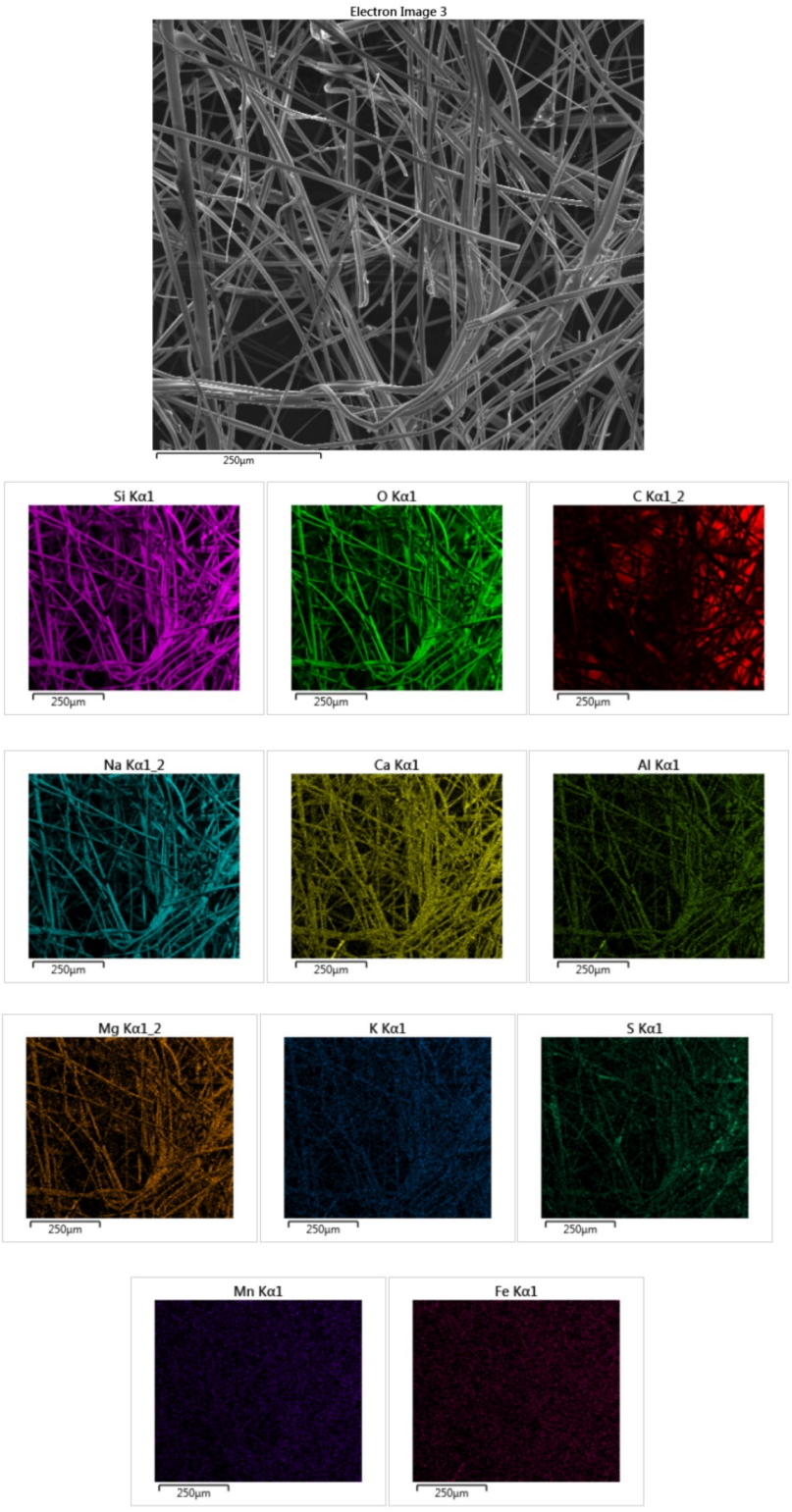

Figure 63 – EDS analysis for glasswool.

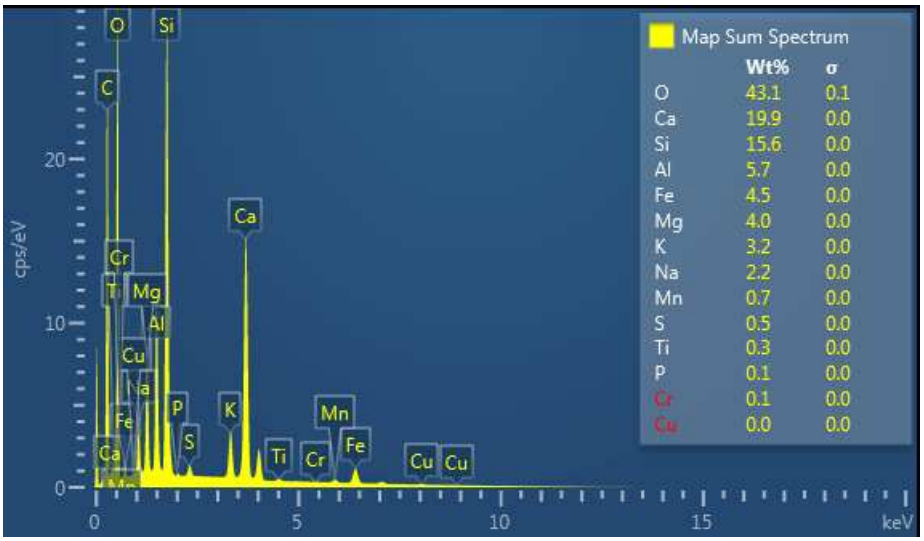

Figure 64 – Chemical spectrum for rockwool using EDS analysis.

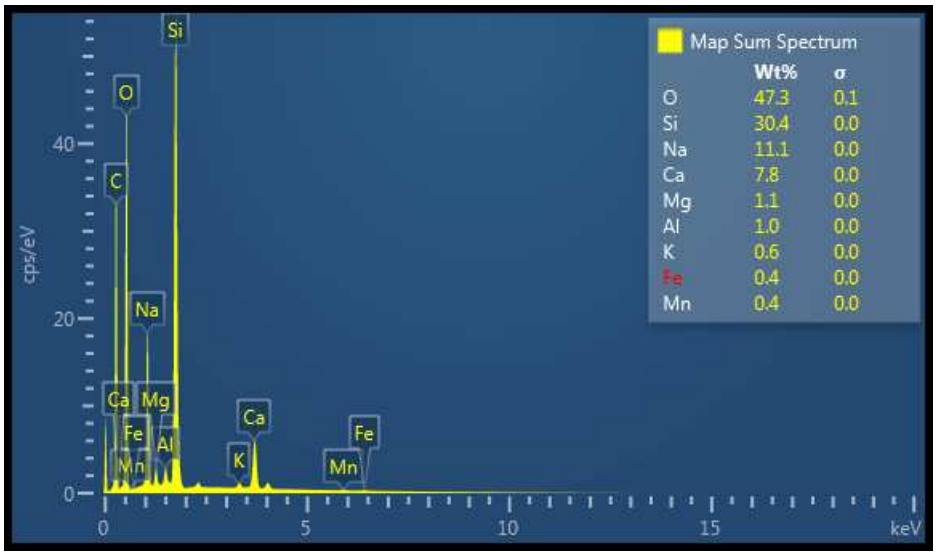

Figure 65 – Chemical spectrum for glasswool using EDS analysis.

APPENDIX C – NON-LINEAR LEAST SQUARES METHOD

In the curve fitting using the Non-linear Least Squares Method, the expression for the sound absorption coefficient (α at Eq. 2.44), for samples with mesopores not filled (model described in Sec. 2.5.3.1) and for samples with mesopores filled (model described in Sec. 2.5.3.2) were adjusted to the experimental data of sound absorption coefficient obtained in Section 4.1.1.

The adjusted curve obtained with the Non-Linear Least Squares Method comes from the minimization of the function Q, which is the squared deviation between the measured values of the sound absorption coefficient and the sound absorption analytical model equation $\alpha = f(\omega_i, \vec{\beta})$, where $\vec{\beta}$ (β_1, β_2 and β_3) are the unknown parameters of the problem. Q is given by (NIST/SEMATECH, 2018):

$$Q = \sum_{i=1}^{n} (\alpha_{mi} - f(\omega_i, \vec{\beta}))^2 \tag{C.1}$$

where i indicates each frequency value that was observed and α_{mi} is the measured sound absorption coefficient at the i-th frequency.

As a result of the minimization process, a value $\hat{Q}$, which is the minimum value for the function Q, is found. Considering this solution, $\vec{\beta}$ (real values which are unknown) assume numerical values of $\hat{\vec{\beta}}$ ($\hat{\beta}_1, \hat{\beta}_2$ and $\hat{\beta}_3$), optimal values, in the minimum least squares sense, which leads to the value $\hat{Q}$ (NIST/SEMATECH, 2018).

For the linear case of the least squares method, the minimization of Q can be calculated analytically. However, for the non-linear case, it is necessary to use a minimization algorithms, which also involves the use of starting values for the unknown parameters.

An example of a linear case least-squares method for a given data is presented in Fig.66, where the points are data, the solid line is a curve fitting based on the estimated parameters and the dashed line is the curve based on the true parameters (in this case known) (NIST/SEMATECH, 2018).

In this example, the curve with estimated parameters and the curve with true parameters are almost identical, because the data (points) were simulated. In the case of real data, it is not possible to compare the curve of the estimated parameters with the curve of the real parameters, which are unknown. To quantify if the curve of estimated parameters is a good estimative of real data, it is necessary to calculate the residual standard deviation ($\hat{\sigma}$), given by:

$$\hat{\sigma} = \sqrt{\frac{\hat{Q}}{n-p}} \tag{C.2}$$

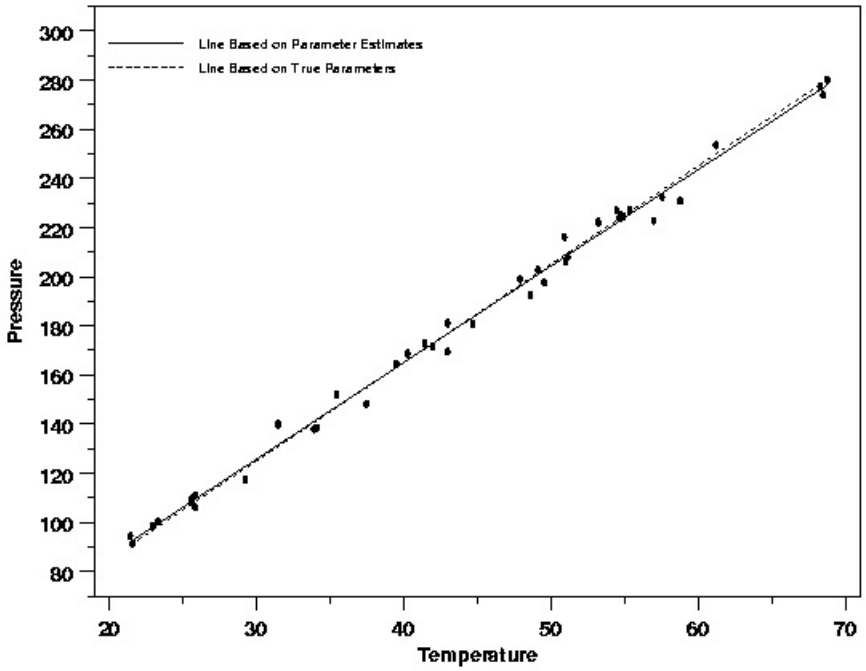

Figure 66 – Example of a curve fitting using linear least-squares method.
Reference: NIST/SEMATECH (2018)

where p is the number of estimated parameters.

The residual standard deviation, $\hat{\sigma}$, could be used to describe how far the curve based on the estimated parameters are from the real data (NIST/SEMATECH, 2018).

APPENDIX D – YOUNG MODULUS MEASUREMENT UNDER COMPRESSIVE LOAD

The standard EN 13161:2015 gives the specification of the proper test to be performed when working with mineral fibers (EN13162, 2015). According to this standard, the Young Modulus under compression of a mineral wool material can be determined using the proceedings of EN 826:2013.

The test according to this standard were executed in the facilities of the Laboratory of Materials Testing at the School of Mechanical Engineering at Unicamp. The equipment utilized is a MTS Testing Machine, model 810-FlexTest40 with a load capacity of 100 kN and a load cell of 1,5 kN. The equipment calibration guarantees a precision of 1% for the measurement of displacement and force.

The samples were taken from two different panels and different positions on the same panel. The samples used are of the size of 100×100 mm. The samples were submitted first to a pre-load of 250 Pa and the thickness (d_0) of the sample was determined under this pre-load. After the specimen was compressed at a constant speed of $0.1d_0$ (EN826, 2013) until 60% strain. Force and displacement were registered and the elasticity modulus was calculated in reference of the region around 10% strain. Figure 67 shows one of the samples tested and the MTS Testing Machine.

Figure 67 – Sample under compressive load in MTS testing machine.

The results obtained for this five samples of rockwool and glasswool are showed in Tabs. 33 and 34, respectively. Also, the standard deviation for the elasticity modulus value

for each material. The value of standard deviation corresponds to 30% of the mean value of rockwool and 25% of the mean value of glasswool. This is caused by the spatial heterogeneities of the material.

Table 33 – Young Modulus of compression for Rockwool.

Sample	**E (*kPa*)**
1	138.170
2	174.720
3	876.24
4	108.600
5	181.600
Mean Value	138.143
Standard Deviation	40.777

Table 34 – Young Modulus of compression for Glasswool.

Sample	**E (*kPa*)**
1	3.009
2	2.213
3	1.724
4	3.070
5	1.9667
Mean Value	2.396
Standard Deviation	0.612

ANNEX A – IMAGE USAGE PERMISSIONS

ELSEVIER LICENSE
TERMS AND CONDITIONS

Apr 19, 2018

This Agreement between Mrs. Giovanna Pisicchio Zanoni ("You") and Elsevier ("Elsevier") consists of your license details and the terms and conditions provided by Elsevier and Copyright Clearance Center.

License Number	4323261333655
License date	Apr 06, 2018
Licensed Content Publisher	Elsevier
Licensed Content Publication	Applied Acoustics
Licensed Content Title	On the use of porous inclusions to improve the acoustical response of porous materials: Analytical model and experimental verification
Licensed Content Author	E. Gourdon,M. Seppi
Licensed Content Date	Apr 1, 2010
Licensed Content Volume	71
Licensed Content Issue	4
Licensed Content Pages	16
Start Page	283
End Page	298
Type of Use	reuse in a thesis/dissertation
Portion	figures/tables/illustrations
Number of figures/tables/illustrations	3
Format	electronic
Are you the author of this Elsevier article?	No
Will you be translating?	No
Original figure numbers	Fig.1, Fig.9, Fig. 16
Title of your thesis/dissertation	Acoustical Characterization of double posity materials using mineral wools
Expected completion date	May 2018
Estimated size (number of pages)	117
Requestor Location	Mrs. Giovanna Pisicchio Zanoni Rua Mendeleyev,200 Campinas, Sao Paulo 13083-860 Brazil Attn: Mrs. Giovanna Pisicchio Zanoni
Publisher Tax ID	GB 494 6272 12
Total	0.00 USD
Terms and Conditions	

INTRODUCTION

1. The publisher for this copyrighted material is Elsevier. By clicking "accept" in connection with completing this licensing transaction, you agree that the following terms and conditions apply to this transaction (along with the Billing and Payment terms and conditions

established by Copyright Clearance Center, Inc. ("CCC"), at the time that you opened your Rightslink account and that are available at any time at http://myaccount.copyright.com).

GENERAL TERMS

2. Elsevier hereby grants you permission to reproduce the aforementioned material subject to the terms and conditions indicated.

3. Acknowledgement: If any part of the material to be used (for example, figures) has appeared in our publication with credit or acknowledgement to another source, permission must also be sought from that source. If such permission is not obtained then that material may not be included in your publication/copies. Suitable acknowledgement to the source must be made, either as a footnote or in a reference list at the end of your publication, as follows:

"Reprinted from Publication title, Vol /edition number, Author(s), Title of article / title of chapter, Pages No., Copyright (Year), with permission from Elsevier [OR APPLICABLE SOCIETY COPYRIGHT OWNER]." Also Lancet special credit - "Reprinted from The Lancet, Vol. number, Author(s), Title of article, Pages No., Copyright (Year), with permission from Elsevier."

4. Reproduction of this material is confined to the purpose and/or media for which permission is hereby given.

5. Altering/Modifying Material: Not Permitted. However figures and illustrations may be altered/adapted minimally to serve your work. Any other abbreviations, additions, deletions and/or any other alterations shall be made only with prior written authorization of Elsevier Ltd. (Please contact Elsevier at permissions@elsevier.com). No modifications can be made to any Lancet figures/tables and they must be reproduced in full.

6. If the permission fee for the requested use of our material is waived in this instance, please be advised that your future requests for Elsevier materials may attract a fee.

7. Reservation of Rights: Publisher reserves all rights not specifically granted in the combination of (i) the license details provided by you and accepted in the course of this licensing transaction, (ii) these terms and conditions and (iii) CCC's Billing and Payment terms and conditions.

8. License Contingent Upon Payment: While you may exercise the rights licensed immediately upon issuance of the license at the end of the licensing process for the transaction, provided that you have disclosed complete and accurate details of your proposed use, no license is finally effective unless and until full payment is received from you (either by publisher or by CCC) as provided in CCC's Billing and Payment terms and conditions. If full payment is not received on a timely basis, then any license preliminarily granted shall be deemed automatically revoked and shall be void as if never granted. Further, in the event that you breach any of these terms and conditions or any of CCC's Billing and Payment terms and conditions, the license is automatically revoked and shall be void as if never granted. Use of materials as described in a revoked license, as well as any use of the materials beyond the scope of an unrevoked license, may constitute copyright infringement and publisher reserves the right to take any and all action to protect its copyright in the materials.

9. Warranties: Publisher makes no representations or warranties with respect to the licensed material.

10. Indemnity: You hereby indemnify and agree to hold harmless publisher and CCC, and their respective officers, directors, employees and agents, from and against any and all claims arising out of your use of the licensed material other than as specifically authorized pursuant to this license.

11. No Transfer of License: This license is personal to you and may not be sublicensed, assigned, or transferred by you to any other person without publisher's written permission.

12. No Amendment Except in Writing: This license may not be amended except in a writing signed by both parties (or, in the case of publisher, by CCC on publisher's behalf).

13. Objection to Contrary Terms: Publisher hereby objects to any terms contained in any purchase order, acknowledgment, check endorsement or other writing prepared by you, which terms are inconsistent with these terms and conditions or CCC's Billing and Payment terms and conditions. These terms and conditions, together with CCC's Billing and Payment terms and conditions (which are incorporated herein), comprise the entire agreement between you and publisher (and CCC) concerning this licensing transaction. In the event of

any conflict between your obligations established by these terms and conditions and those established by CCC's Billing and Payment terms and conditions, these terms and conditions shall control.

14. Revocation: Elsevier or Copyright Clearance Center may deny the permissions described in this License at their sole discretion, for any reason or no reason, with a full refund payable to you. Notice of such denial will be made using the contact information provided by you. Failure to receive such notice will not alter or invalidate the denial. In no event will Elsevier or Copyright Clearance Center be responsible or liable for any costs, expenses or damage incurred by you as a result of a denial of your permission request, other than a refund of the amount(s) paid by you to Elsevier and/or Copyright Clearance Center for denied permissions.

LIMITED LICENSE

The following terms and conditions apply only to specific license types:

15. **Translation**: This permission is granted for non-exclusive world **English** rights only unless your license was granted for translation rights. If you licensed translation rights you may only translate this content into the languages you requested. A professional translator must perform all translations and reproduce the content word for word preserving the integrity of the article.

16. **Posting licensed content on any Website**: The following terms and conditions apply as follows: Licensing material from an Elsevier journal: All content posted to the web site must maintain the copyright information line on the bottom of each image; A hyper-text must be included to the Homepage of the journal from which you are licensing at http://www.sciencedirect.com/science/journal/xxxxx or the Elsevier homepage for books at http://www.elsevier.com; Central Storage: This license does not include permission for a scanned version of the material to be stored in a central repository such as that provided by Heron/XanEdu.

Licensing material from an Elsevier book: A hyper-text link must be included to the Elsevier homepage at http://www.elsevier.com . All content posted to the web site must maintain the copyright information line on the bottom of each image.

Posting licensed content on Electronic reserve: In addition to the above the following clauses are applicable: The web site must be password-protected and made available only to bona fide students registered on a relevant course. This permission is granted for 1 year only. You may obtain a new license for future website posting.

17. **For journal authors:** the following clauses are applicable in addition to the above:

Preprints:

A preprint is an author's own write-up of research results and analysis, it has not been peer-reviewed, nor has it had any other value added to it by a publisher (such as formatting, copyright, technical enhancement etc.).

Authors can share their preprints anywhere at any time. Preprints should not be added to or enhanced in any way in order to appear more like, or to substitute for, the final versions of articles however authors can update their preprints on arXiv or RePEc with their Accepted Author Manuscript (see below).

If accepted for publication, we encourage authors to link from the preprint to their formal publication via its DOI. Millions of researchers have access to the formal publications on ScienceDirect, and so links will help users to find, access, cite and use the best available version. Please note that Cell Press, The Lancet and some society-owned have different preprint policies. Information on these policies is available on the journal homepage.

Accepted Author Manuscripts: An accepted author manuscript is the manuscript of an article that has been accepted for publication and which typically includes author-incorporated changes suggested during submission, peer review and editor-author communications.

Authors can share their accepted author manuscript:

- immediately
  - via their non-commercial person homepage or blog
  - by updating a preprint in arXiv or RePEc with the accepted manuscript

- via their research institute or institutional repository for internal institutional uses or as part of an invitation-only research collaboration work-group
- directly by providing copies to their students or to research collaborators for their personal use
- for private scholarly sharing as part of an invitation-only work group on commercial sites with which Elsevier has an agreement

- After the embargo period
  - via non-commercial hosting platforms such as their institutional repository
  - via commercial sites with which Elsevier has an agreement

In all cases accepted manuscripts should:

- link to the formal publication via its DOI
- bear a CC-BY-NC-ND license - this is easy to do
- if aggregated with other manuscripts, for example in a repository or other site, be shared in alignment with our hosting policy not be added to or enhanced in any way to appear more like, or to substitute for, the published journal article.

Published journal article (JPA): A published journal article (PJA) is the definitive final record of published research that appears or will appear in the journal and embodies all value-adding publishing activities including peer review co-ordination, copy-editing, formatting, (if relevant) pagination and online enrichment.
Policies for sharing publishing journal articles differ for subscription and gold open access articles:
Subscription Articles: If you are an author, please share a link to your article rather than the full-text. Millions of researchers have access to the formal publications on ScienceDirect, and so links will help your users to find, access, cite, and use the best available version.
Theses and dissertations which contain embedded PJAs as part of the formal submission can be posted publicly by the awarding institution with DOI links back to the formal publications on ScienceDirect.
If you are affiliated with a library that subscribes to ScienceDirect you have additional private sharing rights for others' research accessed under that agreement. This includes use for classroom teaching and internal training at the institution (including use in course packs and courseware programs), and inclusion of the article for grant funding purposes.
Gold Open Access Articles: May be shared according to the author-selected end-user license and should contain a CrossMark logo, the end user license, and a DOI link to the formal publication on ScienceDirect.
Please refer to Elsevier's posting policy for further information.
18. **For book authors** the following clauses are applicable in addition to the above:
Authors are permitted to place a brief summary of their work online only. You are not allowed to download and post the published electronic version of your chapter, nor may you scan the printed edition to create an electronic version. **Posting to a repository:** Authors are permitted to post a summary of their chapter only in their institution's repository.
19. **Thesis/Dissertation**: If your license is for use in a thesis/dissertation your thesis may be submitted to your institution in either print or electronic form. Should your thesis be published commercially, please reapply for permission. These requirements include permission for the Library and Archives of Canada to supply single copies, on demand, of the complete thesis and include permission for Proquest/UMI to supply single copies, on demand, of the complete thesis. Should your thesis be published commercially, please reapply for permission. Theses and dissertations which contain embedded PJAs as part of the formal submission can be posted publicly by the awarding institution with DOI links back to the formal publications on ScienceDirect.

Elsevier Open Access Terms and Conditions
You can publish open access with Elsevier in hundreds of open access journals or in nearly 2000 established subscription journals that support open access publishing. Permitted third party re-use of these open access articles is defined by the author's choice of Creative Commons user license. See our open access license policy for more information.

Terms & Conditions applicable to all Open Access articles published with Elsevier:
Any reuse of the article must not represent the author as endorsing the adaptation of the article nor should the article be modified in such a way as to damage the author's honour or reputation. If any changes have been made, such changes must be clearly indicated.
The author(s) must be appropriately credited and we ask that you include the end user license and a DOI link to the formal publication on ScienceDirect.
If any part of the material to be used (for example, figures) has appeared in our publication with credit or acknowledgement to another source it is the responsibility of the user to ensure their reuse complies with the terms and conditions determined by the rights holder.
Additional Terms & Conditions applicable to each Creative Commons user license:
CC BY: The CC-BY license allows users to copy, to create extracts, abstracts and new works from the Article, to alter and revise the Article and to make commercial use of the Article (including reuse and/or resale of the Article by commercial entities), provided the user gives appropriate credit (with a link to the formal publication through the relevant DOI), provides a link to the license, indicates if changes were made and the licensor is not represented as endorsing the use made of the work. The full details of the license are available at http://creativecommons.org/licenses/by/4.0.
CC BY NC SA: The CC BY-NC-SA license allows users to copy, to create extracts, abstracts and new works from the Article, to alter and revise the Article, provided this is not done for commercial purposes, and that the user gives appropriate credit (with a link to the formal publication through the relevant DOI), provides a link to the license, indicates if changes were made and the licensor is not represented as endorsing the use made of the work. Further, any new works must be made available on the same conditions. The full details of the license are available at http://creativecommons.org/licenses/by-nc-sa/4.0.
CC BY NC ND: The CC BY-NC-ND license allows users to copy and distribute the Article, provided this is not done for commercial purposes and further does not permit distribution of the Article if it is changed or edited in any way, and provided the user gives appropriate credit (with a link to the formal publication through the relevant DOI), provides a link to the license, and that the licensor is not represented as endorsing the use made of the work. The full details of the license are available at http://creativecommons.org/licenses/by-nc-nd/4.0.
Any commercial reuse of Open Access articles published with a CC BY NC SA or CC BY NC ND license requires permission from Elsevier and will be subject to a fee.
Commercial reuse includes:

- Associating advertising with the full text of the Article
- Charging fees for document delivery or access
- Article aggregation
- Systematic distribution via e-mail lists or share buttons

Posting or linking by commercial companies for use by customers of those companies.

20. **Other Conditions**:

v1.9

Questions? customercare@copyright.com or +1-855-239-3415 (toll free in the US) or +1-978-646-2777.

Therms and conditions are the same from the previous case.